

Chapter 3

Establishment of a culture model for network activity in neuronal ensembles

3.1 Introduction

As reviewed in section 1.1, neuronal cultures grown on multi electrode arrays have emerged as a successful model for studying generic properties of neuronal ensembles at the network level. The overall purpose of this Ph.D work is to provide this model system with an added functionality of phasic volume transmission, thus achieving a novel experimental platform for studying how fine temporal feature of extrasynaptic agonist concentrations interact with the activity. In this first chapter we describe the establishment of the standard neuronal cultures on MEA model system within our laboratory group. We followed their development for over 3 weeks *in vitro* and demonstrated that they develop normally and exhibit hallmark network activity, both spontaneous and evoked, and comply in characteristics with the literature gold standard.

To date, MEA investigation have been dominated by use of primary cultures derived from rat. However, mouse is generally a more popular neuroscience model and offers a by far greater library of molecular and genetic tools so using it as a tissue source might be beneficial. Thus, an additional contribution presented in this chapter is the examination of mouse based cultures and comparison with rat preparations in the context of MEA investigations. We found that the mouse cultures were difficult to culture on the MEA surface and exhibited a delayed synaptic maturation as compared to their rat counterparts. Nevertheless, mouse cortical cultures that were able to develop exhibited all the richness of network phenomena described in rat literature.

Finally, prior to engaging in the development of the microfluidics system for rapid pulsing

we took the chance to explore generating a slower phasic dopamine signalling model in these traditional experimental systems by manually pipetting the agonist (in this case dopamine) onto the culture followed by replacement of the media. We used this approach to revisit the long standing issue of plasticity in these systems.

Synaptic plasticity without neuromodulation in neuronal cultures on MEA has been controversial as multiple reports produced contradictory or negative results (reviewed further in section 3.4). This in contrast to slices and *in vivo* systems where activity dependent plasticity induced through stimulation or behavioural paradigms is well established [1]. It should be noted that spike timing dependent plasticity had been demonstrated in hippocampal cultures for pre and post synaptic neuron pairs explicitly controlled and monitored via patch clamp [2]. The lack of success on MEAs cannot, therefore, be attributed so a skewed biology of neurons in culture and it is not yet clear if it is related to the poorer sensitivity of the extracellular recordings (sensitive only to super-threshold processes), to the culture network topology which needs to be accounted for in the stimulation protocols, or to the absence of neuromodulators. Indeed that dopamine modulates plasticity in culture has been established but using bath application therefore only interrogating tonic effects [3, 4].

Thus, as a final step in this chapter, we revisited the question of plasticity induction and found that a standard tetanization protocol does not produce a measurable change in evoked responses or in functional connectivity in our cultures. We then explored whether slow pulsing of dopamine by manually adding it during the plasticity-induction phase (tetanization) and washing it away immediately after could have an enabling effect on plasticity. We found that the altered protocol results in a change to activity and connectivity measures but argue that the effect of the washing cannot be easily separated from that of the dopamine, hence confusing the interpretation. This chapter thus serves to establish the multi electrode array electrophysiology technique and to provide motivation for the development of the microfluidics technology in the following chapters.

3.2 Development of spontaneous activity in Mouse cultures

Primary mouse embryonic cortical cultures were seeded on pre-coated MEAs as described in sections 2.3 and 2.4. All MEAs used for the work undertaken in this chapter are of 8x8 configuration with $30\mu m$ electrodes and $200\mu m$ electrode spacing (see appendix A.1 for data sheets).

Figure 3.1 A-C shows microscope images of a representative culture over 18 days in culture. The images show how over the first few days the cells became polarized and extended neurites and dendrites. As these continued to grow, branch and generate synaptic contacts the culture obtained a weblike appearance. In later days of development an obvious mass of extracellular tissue was evident in between the cells covering the previously bare glass

and engulfing the fine cellular processes. In the case of the mouse cultures, many of the preparations did not develop properly whereby, despite good initial adhesion, the majority of the plated cells did not continue differentiating and after a few days detached from the surface and degenerated (figure 3.1 D). This was the case for over half of plated cultures and these were discarded from the experiment. Cultures prepared from rat embryos did not present this sort of inconsistency and generally developed at a high success rate despite using the same MEAs and generally same coating and seeding procedures.

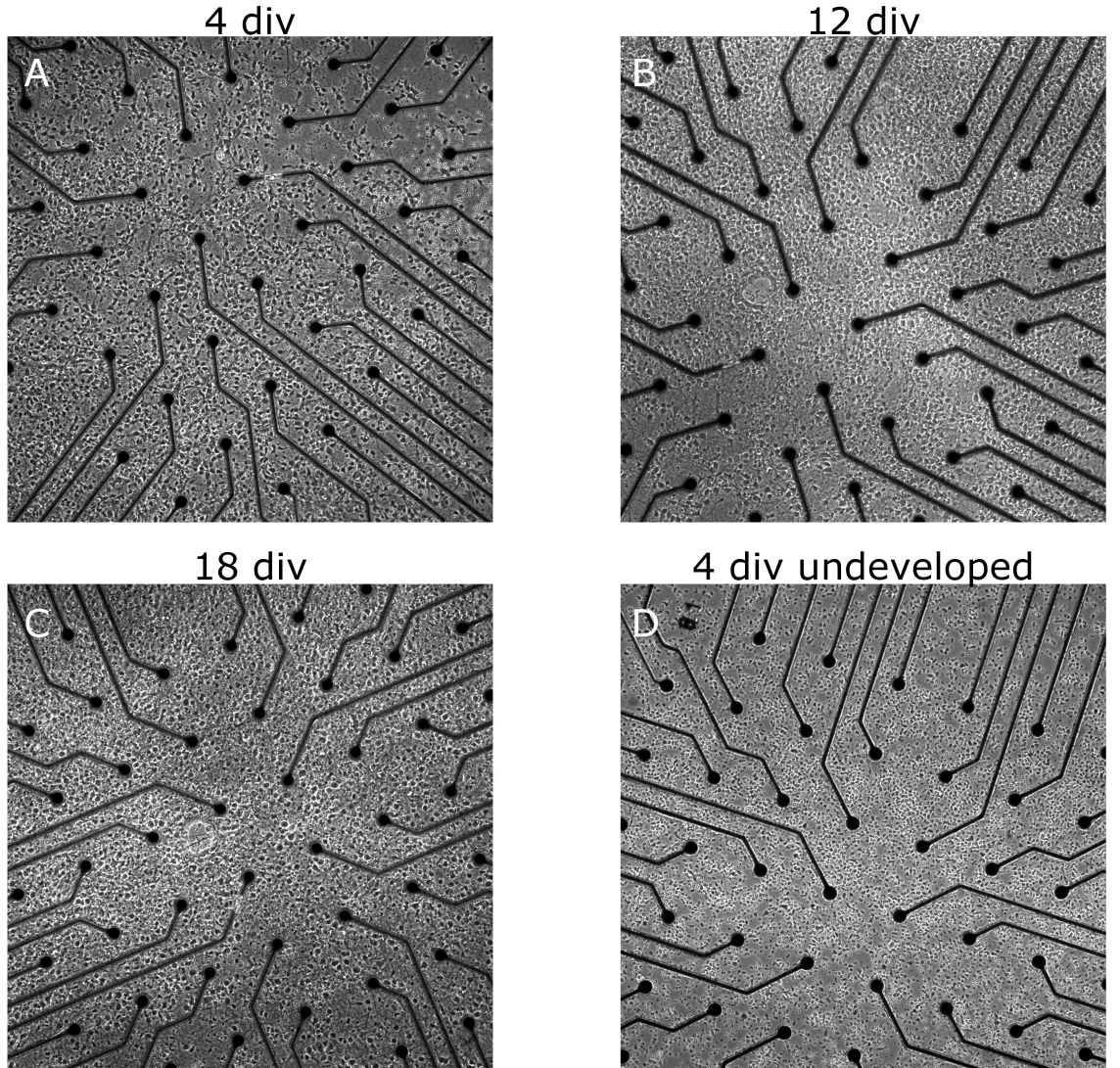


Figure 3.1: Cortical mouse cultures develop to become a densely interconnected neural tissue. (A-C) Cortical culture prepared from mice embryos and plated on micro-electrode arrays imaged on several time points over development. by 4 days *in vitro* most of the cells show an obvious polarized neuronal morphology and extend neurites. At 12 days *in vitro* a thick ECM tissue is evident between the cells (D) Example of a seeded culture that didn't show proper development. The electrodes are $30\mu m$ wide and spaced $200\mu m$ apart.

We monitored the activity of the mouse cultures for 3 weeks in *in vitro*. The analysis

performed throughout this thesis is restricted solely to spiking activity and lower frequencies associated with local field potentials were filtered out of the data. Spike detection was performed through a combination of match filtering and simple threshold crossing. A second pre-analysis step detected and removed erroneous spike waveforms induced by electromagnetic noise and which generated synchronized spiking events across several channels (see section 2.5 for full description of the pre-analysis). No spike sorting was attempted as this was shown to be ineffective in culture [5].

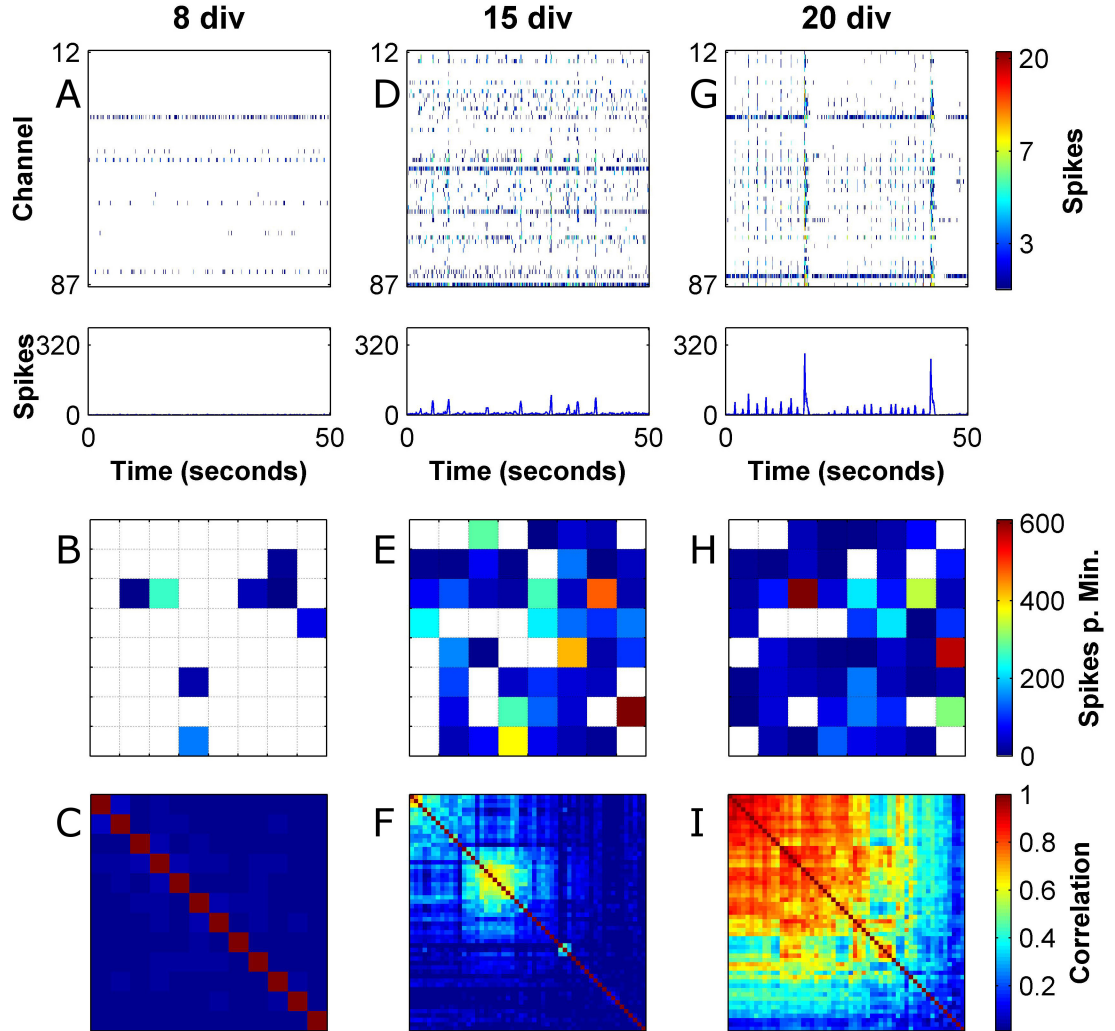


Figure 3.2: Spontaneous activity in mouse culture develops from tonic firing into synchronized bursting events. (A,D,G) Raster plot of spontaneous activity in mouse culture in 3 developmental time points exhibiting the change in the activity structure. Rasters plots are presented in 100ms bins. Bottom panels show summation of raster over all channels. (B,E,H) Activity maps showing the spatial organization of activity on the MEA in the same time points. (C,F,I) Dendrogram- sorted correlation matrices showing groupings of channels into correlated blocks.

Virtually no spikes were recorded until approximately 5 days *in vitro*, at which point tonic firing started to emerge in some of the channels. Beyond this point, the proportion of active channels and measured activity increased until reaching a plato at about 13 days *in vitro* (figure 3.3). The development of synchronization in the cultures is exemplified in Figure 3.2 which shows raster plots at several developmental stages along with the associated mean firing rate maps and dendrogram-ordered cross channel correlation matrices. At 8 days *in vitro* only a small proportion of the channels was tonically active and showed regular spiking (figure 3.2 A). At this point there was very little correlation across the channels suggesting that the measured spike trains aren't driven by synaptic integration but rather controlled through intrinsic neuronal excitability. At 15 days *in vitro* most of the MEA channels exhibited spiking activity (figure 3.2 D). At this point some correlated spiking events (network bursts) began to emerge although most of the the activity was still regular and uncorrelated. These network bursts were not easily discernible in the multi channel raster plot but were evident as large peaks in the summated network activity and as increased correlations between a subset of the channels. To appreciate the significance of the observed correlations, we generated surrogate independent spike rasters where the spikes trains were drawn from an independent Poisson processes with rate parameters as in the original channels (see section 2.5.3). For the data shown in figure 3.2, the maximal observed correlations between two different channels in the surrogate independent spike rasters were 0.05, 0.05 and 0.07 for 8, 15 and 20 days *in vitro*, respectively. These values are negligible compared to the observed values in the correlation matrices for 15 and 20 days *in vitro* and therefore indicate a genuine coupling between the measured neurons. Towards the end of the 3rd week (here 20 days *in vitro*) most of the activity in the cultures was restricted to the network bursts (figures 3.2 G and 3.4 E).

During the early phases of synchronicity (beginning of 3rd week, here 15 days *in vitro*) it was common to observe more than one synchronized cluster of channels in the dendrogram-sorted correlation matrices (figure 3.2 F). Nevertheless, correlations between these clusters continued to develop to the point where the entire culture became a single synchronized unit (end of 3rd week, figure 3.2 I). Previous work showed that applying synaptic blockers at non saturating quantities to fully developed neuronal cultures reveals an underlying modular connectivity pattern through breaking the weaker links between modules while still preserving denser intra-module connections [6]. Our results are compatible with this notion of underlying modularity and show that the modules are formed at the earlier stages of synaptic maturation.

3.2.1 Statistics of activity and synchronicity measures

Figure 3.3 shows activity related statistics over our experimental data set comprising 5 mouse cultures. Long term electrophysiological studies of this type have been facilitated by the introduction of the MEA technology which easily allows sampling of multiple cells

in parallel and repeatedly over long stretches of time. Patch clamp electrophysiology, in contrast, is usually restricted to a few cells at a time and cultures have to be discarded after a single experimental session as it is harder to maintain the cells healthy and sterile. Nevertheless, MEA developmental studies have been almost completely exclusive to cortical cultures made from rat embryos. Thus, with this study, apart from ascertaining that the cultures are healthy, we examine if there are any developmental differences between mouse and the rat based preparations.

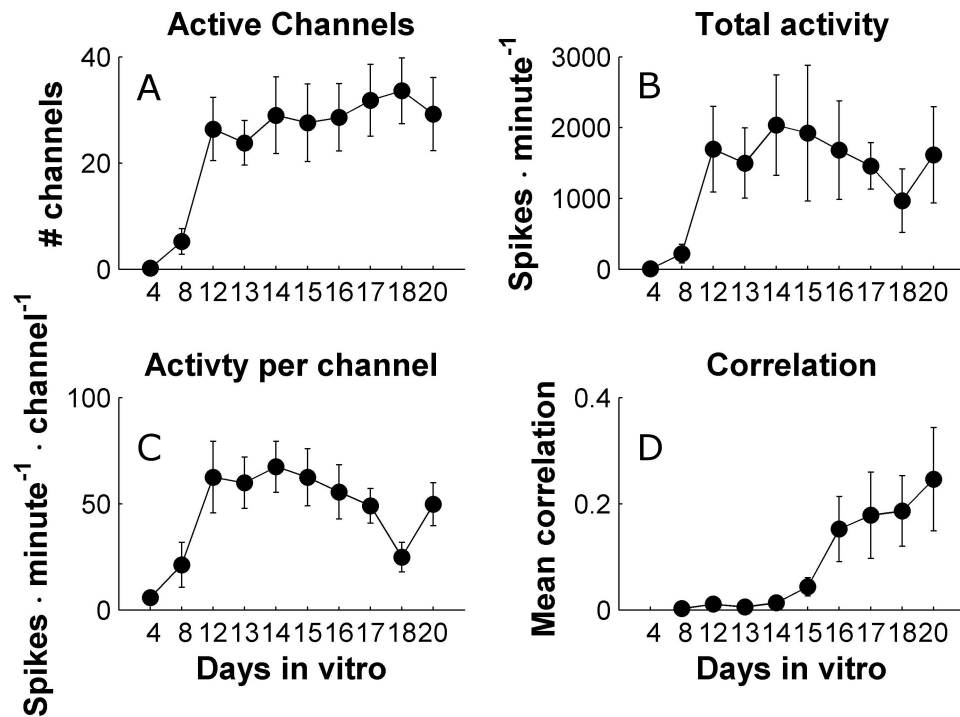


Figure 3.3: Development of synchronicity in mouse cultures lags after activity. (A) Development of the number of active channels as a function of culture age. (B) Development of the total number of spikes recorded on all MEA electrodes. (C) Development of the mean neuron firing rate (average of firing rate over active channels - implied assumption that each electrode records a single neuron). (D) Development of mean correlation. Mean correlation for a recording is the average of the correlation matrix taken without the diagonal. The data is shown as mean and SEM based on n=5 cultures.

The cultures do not become fully active until approximately 2 weeks in culture suggesting that this period of time is required for the seeded progenitor cells to become mature excitable neurons (figure 3.3 A-C). This time frame for activity onset is consistent with rat literature [7, 8, 9] and is generally accepted with regard to culture electrophysiology. After the initial increase, the firing rates (figure 3.3 C) stabilize at around 1Hz and don't exhibit a time dependent trend (1-way ANOVA, p=0.3). The average firing rate per channel is compatible with studies from rat cultures which reported values in the range of 0.4 – 1.5Hz [9, 7, 10, 11]

but the lack of trend is strikingly different as rat cultures are reported to show a marked increase in individual firing rates until 21 days and a decline afterwards [9, 12].

Figure 3.3 D shows the development of correlations in our cultures. The correlation value for a given recording is the mean of the correlation matrix (e.g., figure 3.2 C,F and I) without the diagonal. Evidently, despite the stabilization of the mean unit firing rates at day 13 *in vitro*, significant correlations started to arise only from about 17 days *in vitro*. This suggests that the excitability in the cultures is initially controlled by intrinsic homeostatic mechanisms which are later replaced by synaptic drive. Remarkably, the apparent increase in synaptic efficacy is not accompanied by an increase in spiking activity suggesting that the unit mean firing rate of 1Hz is a controlled quantity which the neurons maintain in the face of a changing network environment around them. Indeed, it has been shown that cultured neurons are capable of rapidly modifying their intrinsic excitability in response to pre-synaptic blockers [11].

To further characterize the spontaneous activity in the cultures we employed a burst detection algorithm as detailed in section 2.5.4 and extracted parameters of burst related measures, shown in figure 3.4. Not surprisingly, the development of bursting activity followed the same pattern as mean correlation and trailed the development of activity by a few days (figure 3.4 A,D compared to figure 3.3 A-C). This separation between measures of pure activity and of those of synchronicity underlines the utility of the MEA system in recognizing and disentangling biological processes that are linked. Previous rat cultures studies report that regular bursting is apparent already towards the end of the 2nd week *in vitro* [7, 8, 9, 12] whereas in our mouse data this was rare. In these reports the evolution of bursts appeared to go hand in hand with the evolution of activity, both of which peaked at 21 days *in vitro* and declined afterwards. As bursting behaviour in our data is a few days delayed and starts in the middle of the 3rd week *in vitro* it is plausible that a similar trend (but delayed) would be observed had we recorded further into the 4th week.

It should be noted that the peak burst rate value observed (15 minute^{-1}) was much higher than the one reported for rat cultures at the same age of development (5 minute^{-1}) [9]. However, we do not believe that this strong discrepancy lies in the difference between the preparations. Rather, our burst detection algorithm (section 2.5.4) uses an innovative approach for identifying synchronized events. Our method computes surrogate spike rasters with identical firing rates as the original data but without correlations to define the burst detection threshold. The thresholds defined in this way are likely to be tighter than for previous approaches where the thresholds were manually selected based on personal preference of how well they fit the data [8, 13]. Since our thresholds are based on an objective criteria we argue that the observed burst rate indeed reflects synchronized events and that the rate of these is actually greater than previously reported.

Further evidence for delayed synaptic maturation is provided by the burst width and burst size measures. Previous work have established that bursts in naive rat cultures exhibit

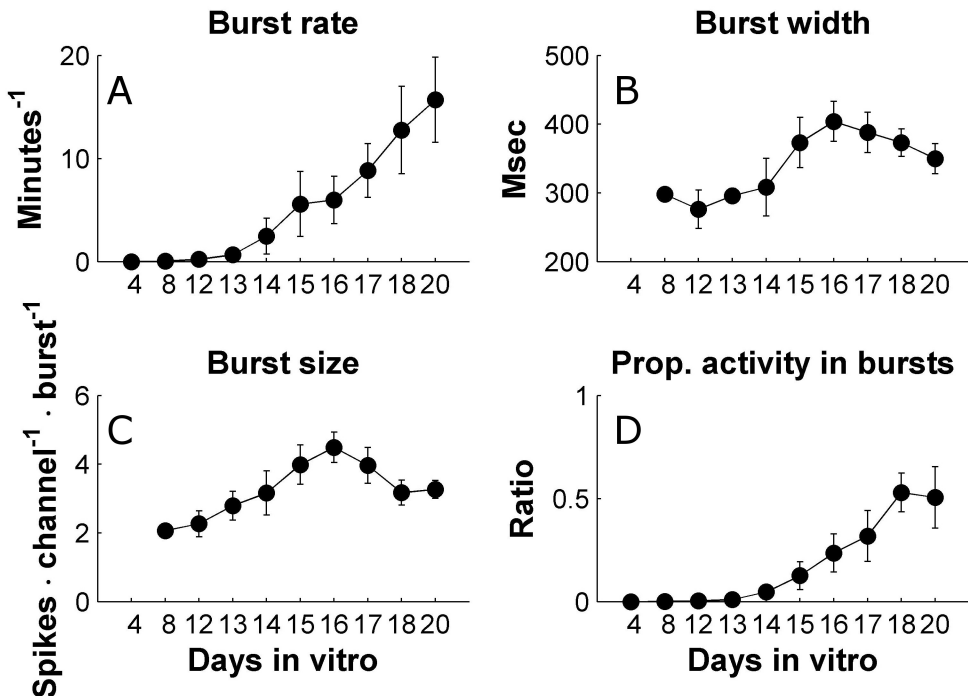


Figure 3.4: **Development of bursting measures in mouse cultures lags behind activity.** (A) Development of burst rate as a function of culture age. (B) Development of burst width. (C) Development of burst size. (D) Development if the ratio between the number of spikes observed with in bursting events and the total recorded spikes. Data is shown as mean and SEM based on n=5 cultures.

wide temporal profiles with long tails of spike discharges that could last up to several seconds [9, 14]. Over the 3rd-4th weeks the burst profiles become narrow and exhibit increasingly faster termination until saturating in the end of the 4th week. This change is attributed to the development of the GABAergic neurotransmission which was shown to occur 1-2 weeks in delay as compared to the glutamatergic system [15]. Hence it has been postulated that feedback loops operating through inhibitory interneurons become functional only in the aforementioned time period [7] (also see an *in vivo* correlate in [16]). In the rat data the bursts show maximal width when they first appear (10-14 days *in vitro*). In our data, a similar trend is observed with peaks appearing in the burst size and burst width measures at 17 days *in vitro*, which is approximately the point when bursting activity became appreciable (time effect was found significant through 1-way ANOVA for both burst size and burst width measures with p=0.035 and 0.028, respectively).

Taken together, the results from the spontaneous activity study demonstrate that, on one hand, the development of neurotransmission and synaptic connections in our mouse cultures appears to be delayed between 3 days to one week. On the other hand, irrespective of the delay, the cultures exhibit all the activity features expected from literature, such as,

homeostatic control of excitability, underlying modularity and development of synchronicity and bursting activity which evolve in accordance with the development of the synaptic networks. Nevertheless, as mentioned in the beginning of this section, the mouse cultures posed an added difficulty of a high culturing failure rate which, together with the delayed electrophysiological development raised concerns regarding their utility and ease of use. We therefore decided that, following the study performed in this chapter, rat based preparations would be used for the remainder of the Ph.D work. The next section will outline a brief pilot study to compare our rat based preparations with the mouse based ones and assert that the former shows an electrophysiological profile in par with the literature.

3.2.2 Comparison between mouse and rat cultures

In order to compare the functional development of mouse based and rat based cultures we recorded spontaneous activity from a set of rat cultures, prepared using a protocol identical to the mouse ones. It should be noted that although the reagents, dissociation techniques and growth conditions were indeed identical, there was still a difference originating from the differing tissue source. The rats were delivered from a private animal facility and operated on within our lab space, whereas the mice were bred in a university based animal facility where they were also operated. The cell suspension for the mice culture therefore had to be carried between buildings before plating which could account for any observed differences. Nevertheless, we believe this to be unlikely.

Figure 3.5 shows a comparison between rat based and mouse based cultures at the same age *in vitro* for several activity and synchronicity measures introduced earlier. A particularly pronounced difference was observed in the closely related measures of correlation and ratio of intra-burst to total activity both of which showed a significantly higher values in the rat cultures (1-sided unbalanced t-test, $p=0.017$ and 0.039 , respectively). These difference demonstrate that mouse cultures exhibited more uncorrelated activity as compared with their rat counterparts. This reiterates the observation discussed in the previous section that the mouse cultures show delayed synaptic development.

Another observed difference is that the mouse cultures showed a significantly higher average unit firing rate (one sided unbalanced t-test, $p=0.048$). This result could be another manifestation of the rat neurons being more attuned to the synaptic drive from the network but is harder to interpret. In any case, the mean values for both preparations types (1Hz and 0.5Hz for mouse and rat, respectively) are within the literature range ($0.4 - 1.5\text{Hz}$).

Both preparations showed a nearly identical burst rate of about 15 minute^{-1} . The burst rate measure is different to the correlation and activity ratio measures in that it counts synchronized events but is indifferent to activity outside such events. This in contrast to the correlation and intra-burst to total spikes ratio measures which are sensitive to activity both inside and outside the synchronized events. The fact that the reduced synaptic coupling in mouse cultures does not affect the burst rate suggests that the this measure is strongly

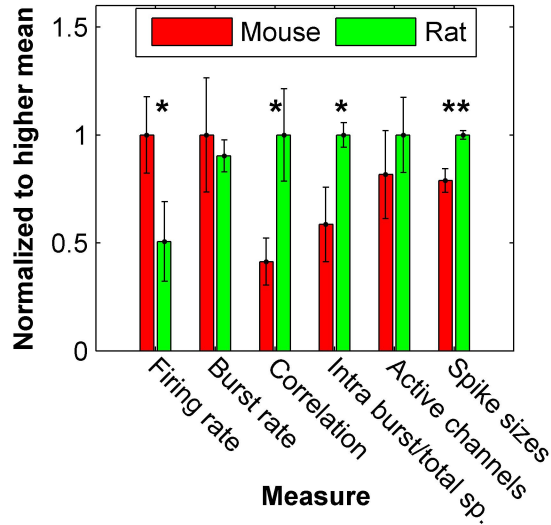


Figure 3.5: **Rat cultures show increased correlation as compared to rat cultures at the same age.** Six measures are considered and are normalized to whatever mean is higher amongst the two compared groups. *, ** indicate statistical significance of the difference between the groups at levels of confidence of 95% and 99%, respectively. Mouse statistics are based on $n=5$ cultures and rat statistics on $n=4$ cultures. Culture ages at the time of recording were selected so that both groups had the same mean age of 19.5 days *in vitro*.

related to the general excitability and not just to the synaptic development.

Finally, the spike sizes measure shows the mean of peak voltage in the recorded extracellular spike waveforms across all mouse and rat recordings (see section 2.5 for example waveforms). Surprisingly, we found a significant reduction in peak voltage for the recording from mouse preparations as compared to the rat preparations. This indicates that the two types of neurons are different in their excitability properties and that, in all likelihood, mouse neurons express a lower density of voltage dependent ion channels.

In summary, the comparison preformed confirmed that the mouse cultures are delayed in synaptic maturation as compared to rat cultures and thereby display reduced correlations at the same age *in vitro*. As far as these results can corroborate, our rat based preparations present all the features and developmental time course that have been described in literature and will therefore will be selected for the work carried out in the following chapters.

3.3 Evoked activity

An important feature of the MEA technology is the ability to induce generation of action potentials through injection of a current waveform into the extracellular electrodes. This is an important functionality as it provides means to provide input to the network and to control the culture activity. Past work have provided effective stimulation protocols and

showed that short current pulses can induce individual action potentials as well as a network response [17, 18]. This methodology was used to study response properties of single isolated neurons over long periods of time [19] and how several stimulation pulses interact with each other as a function of temporal proximity [20, 21, 22]. This approach was used to model sensory input by providing more complex spatio-temporal stimulation pattern and examining the extent to which the information present in the input signal can be decoded from the culture activity [23, 24]. Interestingly, it was shown that high frequency stimulation can break down the synchronized bursting structure of the culture activity, presumably in analogy to brain structures which exhibit higher frequency content when subjected to a high volume of input during active sensory processing [25].

To demonstrate that our system is able to effectively interface with the culture and provide input, we present data from a stimulation session where 120 test pulses were applied every 5 seconds (see section 2.5.2 for technical details). Data for two distinct stimulation sites is shown. Figure 3.6 A-B shows raster plots of the stimulation responses (at the different sites) averaged over all channels in a $500ms$ window after the stimulation pulse, as well as a cumulative PSTH. The PSTH is bimodal with a sharp peak observed within the first $25ms$ after stimulation and a second, significantly wider and less defined peak which lasts to typically lasts about $200ms$ after stimulation. The first peak is considered to represent direct responses, i.e., spikes elicited directly as a result of the stimulation pulse without synaptic mediation. The second peak is thought to be a manifestation of a multi-synaptic reverberating activity in response to the first step of activation. Indeed, it is evident from the response rasters that the first stage of response is significantly more repeatable than the second one which not always present. This is compatible with the above interpretation as direct responses are spikes generated due to a stimulation induced localized depolarization and depend only the specific biophysics and geometry of the neuron so they are expected to occur at a set delay and low jitter. The reverberating response, on the other hand, is a complex phenomena which depends on the network state preceding the stimulus so it stands to reason that it would show large variability or even fail to propagate on occasion. Nevertheless, it should be noted that even the direct responses were far from operating at a 100% success rate, a single neuron reproducibility issue that has been under much debate within neuroscience circles [26, 19].

Comparing between the responses to the two stimulation sites it is evident that they differed in direct responses with stimulations in channel 71 producing a second direct response peak which is also observable as a vertical line in the response rasters. The reverberating response did not show conspicuous differences in shape or latency although it seemed somewhat smaller. Another view on the differences between the two stimulation sites is given in figure 3.6 C-F which show spatially resolved response rasters and response maps for all participating channels, averaged over the stimulations. The spatial response profile appears to be very similar comparing the two stimulation electrodes - each channels showd s similar

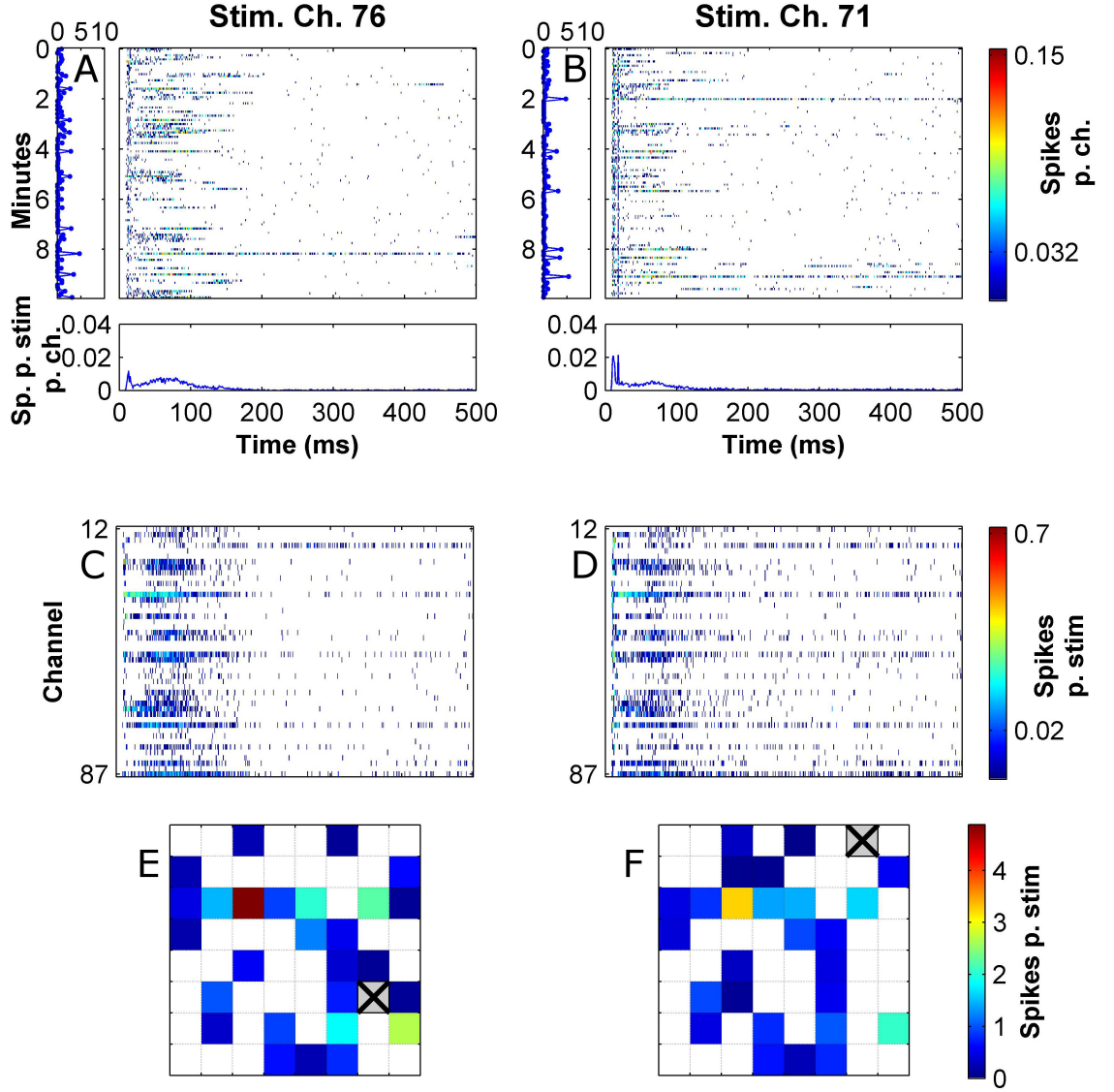


Figure 3.6: Stimulation pulses at different electrodes vary in direct responses but produce a similar reverberative responses. Test stimuli were applied every 5 seconds. (A-B) Main panel: Each line is a response raster for one test stimulus averaged over all channels. Left panel shows the sums of the responses shown in the main panel over the post stimulus observation time window (i.e., number of spikes per channel observed in 500 ms period post stimulation). Bottom panel shows the average of the response rasters over all stimuli. This is the PSTH. (C-D) Spatially resolved PSTHs, i.e., each line is a channel PSTH. (E-F) Stimulation response maps showing the sums of the PSTHs in (C-D) in the actual spatial locations. These response maps only show channels with a stimulation response that is significantly higher than background spontaneous activity for that channel (see section 2.5.2 for selection procedure). A,C,E and B,D,F show response data for two stimulation sessions applied to two different electrodes (indicated in E,F) run one after the other in concession on the same culture.

strength and duration of activation. There are some differences in latency but these were relatively unpronounced, at least to the naked eye. Although we did not study this in depth, it was our impression that different stimulation electrodes differ in mainly whether or not they are able to produce a reverberating response. However, once this response was elicited it seems to be stereotypical, i.e., each culture develops to take on a particular identity which is conjured whenever a synchronized burst occurs regardless of the site of induction or if it is spontaneous or evoked. It has been suggested that the lack of sensory input during culture development drives it into a degenerate state of over connectedness which might explain this rigidity. On the other hand, it should be noted that distinct yet overlapping responses to different stimulation sites have been reported [27]. Additionally, decoding of spatial stimulation information from culture data has been successfully demonstrated [28] so this system might nevertheless model genuine neural coding mechanisms from *in vivo*.

3.4 Plasticity induction in the presence of dopamine

Mature neuronal cultures abide to the principles of spike timing dependent plasticity (STDP), demonstrated in a paired pulse paradigm [2]. Modulation of the effective STDP window by dopamine has also been shown [3]. These results have raised the interesting possibility that neuronal cultures grown on multi electrode arrays could be used to study how plasticity operates at the network level. This sparked a substantial body of work to devise paradigms for induction and observation of plasticity using just the extra cellular network recordings and stimulations. Initial efforts have focused on brief tetanic stimulations inspired by the original experiments discovering LTP and which used this stimulation protocol [29]. Positive reports employing tetanus based induction have reported either a generalized potentiation in evoked responses which could be observed using simple measures such as summated response over all MEA electrodes [30, 31, 32] or more subtle effect that did not involve global change but rather antagonistic changes to the different channels and required more sophisticated multi-variate analyses to observe [33, 34, 35]. The later type of plasticity was observed both in evoked responses as well as in spontaneous activity. Indeed that tetanus induces a global potentiation is not surprising given that the original LTP experiments involved potentiation in the LFP measurements which represent large populations of neurons. However, it is known that neuronal systems employ homeostatic mechanisms to keep the general excitation levels constant [36] so such extreme modifications to activity are likely to be unphysiological. In that sense it is interesting that more subtle forms of plasticity are observed in the multi dimensional aspect of the activity. However, it is unclear why similar protocols produce such difference in outcome in different studies and different labs. Later work has shown that low frequency stimulation protocols can also induce changes in spontaneous activity of the subtle type [34, 37]. This result is interesting as natural input during real-life behavioural learning is probably more similar to such low frequency signals than to tetanus. Obviously, behaviour

in general and learning in particular are a closed loop process and this was modeled, to a certain extent, with feedback systems where the stimulation pattern was directly informed by the preceding neuronal activity [38, 39]. These important works showed that the direction and extent of plasticity can be controlled to follow bespoke criteria and therefore established that they are indeed relevant for goal directed learning.

As mentioned above, the quest to find plasticity in neuronal cultures grown in MEAs has produced successes but also contradictory, controversial and negative reports [27, 40]. Here we provide our own contribution to the discussion by applying one of the reported protocols to our mouse cultures and checking for plasticity. Additionally, as reviewed in section 1.2.1, neuromodulators have been shown to be strongly associated with neuronal plasticity and their presence or absence can strongly affect the direction of change (i.e., potentiation or depression) or even abolish it altogether. Moreover, neuromodulators have been shown to operate in both a tonic and phasic mode, where the phasic discharges are thought to act as a reward signal and whose timings are important for selecting neuronal activity that is relevant for the rewarded behaviour. Since neuromodulators have not been used in conjunction with plasticity and neuronal cultures on MEAs we decided to include a phase within our protocol where dopamine is introduced just for the induction phase and washed away afterwards. This to mimic a phasic mode of dopamine operation and to check if it enables the plasticity.

We elected to use a tetanus based protocol based on [30]. The reasons for selecting this protocol are as follows: Firstly, some of the past plasticity work on MEAs did not include a control to verify that the observed changes are due to the stimulated activity and not an artefact. Although this may seem unscientific it is a consequence of the nature of the system where each sample takes a long time to produce, maintain and measure. As a result, achieving a high n-number for both experiment and control is in some cases impractical. Our protocol works around this by exploiting the fact that neuronal cultures on MEAs can be used continuously for many recordings without compromise so we ran all experimental and control sessions on the same culture consecutively. Secondly, more complicated protocols such as the ones that apply stimulation in feedback from the recorded activity would require a sophisticated drug application system which is not currently available. This protocol includes a tetanus epoch of just a few minutes which offers a convenient time frame for manual addition and washing away of the drug.

Figure 3.7 shows a schematic of the experiment. The protocol catered for examination of both spontaneous activity and evoked responses. Each measurement epoch comprised a period of 10 minute recording spontaneous activity, followed by 4 x 10 minute periods of recording under 0.2 Hz test stimuli applied at 4 different electrodes, respectively. The electrode identities and amplitudes of test stimuli were selected to produce obvious evoked responses based on a pre-experiment examination. The measurement epochs were separated by 3 induction epoch running an 'associative tetanus' as proposed by [30]. 'Associative tetanus' is a stimulation paradigm designed to induce an association between two stimulated

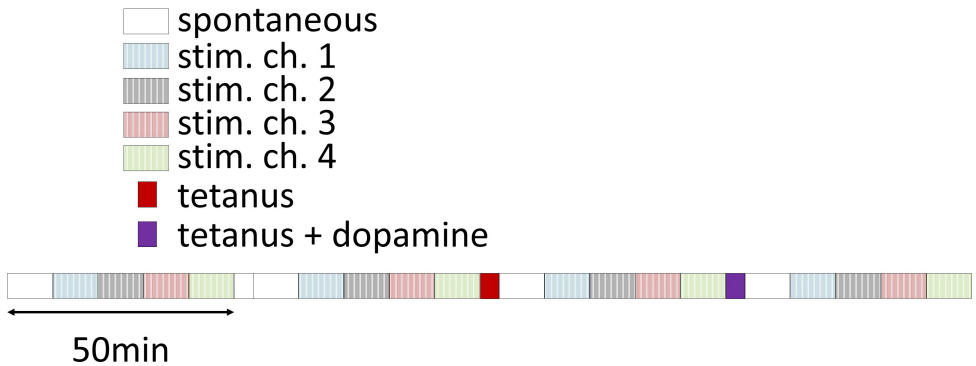


Figure 3.7: Outline of the combined dopamine and tetanus open bath plasticity experiments.

populations. The primary channel produces a tetanus pulse train consisting 50 pulse sets at 0.2Hz each consisting of 50 pulses at 20Hz . The secondary channel produces 50 single pulses at 0.2 Hz in phase with the tetanus pulse sets, i.e., each stimulation pulse in the secondary channel is timed to occur in the middle of a set in the primary channel. The primary and secondary channels were selected randomly out of the 4 stimulation channels used in the measurement epochs. The 3 induction epochs are as follows: (1) a sham (control) 'associative tetanus' executed by the signal generator with pulses of 0mV amplitude. (2) An actual 'associative tetanus' where the amplitudes for the primary and secondary channels are the same as those used in the test stimuli in the same channels during the measurement epochs. (3) An 'associative tetanus' as above where half of the culture media (0.5ml) was first removed for later use and $100\mu\text{M}$ dopamine•HCl was added. After the termination of the tetanus the dopamine containing media was replaced with the portion earlier removed and the final examination epoch was carried through. It should be noted that removal of half of the media during the 3rd induction epoch caused a slight but noticeable increase in the recording noise so the spike detection thresholds in the earlier measurement epochs were matched to the last one to avoid biasing of the results.

3.4.1 Examining changes in response to stimulation

Figure 3.8 shows example stimulation response data for the 4 measurement epochs in one of the tested cultures. Data is presented as explained in section 3.3. Baseline refers to the initial measurement epoch performed prior to any induction epoch. Control refers to the epoch taking place after the sham tetanus and the differences from the preceding epoch reflect spontaneous deviations in the culture activity. Tetanus and tetanus + dopamine are the epochs following the genuine induction phases. The differences between these experimental epochs and their immediate predecessors are compared to the difference between the control and baseline epochs so as to capture the effect of the induction. The baseline, control and tetanus epochs all show a similar PSTH profile and similar channel rasters. However, there

are also some noticeable differences. For example, the latency of the reverberating response seems to increase approximately half way through the control epoch, a change that is carried over to the tetanus epoch. Additionally, the reverberating phase of in the control PSTH is smaller than in the baseline and this is observed as reduced intensity in some of the channel rasters. These un-induced changes demonstrate the importance of employing such control epochs to assess how activity features change spontaneously.

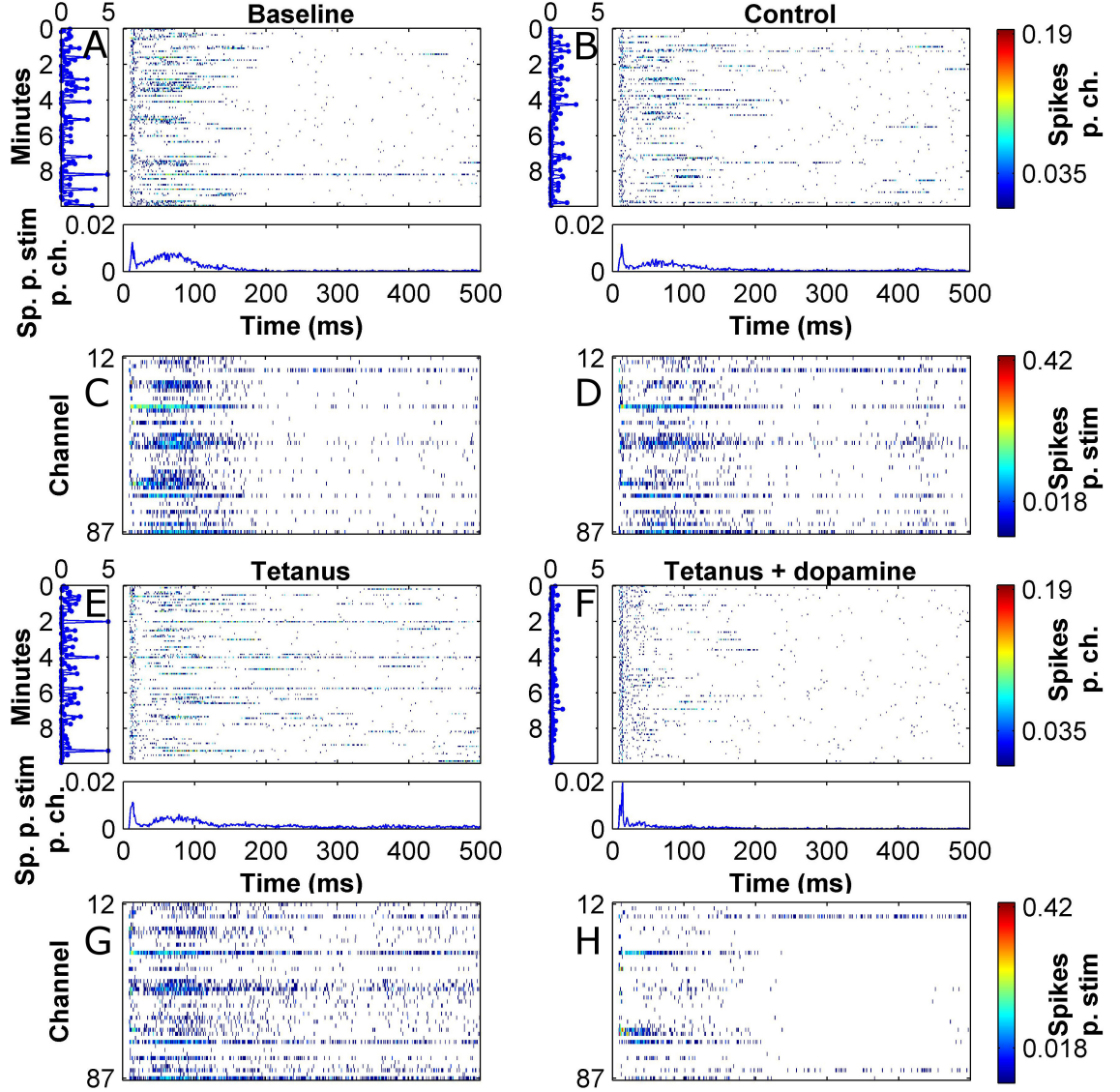


Figure 3.8: Tetanus combined with a dopamine pulse but not tetanus alone induces a depression of evoked responses. (A,B,E,F) Response rasters from the first stimulating electrode of each of the measurement epochs of the induction experiment. These are stimulation resolved (i.e., each line is a response to a single stimulation averaged over all the recording channels). (C,D,G,H) Channel-resolved response rasters of the same stimulation epochs. See caption of figure 3.6 for further details. Note an obvious decrease of evoked responses intensity following the tetanus induction in the presence of dopamine.

The tetanus + dopamine induction resulted in significantly more pronounced modifications to the evoked responses than the preceding inductions. The most obvious difference was the global reduction to the reverberating response in the PSTH. Most of the channels showed a marked decrease in intensity of responses although there were a few that actually increased. Another notable difference is that the direct response had become sharper. This global decrease in response is evident in the response maps in figure 3.9 where the number of responsive channels and their firing rate is markedly smaller after the tetanus + dopamine induction (recall that the response maps show only channels with significantly higher stimulation associated response in comparison with spontaneous activity).

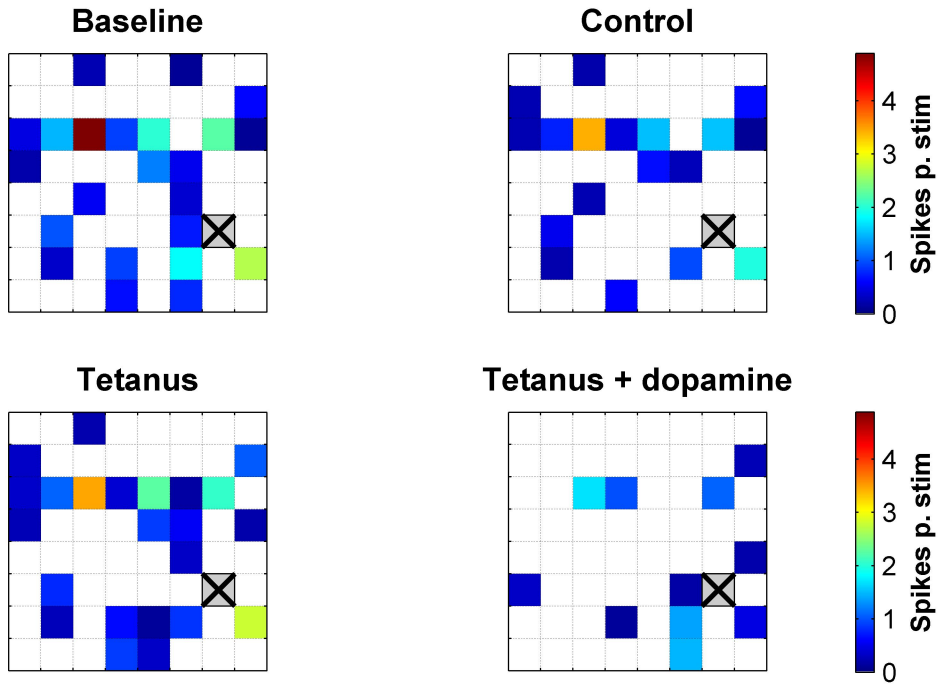


Figure 3.9: Tetanus combined with a dopamine pulse but not tetanus alone induces a reduction in the number of responsive channels. Stimulation response maps of the same data presented in figure 3.8.

Figure 3.10 shows a statistical analysis of the plasticity induction experiments which closely follows the one performed in [30]. In essence, channel responses for each stimulating electrode were compared in a scatter plot of pre induction vs. post induction responses and a linear fit was computed (figure 3.10 A-B). The slope for The 'associative tetanus' induction did not show a statistically significant difference from the one for the sham (control) induction (1.01 ± 0.07 vs. 1.07 ± 0.07 , 2-sided t-test, $p=0.5$). The slope for the induction performed under the presence of dopamine was significantly smaller, though (0.66 ± 0.09 , 2-sided t-test, $p=0.004$), indicating a general depression in evoked responses (i.e., across all channels). The potentiation index analysis provided results to the same effect. This analysis

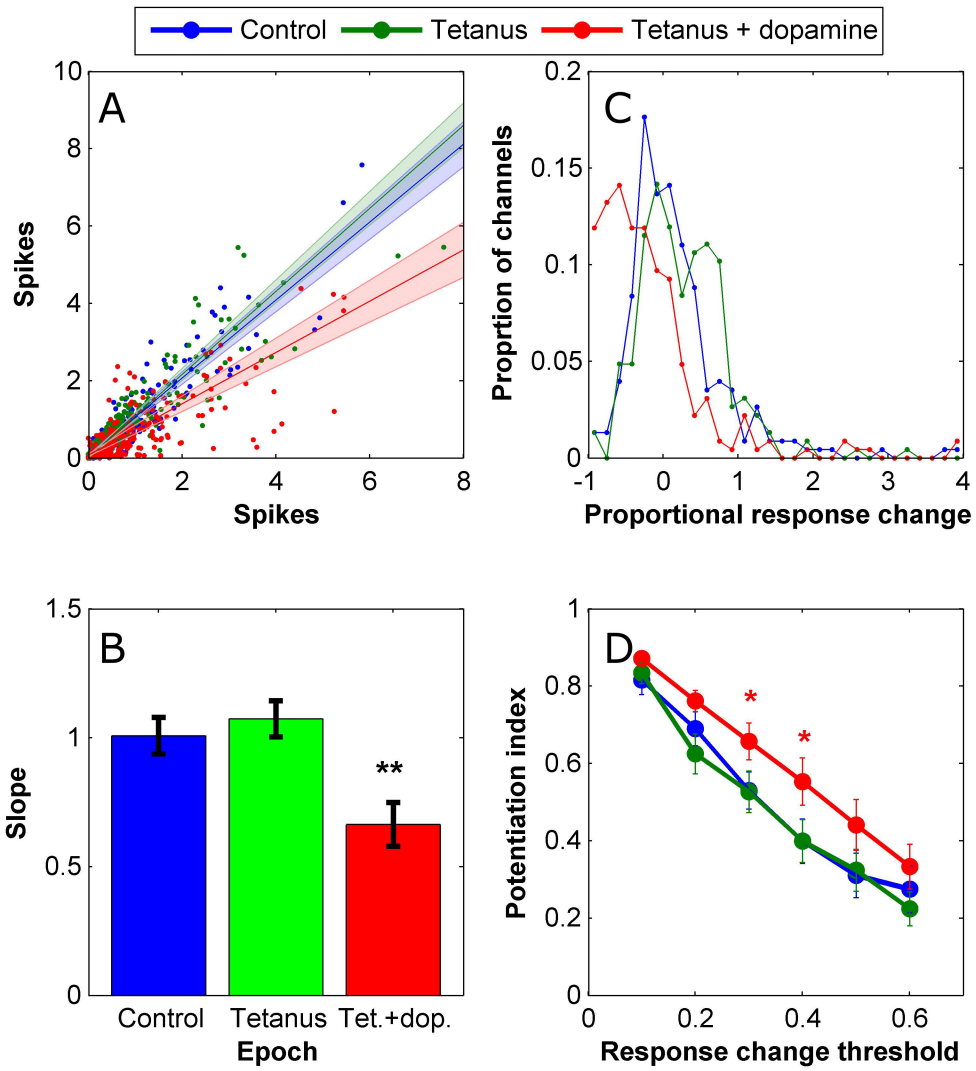


Figure 3.10: **Tetanus combined with a dopamine pulse but not tetanus alone induces a depression of evoked responses.** (A) Scatter plot of pre induction vs. post induction channel responses for the 3 induction steps of our protocol. Data from all tested cultures and from all stimulating electrode are lumped. The analysis, however, considers each of these groups to be an independent data set and fits a line to each. Plotted lines and shaded areas visualize the mean and SEM of these line slopes. Data is based on 4 cultures \times 4 stimulating electrodes = $(n=)$ 16. (B) Comparison of fitted slopes from A. (C) Distributions of proportional changes induced in channel responses for the 3 induction steps of our protocol lumped as in A. For computation of potentiation index (PI) such distributions are generated for each data set. For each of these distributions the PI is the proportion of channels exceeding a threshold level of change. Finally, PI is computed for a range of thresholds and averaged over independent data sets ($n=16$ as in A). (D) Mean + SEM of potentiation index as a function of tested levels of change thresholds.

is based on generating distributions of proportional changes to the channel responses before and after the induction (figure 3.10 C). Potentiation index is a measure for comparing these distributions and is defined as the proportion of channels with absolute change exceeding a predefined threshold. By selecting the threshold correctly, a distinction between the distributions based on their width can be generated even if their mean is the same. In other words, this measure is designed to detect more subtle changes to the network activity that may include some of the channels experiencing large but antagonistic changes which cancel out when looking at the mean. In more common terms, one could say this is a variance or a second order measure. Since the appropriate threshold for making the distinction between the distributions is unknown, potentiation index is computed for several thresholds over the entire range of the data. It should be mentioned that the name 'potentiation index' is somewhat of a misnomer as it refers not to potentiation in the sense of strengthening but to absolute change. At any rate, applying this analysis to our plasticity induction data did not reveal any significant differences between the tetanus and control inductions. The tetanus induction in the presence of dopamine, on the other hand, showed a significantly higher potentiation using change thresholds of 0.3 and 0.4 (figure 3.10 D, 1-sided t-test, $p=0.034$ and 0.039, respectively). This, however, is not surprising given that a general depression was observed in the preceding slopes analysis.

3.4.2 Examining changes in functional connectivity

Since the afore-mentioned analyses did not reveal any tetanus-only induced plasticity we decided to try a yet finer probing of the network activity. This is based on the functional connectivity analysis which was reported to capture plasticity in response to tetanus [34]. Mathematical details and examples for computation of functional connectivity are given in section 2.5.5. In essence, the measure is based on locating peaks in the cross correlation function between channel pairs normalized to the number of spikes in the first channel. The size of the peak reflects the probability of recording a spike in the second channel following a spike in the first one at a time captured by the latency of the peak. This computation therefor results in 2 vectors, one holding peak sizes (also termed FC strengths) and the other peak latencies. Finally, differences in functional connectivity between recording epochs is measured as the Euclidian distance between the appropriate vector from the compared epochs. In our analysis we looked only at distances in the FC strengths vector because situations where the functional connectivity is lost completely (i.e., connection strength becomes 0) do not require special treatment. It has been claimed that this measure is more efficacious at detecting plasticity when computed over spontaneous activity [34] so we indeed used the spontaneous activity periods of recording in our protocol for its computation.

Figure 3.11 shows the changes to the functional connectivity over the different experimental protocols (measured as Euclidian distance from the baseline epoch) as well as the mean channel firing rate. The results show that the tetanus induction itself did not generate

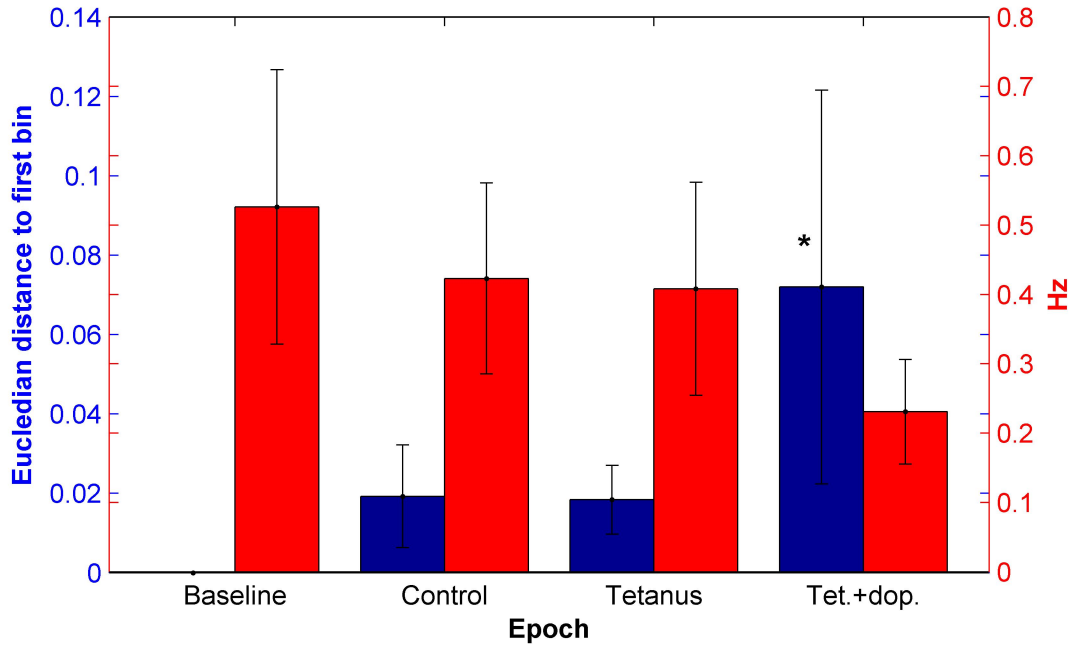


Figure 3.11: **Tetanus combined with a dopamine pulse but not tetanus alone induces a change to functional connectivity as well as a decrease to spontaneous activity.** Blue bars: Euclidean distance of the functional connectivity strength vector from baseline following each induction epoch. Functional connectivity was computed based on the spontaneous activity period in each of the measurement epochs. Functional connectivity computation requires a minimum number of spikes in each of the analyzed channel pairs to generate a meaningful cross correlation function estimation (see section 2.5.5) so only a subset of the possible recording channel pairs normally participate in the analysis. One of the cultures participating the the plasticity induction had to be removed as it had no channel pairs complying with the above criteria. Thus the shown data are based on n=3 cultures with 33, 10 and 179 computable functional connectivity pairs. Red bars: Mean channel firing rates in the same spontaneous activity measurement periods. This data are based on all n=4 participating cultures.

a change to the functional connectivity beyond naturally occurring fluctuations that were already observed after the control induction. A larger change was observed following the tetanus induction in the presence of dopamine which proved to be statistically significant (1-sided t-test, $p=0.026$). However, this change was also accompanied by a strong decrease in the mean channel firing rate which, for this data set, proved to be significant with only 90% confidence (1-sided t-test, $p=0.097$). In light of this change to the averaged culture activity, the observed shift in the functional connectivity measure should be taken with a grain of salt as it was designed to reflect subtle changes to the underlying culture structure in conditions where first order statistics (like mean firing rate) are stable.

3.5 Chapter conclusion

The main purpose of this chapter was to establish the standard neuronal culture on MEAs model system together with the accompanied Matlab analysis and show that the cultures are healthy and exhibit the diverse electrophysiological characteristics which have made them a successful neuroscience model system. Indeed distinct stages of development of network activity were clearly observed. These consisted of initial uncorrelated but widespread firing patterns corresponding to neuronal maturation followed by an increase in correlations and rate of synchronized events which indicate that the synapses are maturing. Further examination of the data revealed evidence for other neurobiological processes that have been described in culture. These included homeostasis of activity rates, existence of strongly intra-connected subnetworks and a gradual temporal narrowing of the synchronized events which has been attributed to a delayed maturation of the GABA neurotransmission system as compared to the glutamatergic one. These processes have not been studied here in depth but are taken as evidence that our cultures are healthy and in par with the literature gold standard.

Another important purpose for the work performed in this chapter is to examine the usability of mouse based cortical culture for MEA studies, as they have been seldom used in this context. We encountered difficulty in getting the mouse cultures to develop well on the MEAs and struggled with sub 50% success rates. In rat cultures, for a seeded culture to not develop well for several weeks was a rarity. Comparing electrophysiological parameters of the two preparations showed that the mouse cultures that did develop had a delayed synaptic maturation as compared to their rat counterparts, manifested in lower correlation values for same age *in vitro* and in synchronized events appearing later than expected from literature. Although the mouse cultures that did survive finally showed all the characteristics that could be expected from this type of preparation, their weakness in development and high failure rate led us to discontinue their use and switch to rat cultures for the following Ph.D chapters.

The final undertaking of this chapter was to explore a protocol for phasic application of dopamine using manual pipetting. We modified a common plasticity protocol to include a step where dopamine is ‘pulsed’ (through manual pipetting and subsequent washing) into the culture during the tetanus induction step. Without any dopamine, we were not able to induce a change in the culture activity, despite reports to the contrary in the paper from which the protocol was adapted. This should not come as a surprise as the literature is controversial in this regard and should just serve as a demonstration that further work is required for these system to serve as a useful model of plasticity. Following a tetanus induction which was performed in the presence of dopamine a significant depression was observed in the evoked responses which measured up to an hour following the induction. The spontaneous activity was also depressed but to a lesser extent. On one hand this could demonstrate and

enabling of LTD by the dopamine. The fact that this effect is present after the dopamine had been removed strengthens the possibility that this is a plasticity effect rather than a result of direct interaction of the cells with the agonist. Indeed a similar experiment had been performed in cortical slices and produced very similar results [41]. On the other hand, it is also known that in neuronal culture the mere action of media replacement drastically reduces activity (this will be made very clear by the results of chapter 5), an effect that could last several hours. Additionally, the presence of dopamine itself is known to have an inhibitory effect in the cortex regardless of plasticity [42, 43] and it is hard to rule out the option that a small concentration of the agonist is still present after the washing step and contributing to the observed effect. Under the constraints of the current bath application methods, it is impossible to run a dopamine pulse without these impinging effects. Indeed we could quantify them by using a set of control experiments but we cannot eliminate them.

To summarize, these dopamine pulsing results are promising in that they suggest a potential for dopamine to enable plastic behaviour in culture. However, this notion wasn't fully proven due to uncertainty about the effects of media replacement and of temporary interaction of dopamine with the neurons. This highlights the need for a precise solution exchange system whereby dopamine can be applied with high spatio-temporal precision and without change to other extracellular ingredients which could interfere with the activity. Such a system would allow interrogation into the fine temporal details of the phasic dopamine and volume transmission processes in general far beyond what was demonstrated in the above-described work. The following chapters in this Ph.D thesis will describe the development and establishment of a microfluidic based rapid solution exchange system where the drug delivery is rapid, precise and decoupled from other changes to the extracellular chemistry.

Chapter 4

Viability of neuronal cultures in microfluidic devices in static conditions and under steady flow

4.1 Introduction

As outlined in section 1.4 the purpose of this Ph.D work is to produce a model for phasic neuromodulator signalling by generating rapid agonist transients onto an entire neuronal culture. This is to be achieved using the interface shifting method in microfluidic devices. Applying this method involves using rapid flow rates at scales of $1 \frac{mm}{s}$ (the rational behind this figure is provided in section 4.2.1). Previous microfluidics work involving primary neurons used such rapid flow rates but just for short experiments lasting between minutes to 2 hours at most [44, 45, 46, 47]. Studies showing long term neuronal culture development under flow used much reduced flow rates where the convective forces were comparable to diffusion [48, 49, 50, 51]. Thus to avoid the complexity involved in getting neuronal cultures to survive long term under rapid flow we elected to follow an experimental paradigm whereby the cultures were initially grown in microfluidic devices in static conditions. After reaching maturity they were subjected to flow only for the duration of the experimental session. The first part of this chapter is dedicated to development of a protocol for long term culturing of primary rat neurons in microfluidic devices. As reviewed in section 1.3.2, this type of protocol is prevalent in the literature but the configuration of our devices, which were designed with the interface shifting method in mind, required specific adaptations.

An important part of the our experimental design is for the culture to be of restricted size (i.e., a microculture). This is necessary, firstly, because the interface shifting routine

involves having a small proportion of the microfluidic channel area chronically exposed to the agonist, even between transients (see section 1.3.1). Thus to avoid such chronic drug exposure, the culture needs to be located entirely outside the chronically exposed area. Secondly, it is important to note that an agonist pulse in interface shifting method actually takes the form of an agonist wave travelling along the long axis of the channel. This means that, depending on the flow rate and the geometry of the culture, cells at different locations along the channel may experience the drug at different times following the pulse command. In phasic neuromodulator signalling, the agonist molecules are secreted from nerve terminals that innervate the entire volume of the target tissue. Consequently, a neuromodulator pulse involves an approximately synchronized increase of agonist concentration over the entire innervated tissue followed by a decrease in concentration as the agonist molecules get locally re-uptaken [52]. It is important to note that, due to inhomogeneities in the spatial distribution of the innervating neuromodulatory fibers, different parts of the tissue still exhibit some delays in exposure to the agonist depending on their proximity to neuromodulatory synapse clusters. Nevertheless, these delays are small compared to the time scales of the global pulse [52, 53]. Because of the functional importance of timing in the neuromodulator signalling, it is essential that the microfluidic model does not exhibit increased delays in arrival of the agonist to different parts of the culture as compared to the *in vivo* tissue. To achieve the right timings, the flow speed and culture size need to be selected so that the drug traversal time across the culture matches the delays in the modeled tissue. The ability to control the culture size is crucial and the second part of this chapter will describe a method for generating microcultures which harbour small specific areas of the channel by utilizing microwells. The viability of these microcultures will be analyzed to establish their usability.

A final important topic that will be covered in this chapter is that of neuronal viability under rapid flow. Primary neurons are considered to be highly sensitive to shear stresses. Since this system is developed with long term plasticity in mind it is important to make sure that the culture is kept viable and functional for at least several hours under the applied shear stresses. It is also important to take into account that a functional neuronal tissue employs a large number of intrinsic volume transmission processes which comprise controlled secretion and uptake of active substances into the ECM (reviewed in section 1.2). These substances include neurotransmitters, hormones, neurotrophic and growth factors and are generally termed conditioning factors. Rapid flow is likely to interrupt with these processes by changing the concentrations of the conditioning factors or their spatial distributions. Since microfluidic flow has been scarcely used with primary neuronal cultures the flow rate limits have not been established and it is currently unclear what is the impact of each of the above-mentioned factors, shear stress and conditioning removal, on the culture viability. To characterize the effect of these factors we performed a viability assay under flow with a range of flow rates and media conditioning levels. In the tested range, we found a strong correlation between conditioning and viability but no shear effect. We established a protocol for media

conditioning which, when used for flow, maintains the culture above the 90% viability mark for over 5 hours. Chapter 5 will further address the question of functionality and will describe a characterization of the network activity under flow.

4.2 Long term neuronal cultures in microfluidic devices

4.2.1 Development of protocol

This section outlines the development of a protocol for long term culturing of primary hippocampal neurons in microfluidic devices. Long term culturing of cortical and hippocampal neurons has been established for over 30 years [54, 55, 56]. Recently, there has been an emerging use of microfluidic devices to culture neurons with increased control over the topology and to access specific neuronal compartments [57, 58, 59]. Nevertheless, neuronal cultures are infamous for their sensitivity to subtleties in the preparation technique and the materials that come in contact with the media or the cells and often require specific adaptations for the specific lab / application [60, 49]. These are discussed next.

Figure 4.1 shows the dimensions of the devices used in this study. The dimensions were selected so that, given the volumetric flow rates allowed by our flow system, a flow speed would be produced that is compatible with the desired agonist exposure times. Thus the main channel width was 1.5mm and the height was $65\mu\text{m}$ giving a cross section of $\approx 0.1\mu\text{m}^2$. Using a flow rate of 100nl/s gives an averaged flow speed of 1mm/s . Assuming that the long dimension of the culture would be less than a millimeter and that the culture would be positioned less than a millimeter from the agonist port then the agonist should reach the culture within a second and clear it a second later, which is the correct order of magnitude for neuromodulator phasic signalling [53]. Obviously this is just a back of the envelope calculation which does not take into account complexities in fluid dynamics and delays inherent to the flow switching system and its purpose is to provide a relevant geometry. A more rigorous examination of pulsing time scales will be performed in chapter 6 where the final microculture pulsing system is described.

The devices were bonded to glass cover slips using plasma bonding (see section 2.2 for details and more illustration of the assembled devices), oven sterilized, and then subjected to PLL surface treatment as detailed in section 2.3.

Due to the need to interface with a flow system, the microfluidic devices used in this work were made with biopsy punched ports of $\approx 0.8\text{mm}$ diameter which allow connection to the flow tubing by simple pressure fitting. This design contrasts with standard neuroscience oriented microfluidic devices where the ports are typically of 8mm diameter [57]. In these standard devices the seeding proceeds through pipetting of the cell solution into the ports and allowing the cells to flow through the channel (flow is enabled by controlling for a differential media height across the inlet and outlet ports). In the case of these standard devices, the

ports function as de facto reservoirs by holding a significant volume of media ($400\mu L$ each) and therefore protect the device for dehydration and serve as a source of nutrients. Due to the smaller port size in our devices, plating was performed by injecting the cells into the inlet port using a gel loading tip. The volume of injection was selected to be larger than the internal volume of the device so as to fully flood it with cells. The devices used here had an internal volume smaller than $1\mu L$ (figure 4.1) and the injection volume was $2\mu L$. After completion of the injection the cells were left suspended in the channel volume and were allowed to settle down in the incubator. The lack of flow following the cell injection made this protocol more consistent than the flow based seeding in standard devices. In those cases too strong of a flow ends up in having most of the cells flow through the device without settling and therefore in inconsistent seeding densities. On the other hand, a down side to our design is that due to their smaller diameter, the ports in our devices only hold about $2.5\mu L$ of media each and therefore cannot effectively fulfill the role of media reservoirs.

The following subsections will outline the major steps taken during the development of the protocol to circumvent the issues encountered along the way. The development of the protocol did not include an in depth scientific investigation to prove all the observed effects and interactions as doing so would have taken a long time and would have been counter productive with respect to the global project. The information is therefore not statistically complete and is presented in the form of examples which are meant to provide an intuitive and heuristic guide for scientists who would want to employ these techniques in the future.

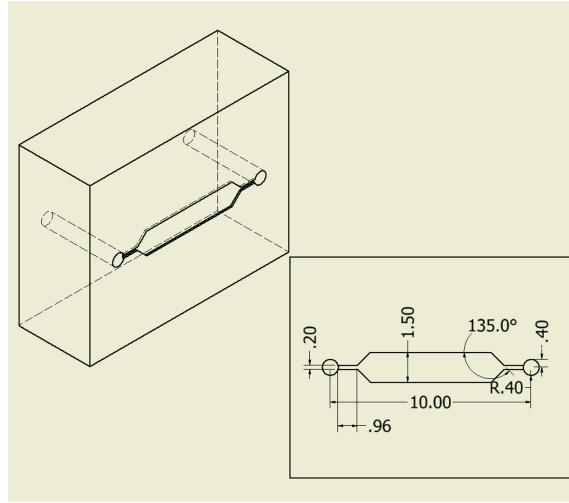


Figure 4.1: Schematics of the standard single layer microfluidic devices. All measurements listed in mm. Standard single layer microfluidic channels used in this section comprised both 2-port and 3-port (y-shaped) configuration. Only the 2-port configuration is presented here for simplicity.

4.2.1.1 Evaporation and surface chemistry considerations

The initial incubation configuration explored was to apply a $200\mu L$ drop of media to the top of the PDMS surface to act as a media reservoir from which nutrients are exchanged and to preserve the aquatic environment. To minimize evaporation, the devices were further kept in a closed petri dish next to a dish with $1mL$ DDW. The petri dish was kept in a humidified CO₂ incubator (Figure 4.2 A). The initial configuration also incorporated a 30 minute incubation with PLL solution as surface preparation. Cultures seeded in this configuration did not develop long term. The cells were initially healthy and adhered to the surface but the adhesion was non-uniform and by 5 days *in vitro* the cultures degenerated completely (figure 4.2 C-D). The main issue associated with this device configuration was that evaporation from the media on top of the devices was causing a rapid increase in the media osmolarity at a rate intolerable by the cells. We quantified this effect by measuring the osmolarity (Osmomat 030 by Gonotec) of the media on top 15 such devices after an overnight incubation. We found that the osmolarity drifted by $126 \pm 97mOsm$ overnight, implying an evaporation rate of $49 \pm 20\frac{\mu L}{day}$.

We tried to circumvent the evaporation issue by changing the drop on top of the devices every day (as opposed to twice weekly) and assessed the effectiveness by following the osmolarity of 4 devices for several days following the plating. Figure 4.2 B shows that the osmolarity in this case was stable but still very high (typical osmotic strength values for cell culture media is $\approx 300mOsm$ and the osmolarity of our Neurobasal growth media is $225mOsm$). A better solution was provided by switching to a maintenance routine where the devices were fully immersed in $2.5 - 3mL$ of culture media for the duration of the culture development (figure 4.3). Full details of this routine are provided in section 2.4. The volumes of media applied to each sample in this approach are comparable to what is used in standard cell culture samples so media could be changed just twice a week without incurring excessive osmotic drifts. After 3 weeks of culturing in this approach, media osmolarity never drifted more than $30mOsm$. Beyond this, the initial patchiness in adhesion led us to suspect that 30 minutes of PLL incubation, which is adequate for standard open surfaces, might be insufficient in the case of microfluidic devices where the extreme surface to volume ratio might cause an increased flux of PLL molecules into the PDMS and reduce the effective concentration available for the glass surface. Consequently, we also modified the protocol to an overnight PLL incubation. With this modified protocol we were able to sustain neuronal cultures for long term (figure 4.4) but still not ideally, as will be described in the next section.

4.2.1.2 Considerations of factor circulation

Figure 4.4 A-B shows microscope images of two sides of an example device 12 days after seeding during which it was maintained using the modified protocol as described above. The

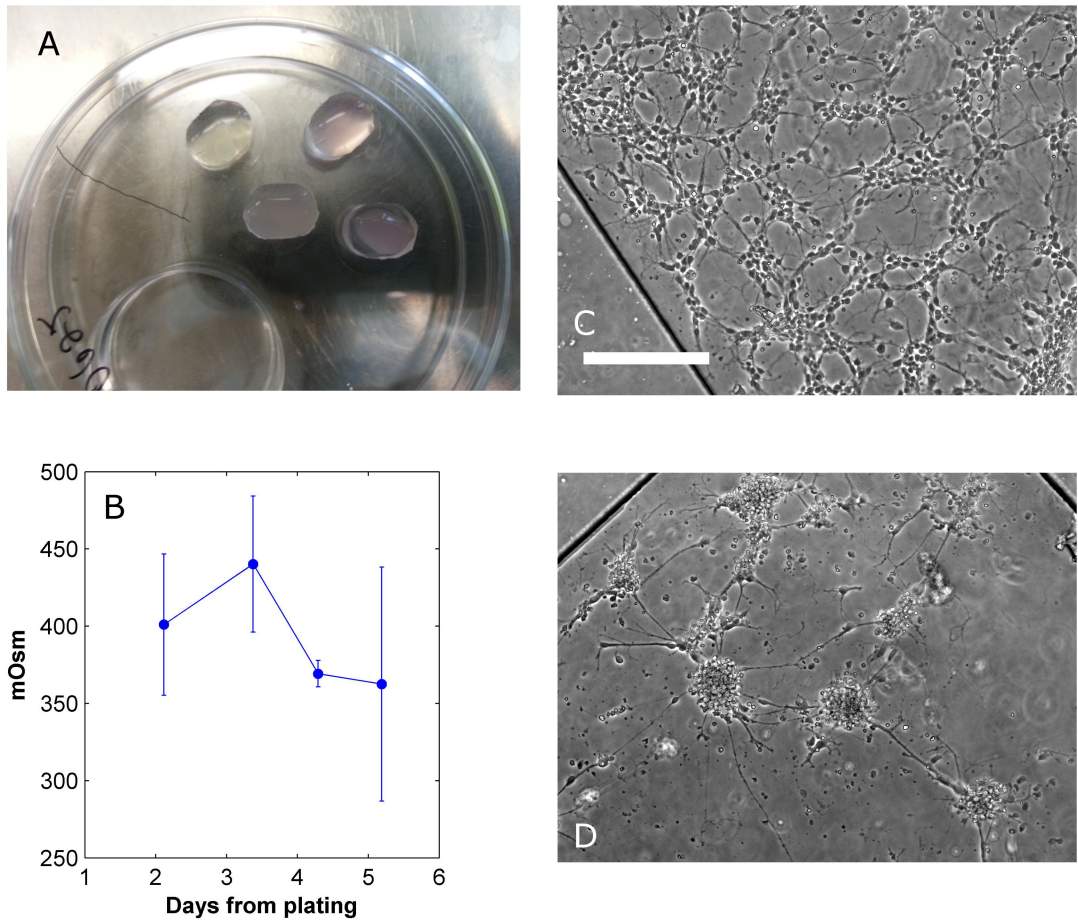


Figure 4.2: The ‘drop on top’ configuration results in excessive osmotic drifts and degeneration of the cultures. (A) Top view of a group of devices illustrating the ‘drop on top’ approach. (B) Osmolarity measurements taken from the drops on top of the devices in A during a maintenance protocol where the drop on top was changed every day. (C-D) Images of a culture growing in the ‘drop on top’ configuration and where the drop was changed only twice weekly. Images are at 2 and 5 days *in vitro*, respectively. Scale bar is $200\mu\text{m}$ long and is consistent for both images C and D.

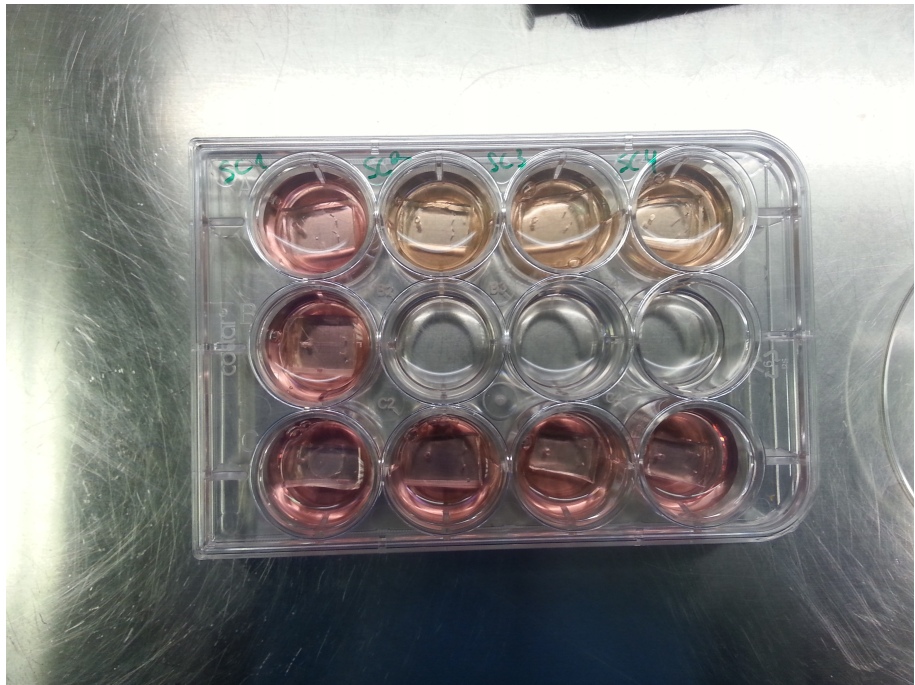


Figure 4.3: **The immersion configuration.** In this configuration, the devices were immersed in 12-wells with $2.5 - 3ml$ media each to prevent excessive osmotic drifts. This configuration required immersion 24 hours prior to seeding to release air trapped in the PDMS.

part of the culture residing in the vicinity of the seeding port did not develop properly and was mostly degenerate. Remarkably, the part of the very same culture residing on the side opposite to the seeding port was able to develop properly and maintain a healthy appearance for several weeks. A hint as to the mechanism operating behind the above phenomena comes from devices where one of the ports was punched to be twice as big (figure 4.4 C-D). In this case the cells were seeded from one of the ports opposite to the large port. In these large port devices the whole culture developed healthily without any significant spatial differences. Another clue was provided by our exploration of devices with a larger architecture where the height of the channel was $1mm$ and its internal volume $\approx 20\mu L$. The density of the plating solution for these devices was calculated so that the plated area density would be as in the small devices, $2600 \frac{cells}{mm^2}$. Nevertheless, culture grown in these larger devices never exhibited any sign of such spatially arranged degeneration and typically developed well for several weeks (results not shown). We argued that the most likely explanation for the above observations is that the configuration of small devices and small ports does not provide adequate circulation to remove metabolic by-products and provide fresh nutrients to all parts of the culture. The fact that the degeneration occurred in proximity to the seeding port could be explained either by the port being blocked by lumps of cells or by a existence of a gradient of cell density along the channel. In both cases there would be a large unmet circulatory demand around the seeding port. In the case of the large port or the large devices,

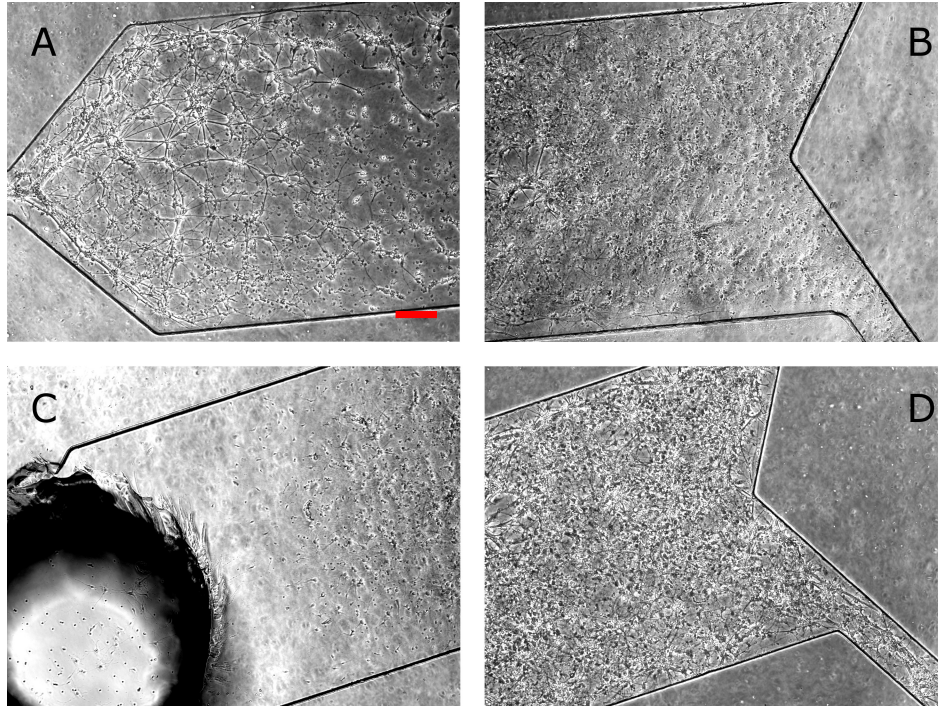


Figure 4.4: A circulation bottleneck can emerge in microfluidic devices. (A-B) Images of a culture growing in 3-port microfluidic devices where all the ports are 0.8mm in diameter. The images show the culture condition in the seeding port side and in the other side, respectively. (C-D) Images of a culture growing in 3-port microfluidic devices where one of the ports is twice as big (1.5mm). Images show culture condition in both sides of the device as before. Images were taken at 12 days *in vitro*. Seeding solution density was of $40 \times 10^6 \frac{\text{cells}}{\text{ml}}$ which is equivalent to $2600 \frac{\text{cells}}{\text{mm}^2}$ assuming homogenous distribution of the cells. Devices were maintained as described in section 2.4. Scale bar is $200\mu\text{m}$ long and is consistent across all images.

a stronger diffusive coupling between the culture and the external bulk media is enabled so in those cases circulation was not an issue. Since the configuration of small devices and small ports was required to properly interface with the flow tubing and to reach the required flow speeds we experimented with reduced plating densities in hope that these will have reduced circulatory demands. Indeed we found that by decreasing the plating density 6 fold (giving an area density of $\approx 450 \frac{\text{cells}}{\text{mm}^2}$) the spatially arranged degeneration phenomenon disappeared.

The observations described in this section demonstrate how microfluidic technology can impose conditions that are not normally met in standard preparations. The area density of $2600 \frac{\text{cells}}{\text{mm}^2}$ seeded in the earlier versions of the protocol is high but still commonly used for many applications involving neuronal culture. In those cases the culture is in immediate contact with a large volume of bulk media which readily supplies nutrients and removes by-products via diffusion. In our microfluidic devices, the internal volume of media is 3 orders of magnitude reduced ($\approx 1\mu\text{L}$) and it is only in this extreme configuration that circulation

becomes an issue. This situation is similar to cases where non-vascularized 3D cultures develop a necrotic core due to the lack of oxygen and nutrient penetration.

4.2.1.3 Alternative bonding methods

Plasma bonding is a lengthy process that needs to be applied to each sample separately and therefore is not well suited for producing large quantities of devices. Additionally, it is not practical for more complex devices involving several layers as having to apply plasma bonding methodology to each layer separately makes the production of every single device very tedious. Consequently, we experimented with alternative bonding approaches that have been recently suggested for assembly of microfluidic devices [61, 62]. Complete protocols and illustrations are provided in section 2.2.

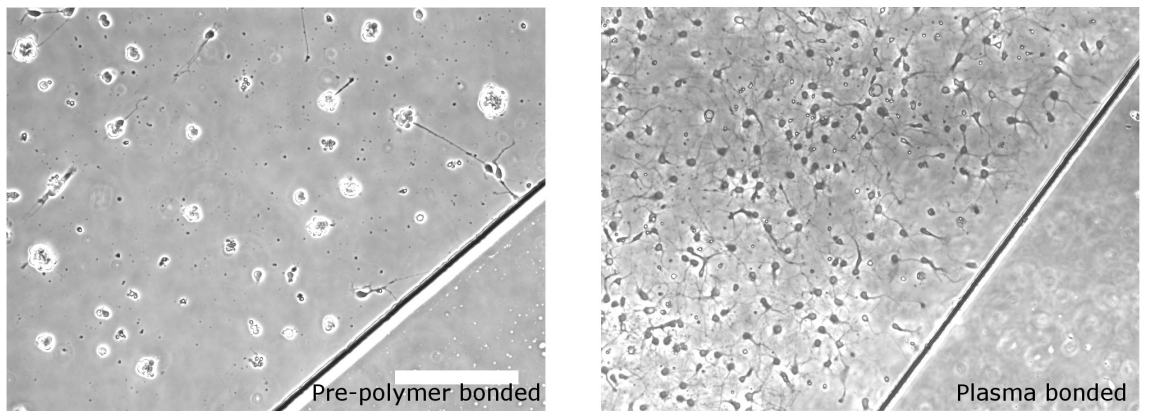


Figure 4.5: Contamination associated with pre-polymer bonding renders the surface unsuitable for neuronal adhesion. Images comparing a culture growing in pre-polymer bonded devices to one growing in plasma bonded devices. The images were taken at 5 days *in vitro*. Following bonding, the devices were subjected to identical surface preparation, seeding (density $7 \times 10^6 \frac{\text{cells}}{\text{ml}}$), and maintenance protocols (see sections 2.3 and 2.4). Scale bar is $200\mu\text{m}$ long and is consistent across both images.

The first approach attempted was to use the PDMS polymerization catalyst as an intermediate layer between the glass and PDMS bulk. The PDMS is dipped in catalyst solution, placed on top of the glass substrate and left to cure. This apparently induces further polymerization as well as partial covalent binding with the glass and results in a bond strength comparable or greater than plasma bonding [61]. We were able to achieve adequate bonding using this method but unfortunately the internal device surface proved to be completely inadequate for neuronal growth (figure 4.5. Interestingly, such a problem was not presented for other cell types such as astrocytes and HEK cells (data not shown)). This issue serves as another demonstration of the specific demands that are presented by neuronal culture. It is known that PDMS, when in contact with a surface, can contaminate the exposed areas around the point of contact through ‘leaching’ of PDMS oligomers or curing agent molecules. Indeed it has been shown that PDMS sometime acts as a source of contamination interfering

with neuronal growth inside microfluidic devices [49]. The lack of adhesion reported here for the pre-polymer bound devices is probably an extreme manifestation of exactly these contamination processes.

A different bonding alternative explored was that of using double sided silicone transfer tape [62]. In this case channel features are not engraved into the PDMS through soft-lithography but simply cut out of the tape which is consequently joined with the glass surface. A square PDMS bulk with punched ports is joined to the top side of the tape to complete the body of the device. Since this method does not disrupt the surface coating of the non taped parts of the glass and can be performed in a sterile hood it opens the door for a new surface treatment approach. With tape based assembly the device can be taped to a pre-treated glass (surface-then-bond) whereas previously, with plasma bonding, the surface coating chemicals had to be introduced and incubated in the assembled device (bond-then-surface). This shift in paradigm allows to utilize the device geometry to control which parts of the treated surface will be exposed and available for culture adhesion and therefore offers an easy way of controlling its shape and size. This concept will be critical for the establishment of the microculture geometry in chapter 6.

Figure 4.6 compares cultures grown in plasma bonded devices to ones grown in tape based and using the surface treatment paradigms appropriately as discussed above. The cultures are indistinguishable and appear to develop identically over the 12 days of inspection. This shows that the silicone tape is safe for use with neuronal culture and does not leach significant amount of toxins onto the surface or media. This tape based assembly approach will be cardinal for the multilayered devices described in chapters 5 and 6.

4.2.1.4 Extraction of PDMS

PDMS extraction is the last topic described with regards to the development of the basic protocol. As was apparent from the results of section 4.2.1.3, traces of curing agent or short oligomer chains can be harmful to neuronal cultures grown in the presence of PDMS. Indeed, even though the maintenance protocol achieved in section 4.2.1.2 did generally sustain neuronal cultures for at a couple of weeks *in vitro*, there were occasions where the cultures did not develop adequately. We reasoned that PDMS leaching might play a role in that inconsistency and therefore decided to try and employ a protocol for extraction of toxic species out of the cured devices. The protocol follows the suggestion from [49] and is detailed in section 2.1. Figure 4.7 compares cultures grown in standard devices to those grown in extracted devices from the same plating and using the same maintenance protocol. In this plating, the cultures in standard devices seemed to fasciculate early on and completely degenerated by 12 days *in vitro* ($n=5$). In the extracted devices ($n=10$) there was no sign of such degeneration. It should be noted that the extraction process involves immersing the devices in highly toxic solvents such as pentane and xylenes. When these are not properly oven-baked out of the devices a highly violent toxic effect is generated with the cells dying

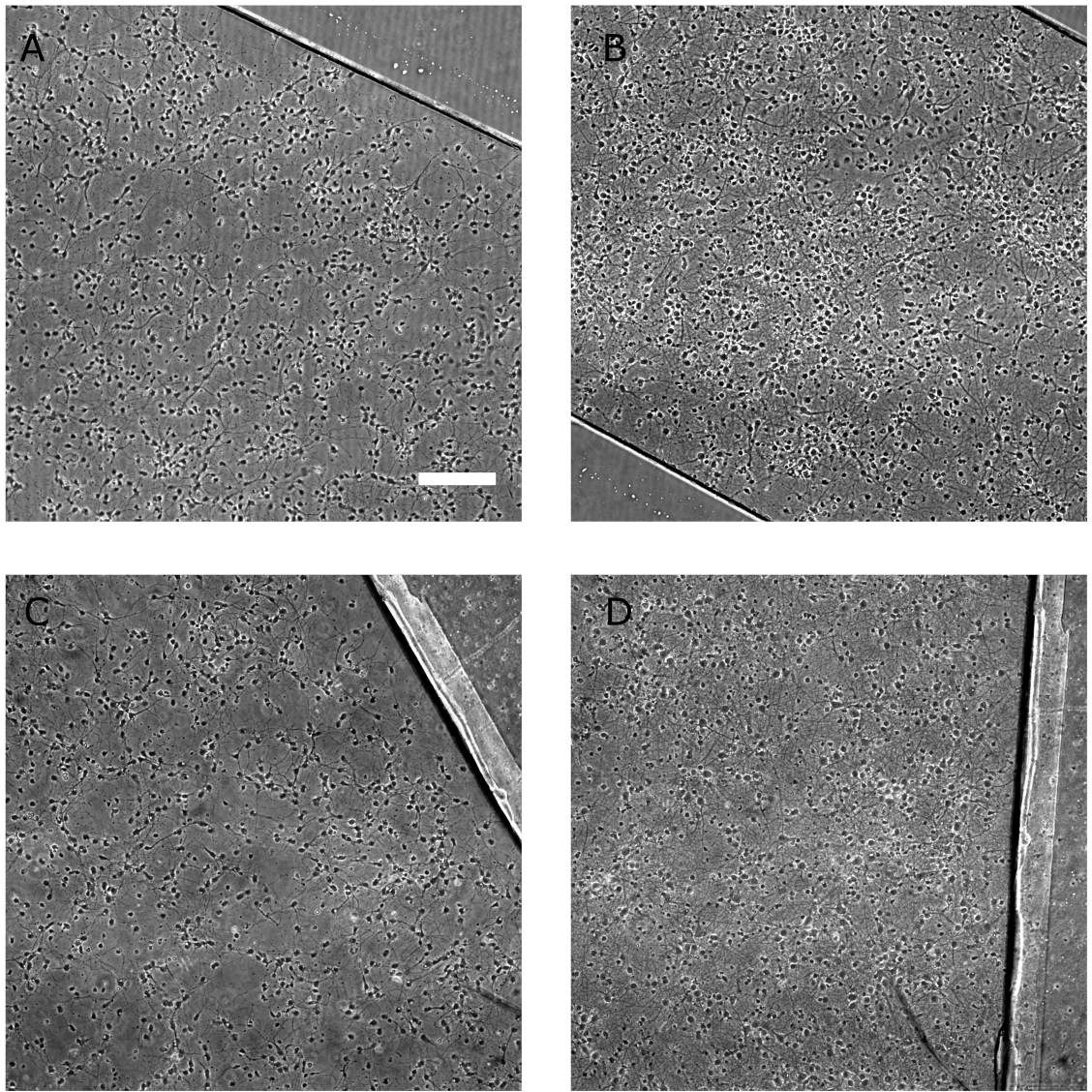


Figure 4.6: Tape based device architecture is fully compatible with neuronal culture. (A-B) Cultures growing in plasma bonded devices at ages 5 and 12 days *in vitro*, respectively. (C-D) Cultures growing in tape based devices at different stages of development as above. Plasma bonded devices were subjected to ‘bond-then-surface’ surface preparation approach whereas tape based devices were subjected to ‘surface-then-bond’ (see section 2.3). Both devices were seeded and maintained as described in section 2.4. Seeding density was $7 \times 10^6 \frac{\text{cells}}{\text{ml}}$. Scale bar is $200\mu\text{m}$ long and is consistent across all images.

immediately upon seeding (figure 4.7 C). Faulty development in non-extracted devices was not always observed and could be attributed to a specific PDMS mixing batch or to interactions with other factors. Nevertheless, to maximize the consistency of the preparations we added PDMS extraction to the standard protocol.

To summarize, we have developed a protocol for long term growth of neuronal culture in planar (1-layer) microfluidic devices. We reviewed what we consider to be the important

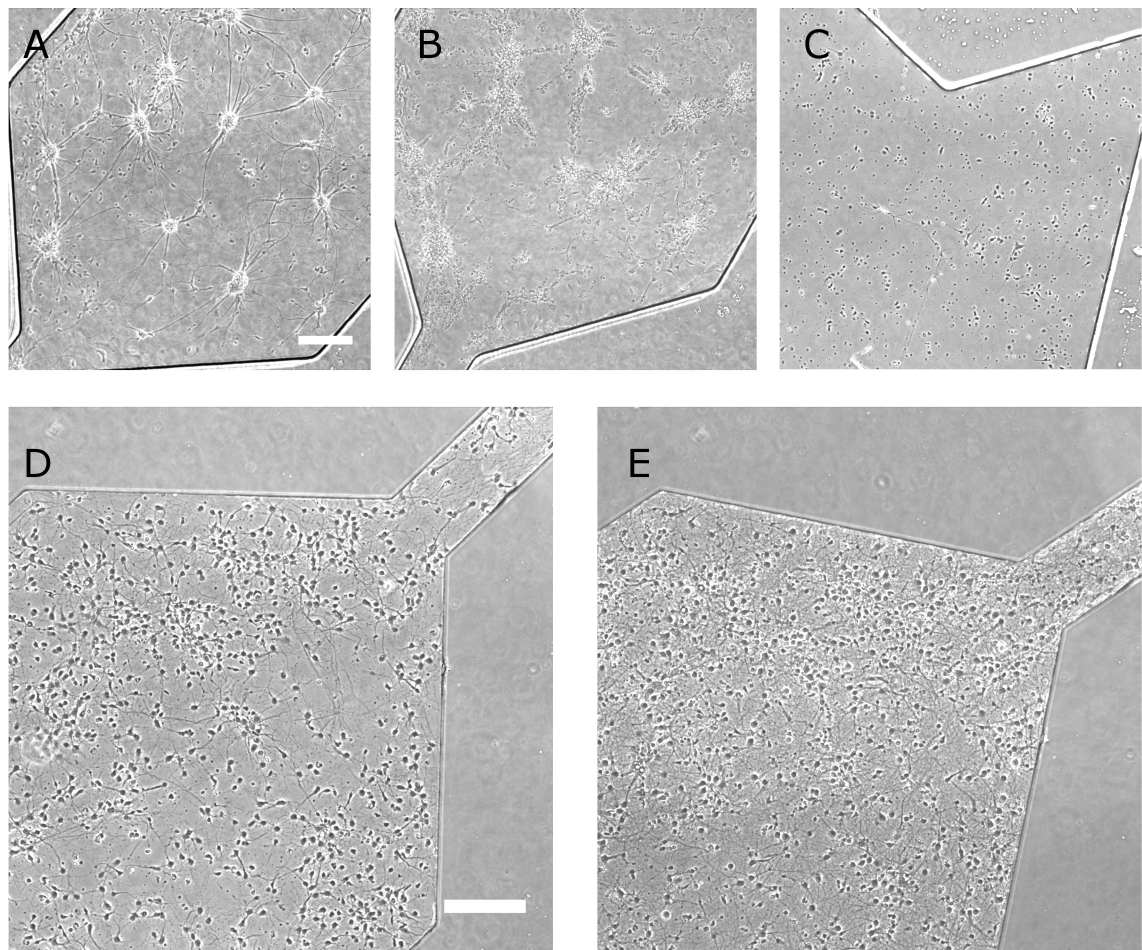


Figure 4.7: Non extracted PDMS devices can leach out chemicals that are harmful to neuronal growth. (A-B) Neuronal culture exhibiting adhesion and development issues that are thought to arise from PDMS leaching. Same culture is shown at ages 5 and 12 days *in vitro*, respectively. (C) Culture seeded in a device made from extracted PDMS which was not baked long enough for removal of noxious extraction chemicals. Image was taken at 2 days *in vitro*. (D-E) Cultures grown in extracted PDMS devices at 5 and 12 days *in vitro*, respectively. These images represent the typical cultures achieved for the final protocol incorporating all the principles discussed in this section. All devices were plasma bonded (section 2.1), subjected to ‘bond-then-surface’ surface preparation (section 2.3), seeded at a density of $7 \times 10^6 \frac{\text{cells}}{\text{ml}}$ and maintained according to section 2.4. Scale bar is $200\mu\text{m}$ long and is consistent across all images.

factors in the development of such protocols, namely, osmolarity, circulation of nutrients and oxygen, ease of assembly and leaching of chemicals from the construction materials (usually PDMS). Full details of the final protocol are provided in section 2.4. This protocol is the basis for all the subsequent device types used in this Ph.D thesis. All of them will use the same preparation and maintenance routines and will differ only in the seeding density and volume which require adaptation to the specific device and culture geometry.

4.2.2 Growing microcultures in plasma bonded devices

As explained in section 4.1, controlling the physical extent of the culture is necessary in order to apply the interface shifting method in a way that produces physiologically relevant concentration pulses. Here we describe confinement of the cultures into microwells of a desired size. To add microwells to our device geometry, we produced a PDMS sheet with rectangular holes via thin film spinning on a silicon/SU-8 mold comprising pillars in the shape of the required microwells (see section 2.1). To assemble the devices, the PDMS sheet was placed on a glass coverslip forming a reversible hydrophobic bond. The PDMS bulk with the engraved channel (as in figure 4.1) was then plasma bonded to the PDMS sheet while being manually aligned to position the microwell within the channel borders (figure 4.8). The devices were seeded at density of $20 \times 10^6 \frac{\text{cells}}{\text{ml}}$ and volume of $2\mu\text{L}$. The seeding filled the entire device volume with cells which settled arbitrarily on the exposed PDMS or inside the microwells. After the initial seeding the devices were inspected under the microscope to check if there is adequate inhabitation of the microwells and subjected to flushing and re-seeding as necessary. As shown in figure 2.1.2, an undesirable side effect of the way the PDMS sheet was manufactured is that the microwells are produced with an elevated ridge around them. The ridge caused a directing of the cells around the microwells rather than into them which was the main reason why flushing and re-seeding was necessary at times. After obtaining adequate microwell inhabitation, the devices were left in the incubator for 2-3 hours for initial adhesion of the cells, then media was pulled through with a 1ml syringe. This pulling had a differential effect on the cells depending on their location, i.e., most of the cells on the PDMS surface were ripped off and removed by the pulling whereas the cells in the wells tended to stay put as they were protected from the shear. In this way, isolated neuronal microcultures were generated and they were maintained as described in section 2.4.

Section 4.2.1.2 highlighted how, due to the small internal volume and narrow ports, our microfluidic devices can limit nutrient and oxygen circulation to the extent that necrosis is induced. In the case of the microcultures, however, the opposite extremity of factor circulation seemed to present itself. Initial attempts to grow microcultures under the the afore-mentioned maintenance protocol resulted in the cells showing an initially good adhesion but failing to show any subsequent development and degenerating altogether by 5 days *in vitro* (figure 4.9). This degeneration was similar in time scales to the one caused by the osmotic drift but seemed to be more aggressive as the cells did very little even in the direction of initial sprouting of neurites. This type of degeneration is known to occur in small / low density cultures even in standard preparations (i.e., open surfaces, not microfluidic devices) [60] where it is presumed that the neurons are not able to generate a sufficient concentration of conditioning factors around them to sustain their development. The typical solution in this situation is to grow the cultures in proximity to a large pure astrocyte culture which shares the same media and secretes the required conditioning factors. This auxiliary astrocyte culture is sometimes termed support culture. We followed this approach by adding two

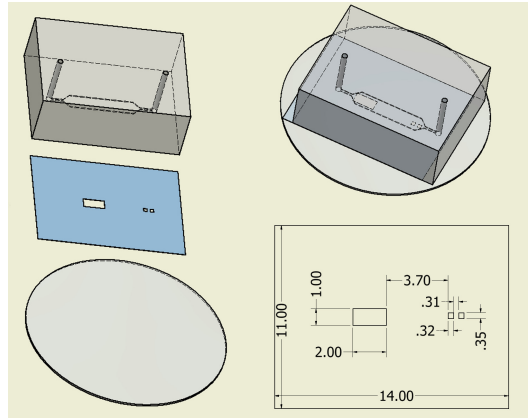


Figure 4.8: Schematics of the 2-layered microfluidic devices with microwells. The three components (PDMS bulk with an engraved microchannel, PDMS sheet and coverslip glass) of the device are shown separately and after bonding to illustrate how the the microwells are aligned to be within the channel boundaries. Dimensions of PDMS sheet are also presented in mm units. In this case, the microwells were of size $350 \times 320\mu\text{m}^2$. Dimensions of microchannel are as in figure 4.1.

levels of support culture. One was harboured in a large well situated within the device several millimeters away from the microcultures (see figure 4.8). A second one was a large culture plated outside the devices on the bare cover slip glass around the PDMS bulk. We found that the presence of these support cultures indeed prevented the afore-mentioned degeneration (figure 4.10) and that both of them together were required for best results (data note shown). We did not attempt growing pure astrocyte cultures for this as regular cortical cultures (which contain astrocytes) seemed sufficient to produce a beneficial effect.

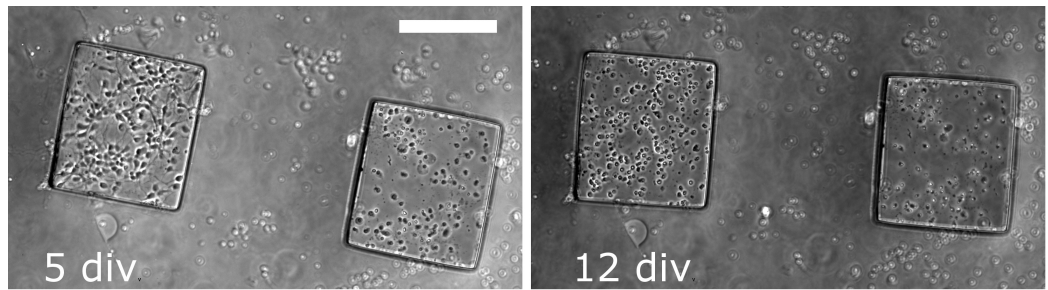


Figure 4.9: Neuronal microcultures do not develop without a support culture. Representative images of microcultures developing without seeding a support culture outside the device. The microwells were of size $300 \times 270\mu\text{m}^2$. Scale bar is $200\mu\text{m}$ long and is consistent across both images.

Since such microcultures are not a standard neuroscience model preparation in and it is unknown what is the smallest size they can be made while still developing properly, we decided to conduct a quantitative examination of their viability. To that end, we designed devices with 3 different microwell sizes and followed their development over 12 days *in*

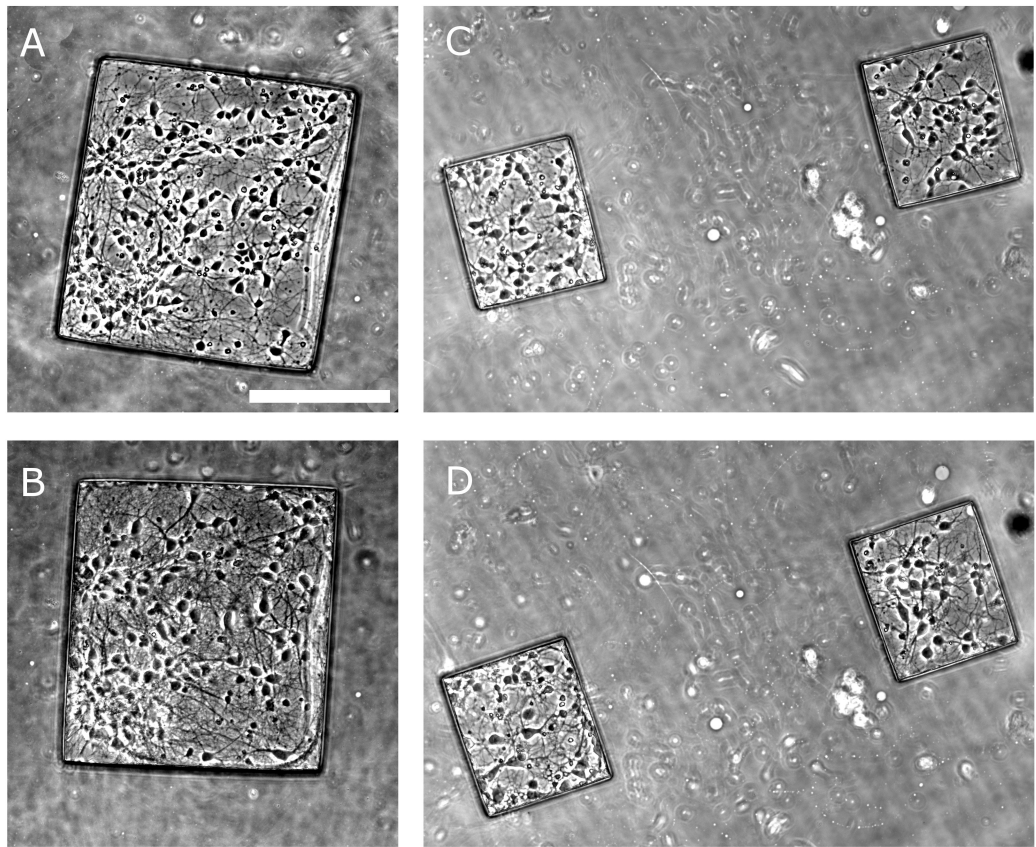


Figure 4.10: Development of neuronal microcultures. (A-B) Images of a neuronal microculture growing in a microwell of size $400 \times 370\mu m^2$ at 5 and 12 days *in vitro*. (C-D) Images of two neuronal microcultures at developmental stages as above in microwells of size $220 \times 190\mu m^2$. Microcultures were seeded at a density of $20 \times 10^6 \frac{cells}{ml}$, flushed and maintained as described in section 2.4. Scale bar is $200\mu m$ long and is consistent across all images.

in vitro. We counted the number of healthy cells in bright field images taken at 1, 5, 12 days *in vitro* and calculated the proportion of cells dying between consecutive counting time points. This data are presented in figure 4.11 as a function of the density of cells in the well at the preceding time point and grouped by well size. This is compared to the same statistic computed in the same way for images of the standard cultures from section 4.2.1 referred to here as macrocultures. It is evident from figure 4.11 A that, regardless of microwell size, the microculture death rates are strongly and negatively correlated with their density. This was corroborated with a linear regression analysis giving a statistically significant linear correlation (F-test, $p = 2 \times 10^{-4}$). The macrocultures did not show such a density associated death rate (F-test, $p = 0.26$) but the macroculture densities were much less variable so the analyzed density range was smaller. The averaged death rates of the macro- and microcultures are compared in figure 4.11 B. Microcultures of all 3 sizes exhibited a significantly higher death rate than the macrocultures (unbalanced t-test, $p =$

2×10^{-5} , 0.0012, 0.0027 for well edge sizes 200, 300, 400 μm , respectively).

Since microculture densities appeared to be a key factor in their long term viability we also performed a similar comparison with the microculture data restricted just to densities higher than $1500 \frac{\text{cells}}{\text{mm}^2}$. This density threshold was selected because the data beyond it did not show a density dependent trend which meant that the beneficial effects were saturated. Indeed the death rates at such high density microcultures were reduced and the large 400 μm ones exhibited death rates indistinguishable from those in macrocultures (unbalanced t-test, $p=0.23$). Smaller high density microcultures of sizes 200 and 300 μm still showed a significantly larger death rate (unbalanced t-test, $p=0.0012$ and 0.0012, respectively).

The above data are consistent with the notion that neuronal cultures need to generate an environment of conditioning factors around the cells to support their own development. Since this environment comprises secreted factors its buildup would strongly depend on the density and the size of the culture. Indeed the effect of both of these parameters is evident in the data shown here and a practical heuristic emerges that microcultures larger than $400 \times 400 \mu\text{m}^2$ and denser than $1500 \frac{\text{cell}}{\text{mm}^2}$ have a potential of developing as well as macrocultures.

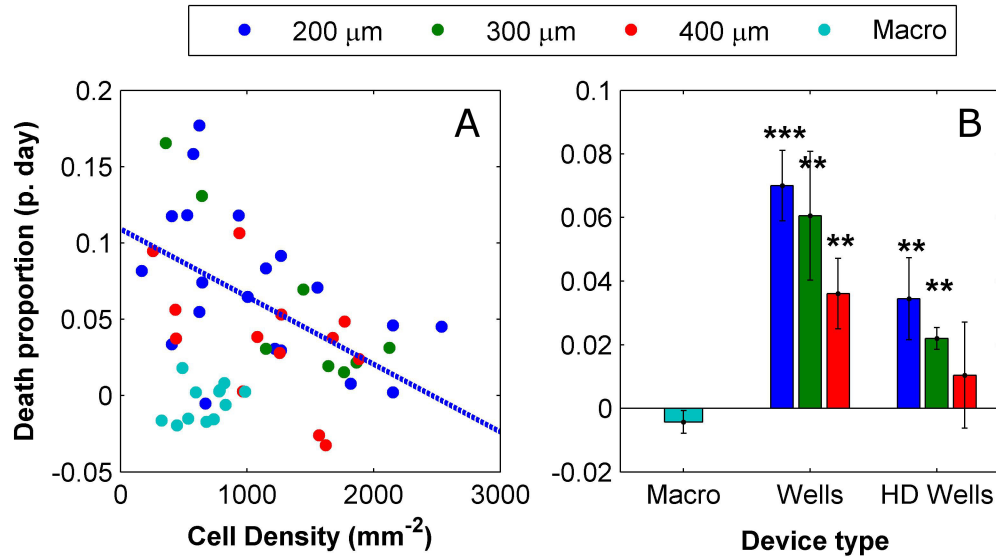


Figure 4.11: The viability of the microcultures is correlated with their density and size. (A) Scatter plot of the proportion of dead cells observed in the microcultures and macrocultures between consecutive counting time points as a function of microculture density. Each point represents a comparison between counts at 2 consecutive time points. Cells were counted at 1, 5 and 12 days *in vitro*. Death proportion is normalized to the number of days between the counts. Data is color coded according to microwell size or if it is a macroculture. (B) Comparison of mean proportional death rates between all the microcultures or microcultures with density higher than $1500 \frac{\text{cells}}{\text{mm}^2}$ and macrocultures. The data is based on 44 microcultures and 9 macrocultures from 4 different platings.

We would like to conclude this section by making a note about the quality of isolation of the microcultures. Since the devices considered here were assembled using plasma bonding, the surface treatment had to follow the ‘bind-then-surface’ approach. This means that the assembled devices were filled and incubated with surface coating solution (PLL) so all exposed internal surfaces were actually chemically prepared for cell adhesion. This means that cells from within the wells were free to send out neurites out onto the PDMS surface and even to migrate there. Additionally, the flushing procedure applied after the seeding was imperfect and sometimes left a substantial amount of cells on the PDMS sheet surface. This lack of restriction meant that after two weeks of growth the microcultures had significant innervation from neurons outside of the well (figure 4.12). Axons seemed to traverse the entire distance between the the microwells and the large support well which was located 3.7mm away. This lack of isolation defeats the purpose for which the microwells were designed. This issue is solved in chapter 6 where tape based design allows a ‘surface-then-bond’ approach whereby only the well bottom is chemically prepared for cell adhesion.

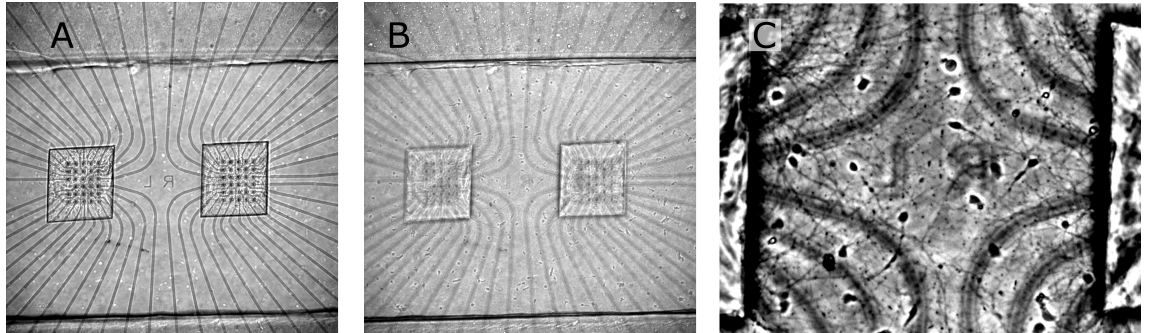


Figure 4.12: Microcultures are not well restricted to the microwell area with bond-then-surface approach. (A) Image of microcultures growing on top of commercial microelectrode arrays at 12 days *in vitro*. (B) Image of the same view field as in A focused on the top surface of the PDMS sheet. This image reveals the substantial inhabitation of the top surface by cells and neurites. (C) A zoom into the area between the microwells in B to highlight the presence of neurons and neurites outside the microwells. Microwells are of sizes $300 \times 270\mu\text{m}^2(L \times W)$ for scale reference.

4.3 Viability of neuronal cultures under steady microfluidic flow

4.3.1 Pilot flow study

The operation of the system in concern involves subjecting the neurons to flow rates in the order of millimeter per second. Thus, in this section as well as in chapter 5, we address the question of how well the cultures perform under flow. Primary neurons are considered to

be highly sensitive to shear stresses so we suspected that subjecting them to flow might be non-trivial and that there might be a limit to how high a flow rate they can bare. Since the interaction of primary neurons with flow is completely uncharted we conducted preliminary experiments where cultures at various ages were subjected to steady flow with growth media while being continuously monitored via time lapse imaging. The flow apparatus used for these experiments is described in section 2.8. These experiments seemed to develop in a stereotypical pattern: shortly after initiation of flow, the cells started losing the surface adhesion which was manifested by obvious fasciculation. In younger cultures where not too much ECM tissue had been built it could be observed that the fasciculation was accompanied by a retraction of processes (figure 4.13). By 20 hours, most of the cells appeared to degenerate. In older cultures rich in ECM this degeneration also involved complete detachment of the tissue, which was left floating inside the device volume.

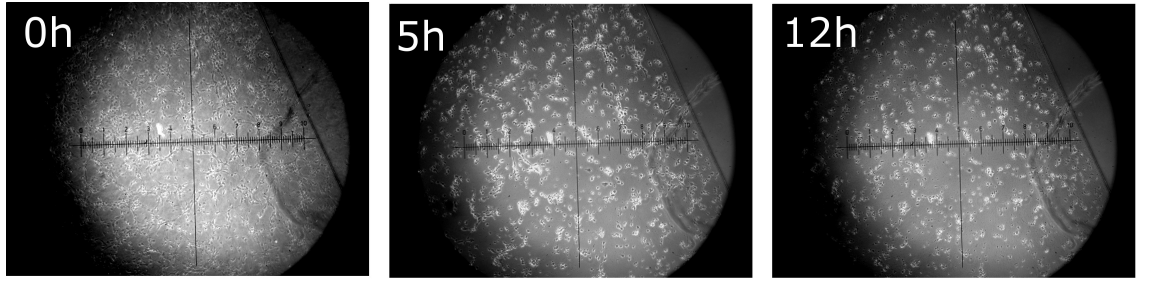


Figure 4.13: Neuronal cultures exposed to steady flow lose their surface adhesion, retract their processes and degenerate after several hours. Time lapse of a neuronal culture grown in the standard 1-layer microfluidic devices (section 4.2.1) placed under flow at 1 day *in vitro*. The flow rate was $1 \frac{nl}{s}$. Scale units: $\approx 100\mu m$

Initial experiments were conducted with the devices placed openly in the ambient environment while only plugged into a custom made heater system where heating resistors were brought into contact with the glass and the PDMS bulk and were controlled to $37^\circ C$ [63]. However, we had concerns as to how well this system controls the internal device temperature given that media at room temperature is pumped in. Additionally, maintenance of media CO₂ levels was based on connecting the pressure control system to a 5% CO₂ / 95% air gas supply. This configuration assured that the media in the flow reservoirs were fully CO₂ saturated but there was still a concern that as it travels through the tubes in the ambient air some CO₂ content could escape. To alleviate these issue, we built a custom made compact environmental chamber whose internal environment was controlled to $37^\circ C$ and 5% CO₂ (figure 2.8.1). The flow tubes were introduced into the environmental chamber through a small side hole before connecting to the devices. The tube configuration was purposefully selected such that the total tubing volume outside the environmental chamber was 3 times less than that of the internal tubing ($\approx 16\mu L$ vs. $\approx 60\mu L$). This meant that, while travelling from the reservoir to the device, the media spent triple the time inside the

chamber environment than in the ambient one so any CO₂ lost outside would necessarily have been reabsorbed. We also calculated that the residence time inside the chamber is at least 10 minutes which is more than enough to heat the media to 37°C given the micrometer scale of the tubing (this was verified with an inline flow thermocouple, PH-01, Multi Channel Systems). Nevertheless, the employment of the chamber did little to change the outcome of the flow experiments leading us to conclude that the basic physiological parameters of temperature and media CO₂ saturation did not play a major role in the degeneration.

Since conditioning factors are known to exert a protective effect on neuronal culture [60, 64] we explored the option of using conditioned media, i.e., media taken from a different culture for flow. We found that this had a pronounced effect on the cultures' tolerance in the sense that there was an initial flow period where the cultures' appearance did not seem to change. Additionally, even though fasciculation and degeneration still occurred, they developed much later, typically more than 10 hours into the flow session. Another interesting observation was that the rapid degeneration observed with fresh media flow seemed to occur regardless of the flow rate and presented itself even when the tubes were connected but the flow was set to 0 $\frac{nl}{s}$. These observations suggested that, when using conditioned media, a time window could be present where the culture is functional and useful experiments may be performed. They were also surprising in that the flow rate, i.e., shear, appeared to play a smaller than expected role in the adverse effects of flow. We therefore decided to conduct a systematic study to quantitatively asses the effect of conditioning and shear on the viability under flow and to establish what is the practical experimentation time window. Description of this study follows.

4.3.2 Quantitative viability analysis

Analyzing how media conditioning affects viability under flow requires an analytic measure of conditioning. Since conditioning involves a continuous secretion of factors into the bulk media, it seemed plausible that, a conditioning measure would be proportional to the length of time which the media was in contact with the cells. We produced conditioned by growing cortical rat cultures of prescribed densities in T-25 flasks with prescribed media volumes and without changing of the media. The precise protocol and the conditioning scale are provided in section 2.7. Roughly, every 3.5 days of incubation in the flasks *in vitro* are equivalent to 1 conditioning units.

We ran a large set of steady flow experiments on macrocultures growing in standard 1-layer devices. The experiments were conducted in a range of conditioning levels and flow rates. To provide a quantitative measure of viability these flow experiments also included a propidium iodide assay (protocol and example in section 2.8). In brief, propidium iodide was added to the flow medium so it was present around the cells for the length of the experiment. Intact plasma membranes of healthy cells are impermeable to fluorescent DNA-binding molecule. However, when cells die their nuclear material becomes exposed and

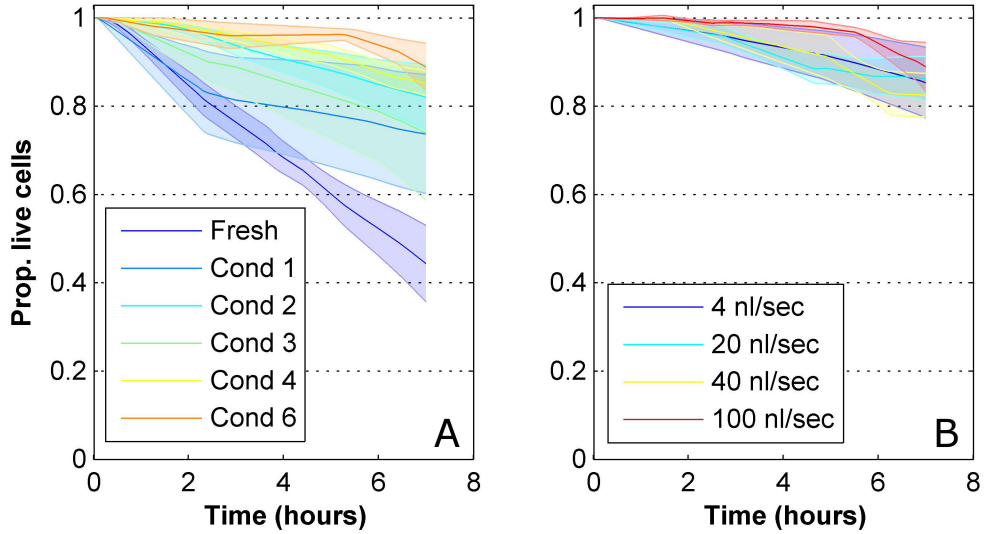


Figure 4.14: Using conditioned media for flow can significantly prolong the culture viability regardless of the flow rate. (A) Averaged viability curves for flow with media of increasing conditioning levels. Every curve averages data from several flow experiments where a propidium iodide assay was used to quantitatively assess the number of dead cells over time (full description is given in full in section 2.8). Example for such individual flow curves can be seen figure 4.15. The flow rate for all experiments was $40 \frac{nl}{s}$. Shaded areas depict the SEM. (B) Averaged viability curves as in A but where the flow rates are varied whereas the conditioning level is fixed at 4. The data is based on 36 experiments from 9 platings. Every curve except for Cond 6 in panel A is the average of at least 3 experiments from 2 different platings. Cond 6 is based on 2 experiments from one plating.

readily serve as a seed for propidium aggregation and therefore appears as a dot in fluorescent microscopy. These dots are counted to provide a quantitative measure of how many cells have died since the initiation of the flow. During a flow experiment fluorescent images were taken every 1-2 hours to generate a curve of the deterioration in viability. Figure 4.14 shows averaged viability curves for a range of conditioning levels where the flow rate is fixed and for a range of flow rates where the conditioning level is fixed. The observations made in the previous section are clearly manifested in these curves: increasing of the conditioning levels is negatively correlated with the death rates whereas increase in flow rates within the tested range is not.

To facilitate the statistical analysis we grouped the conditioning scale into 3 groups: Fresh media (same as before), intermediately conditioned (grouping conditioning levels 1 and 2) and highly conditioned (grouping levels 3-6). Figure 4.15 shows the averaged viability curves generated with new grouping as well as a control curve made without connecting the cultures to the flow system at all (static). The figure also shows a breakdown of the averaged curves into the constituent individual ones per experiment. Since the individual curves did not

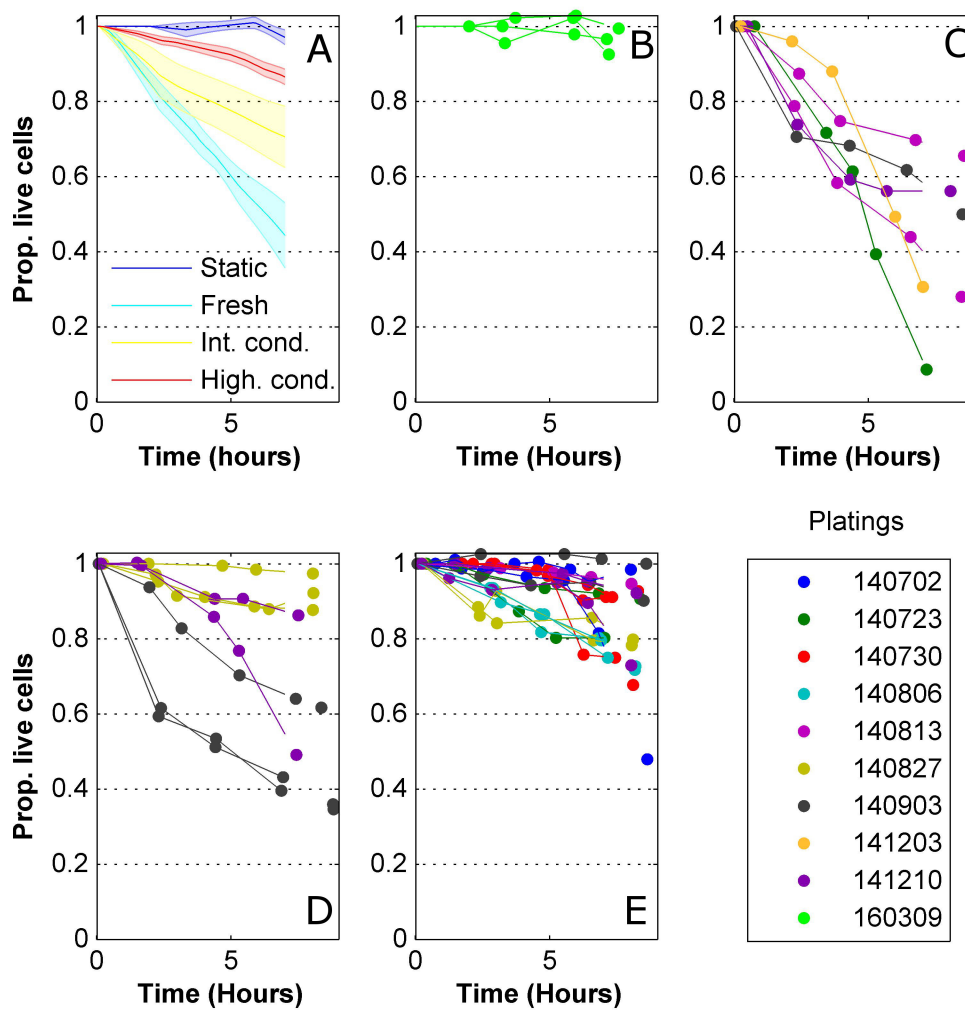


Figure 4.15: **Individual viability curves do not exhibit any common temporal features so their average is linear.** (A) Averaged viability curves for increasing conditioning levels as in figure 4.14 A but with a grouping applied to get improved separation (grouping specified in the text). The flow rate for all experiments was $40 \frac{nl}{s}$. An additional control curve is included where the devices were not connected to the flow system. (B-E) Individual viability curves from the experiments that were averaged in A. Each dot represents a fluorescent image where the number of dead cells were counted. The order of the panels B-E matches the order of the averaged curves as listed in the legend of panel A. Individual curves are color coded according to the date of plating of the given culture.

exhibit any conspicuous common time dependent features and as the averaged curves were strikingly linear we reasoned that a fixed death rate model (linear) would be a plausible a description of this data. In accordance with this notion, the statistical analysis was based on fitting a line to the viability time series of each experiment with a forced intercept at

(time=0, viability=1). The statistical testing was then performed on the fitted slopes and is discussed next.

Figure 4.16 shows a comparison of the fitted death rate slopes for various flow conditions. The conditioning levels of the flow media were shown to have a significant effect on the death rate (Figure 4.16 A, 1-way ANOVA, $p = 1.5 \times 10^{-5}$). However, flow under all conditioning levels still resulted in death rates significantly higher than control (unbalanced t-tests, $p = 2.1 \times 10^{-4}$, 0.049 and 0.021 for fresh media, intermediately conditioned and highly conditioned respectively). Thus we were not able to find a conditioning regime where the cultures were viable for long term under flow. To get an idea as to how much using conditioned media can extend the experimentation time, we calculated how long at least 90% of the cells will be alive, given the established death rates. This provided times of 1.3, 2.5 and 5.6 hours respectively for the 3 conditioning levels at hand. Given that highly conditioned media was used, changing the flow rate did not produce a significant difference (Figure 4.16 B, 1-way ANOVA, $p = 0.91$). The main experiments above were performed with PEEK tubing. We also tested if changing the tubing material would affect the viability under flow. We found that stainless steel tubing gave the same results as the PEEK for flow with highly conditioned media. PTFE tubing, however, was surprisingly associated with a significantly higher rate of degeneration (Figure 4.16 C, unbalanced t-tests, $p = 0.95$ and 7.5×10^{-11} for stainless steel and PTFE tubing, respectively). Thus, The beneficial effect of conditioning seems to be absent when using PTFE. This could suggest that our PTFE tubing absorbs valuable conditioning factors or that it introduces contaminants into the media during flow. We did not further interrogate this non-trivial effect but it is important to make a note of how the tubing selection can affect these types of experiments. Finally, since all the conditioned media in this study was used straight from the culture flask we wanted to check whether it could be stored for later use as that would greatly simplify the experimental design. Consequentially, we extracted highly conditioned media, kept it frozen at -80°C for several weeks and then heated it back up to 37°C prior to using it for flow. We found that the frozen media did not preserve the beneficial effects of the conditioning and resulted in significantly faster death rates as compared to the media used directly from the flasks (4.16 D, unbalanced t-test, $p = 0.0073$). Interestingly, the performance of the frozen media was statistically the same as that of the intermediately conditioned media (unbalanced t-test, $p = 0.59$) so the benefits of conditioning were still partially present. It is likely that some of the conditioning factors degrade over time and are sensitive to freezing and thawing (e.g., large protein molecules) hence the above results.

4.4 Chapter conclusion

In this chapter, we demonstrated a capacity for growing rat macrocultures (standard size) and microcultures in microfluidic devices. The observations made in sections 4.2.1.2 and

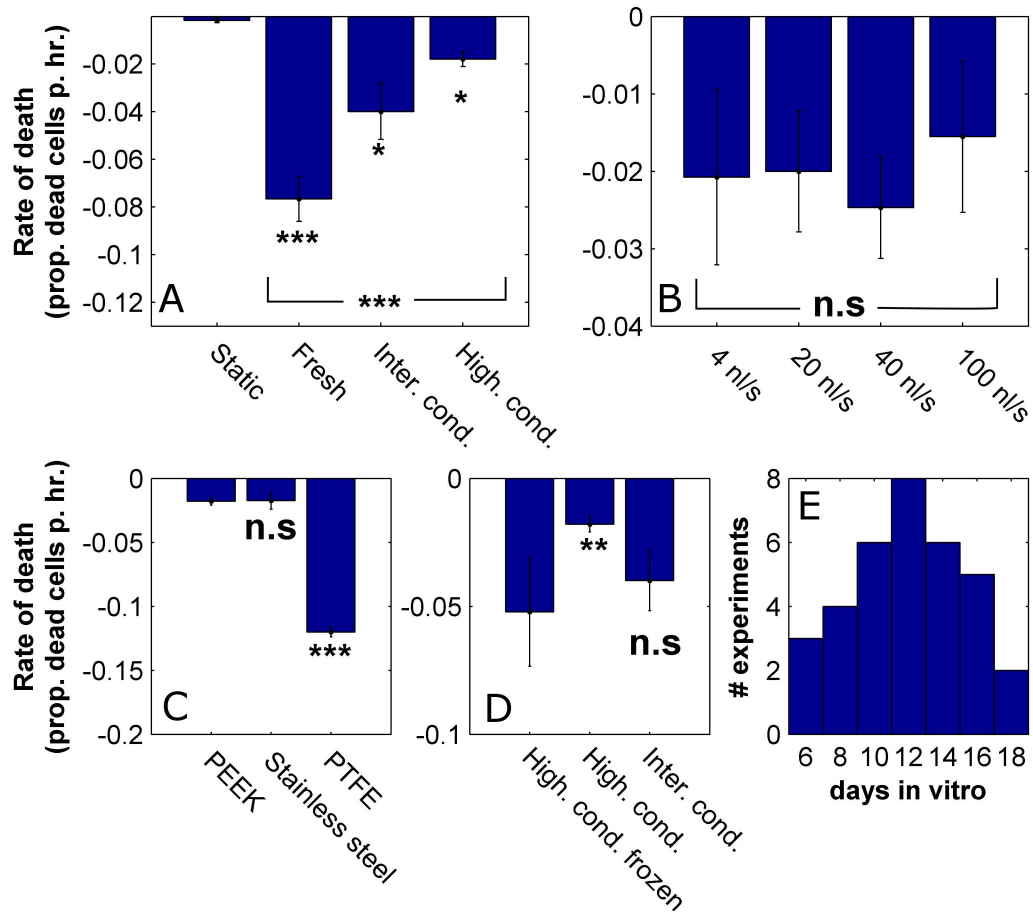


Figure 4.16: Death rates under steady flow depend on media conditioning levels and on the type of flow tubes but not on flow rates in the tested range. (A) Comparison between the measured death rates under steady flow for increasing media conditioning levels and for control devices. Experiments were identical in all other parameters (flow rate $40 \frac{nl}{s}$ and PEEK tubing). **(B)** Comparison between the measured death rates under steady flow for increasing flow rates (all highly conditioned media, PEEK). **(C)** Comparison between the measured death rates under steady flow for different tube types (all highly conditioned media, $40 \frac{nl}{s}$). **(D)** Comparison between the measured death rates for conditioned media that was frozen and re-thawed and conditioned media that was directly used ($40 \frac{nl}{s}$, PEEK). **(E)** Distribution of the ages of the cultures used in this study. The data is based on 49 experiments from 9 platings. Every bar is based on data from at least 3 experiments from 2 different platings except for the static data in panel A and the PTFE data in panel C which are each based on 3 experiments from one plating. Asterisks that group several bars indicate statistical significance of an ANOVA test. Asterisks next to individual bars indicate statistical significance of a t-test between the leftmost condition and the condition at hand. *, **, ***, n.s indicate statistical significance at a level of confidence of 95%, 99%, 99.9% or <95%, respectively.

4.2.2 highlight the challenges that exists in the design of microfluidic devices for neuronal culture in finding a ‘goldilocks’ circulation regime. On one hand, enough nutrients and oxygen need to be allowed into the device to meet the requirements of the culture and, on the other hand, conditioning factors must be prevented from ‘escaping’ as they are required for sustaining the development. The precise design is strongly dependent on the size and density of the culture as these inform its oxygen and nutrient requirements and also the secretion rate of conditioning factors.

In the second part of this chapter we used a viability assay to quantitatively observe the cultures’ health under flow. We found that using highly conditioned media can sustain the viability of the culture for several hours under flow and therefore consider it a promising approach for establishment of the system. Interestingly, the shear rate induced by the flow did not correlate with the viability which suggests that the deleterious effects are mediated solely by removal of conditioning factors and not at all by physical shear. Nevertheless, this is not the only possible interpretation for these results. A related study testing the viability of neuronal culture under a range of flow rates reported a shear threshold associated with culture degeneration [65]. This study found that a compound isolated from brain tissue named Galanin protects the cultures from the shear so, when it is introduced into the flow media, an effective increase in the degeneration threshold is observed. A possible interpretation of our results could therefore be that the conditioned media contains factors similar to Galanin that protect the cells from the shear and therefore effectively increase the flow rate threshold to a level exceeding the tested range. The study presented here cannot unambiguously distinguish the above-described narratives. This issue will be further addressed in the next chapter where electrophysiological measurements under flow will be presented and shed light on the mechanisms by which flow interacts with the culture.

Chapter 5

Activity under steady microfluidic flow

5.1 Introduction

In the previous chapter, we found that when using conditioned media for flow the cultures' viability may be extended so as to allow conducting of useful experiments. The viability assay used, however, is a crude measure of neuronal functionality and indicates that a cell has died only at late stages of apoptosis / necrosis, after the plasma membrane had been breached. This Ph.D work is concerned with how volume transmission interacts with network activity and plasticity so electrophysiological measurements are the relevant measure of functionality. In this chapter, we used multi electrode array electrophysiology to monitor the network activity of the culture as it was subjected to steady microfluidic flow at various flow rates and media formulations. We also explored using a semi-permeable membrane to de-couple the flow from the cells. The media formulation described in the previous chapter as 'highly conditioned' was found in preliminary experiments to be inadequate for electrophysiology under flow as it gave rise to inconsistent results and generally to silencing of most of the activity. Thus, the experiments in this chapter are predominantly based on using conditioned media taken from the same culture dish (i.e., media which the particular tested culture grew in, termed 'self media') and this approach was the one that finally gave usable behaviour. Nevertheless, how flowing with media from other culture dishes affects the activity was also explored.

We found a strong flow rate dependent effect whereby for slow flow rates the network dynamics were preserved. For faster flow rates, a disruption to the network activity was observed consisting a partial silencing of the active MEA channels and a loss of synchronization and of the response to electrical stimulation. This disruption was present even when a semi-permeable membrane was used to de-couple the cells from the flow. Such a membrane was shown to reduce the shear underneath to negligible levels [66] so this observation strongly

suggests that the cause of the effect is a disturbance to the chemistry around the cells. An improvement in the stability of activity was provided by the use of media from older cultures but this was still inconsistent. Finally, we found that typical synchronized network dynamics were preserved in older cultures (aged over 20 days *in vitro*) under fast flow but this was still strongly dependent on the source of the media (self media vs. media from younger culture). We argue that these results indicate an interaction between the flow and intrinsic volume transmission signalling in the tissue and propose that microfluidic flow could potentially be used as a novel assay to study these poorly understood processes. Furthermore, these results highlight the important factors that need to be addressed when designing microfluidic based drug delivery systems to neuronal tissue and the implications for device design are discussed. Most importantly, This study provides a protocol where network activity is preserved under rapid flow and is therefore the basis for the final microculture pulsing system presented in chapter 6.

5.2 Neuronal cultures in cross flow devices on MEAs

Figure 5.1 shows the devices used for the experiments conducted in this chapter. In contrast to the devices used for the viability study in chapter 4, these devices comprised multiple layers so as to allow the inclusion of the semi-permeable membrane (Whatman cyclopore, 100nm pore size, cat. no. 7060-4701). Thus they comprised a flow and cell layers which were joined either to each other or to the membrane from each side, depending on the experiment. Because of the perpendicular arrangement of the flow channel in relation to the cell channel the devices were tagged ‘cross flow’. Since assembly of such multi layered devices through plasma bonding is problematic and since plasma bonding of PDMS to the commercial MEAs could damage the surface and is not practical for re-use, we opted to use the tape technology (section 4.2.1.3). Thus prior to device placement, the MEA surfaces were treated with PEI (section 2.3). In parallel, the device layers were cut out of the 125 μ m silicone transfer tape and aligned using a custom made alignment tool (essentially comprising two pegs holding the layers in place through alignment ports). The assembled devices were oven sterilized and joined with the MEA surfaces, after these have been washed and dried from the PEI solution. The devices were manually aligned to the MEAs in such a way that the intersection area between the flow and cell channels was on top of the central electrode pads area. Since self media is extracted directly from the tested sample we increased the volume of growth media to 4ml per sample to make sure that enough supply would be available for the flow session. We used custom made glass cylinders which were glued to the MEA following the attachment of the devices to hold the media (figure 6.1).

To seed the cross flow devices, the flow channel ports were blocked so as to prevent seeding solution from being diverted through the flow channel. The seeding volume was 3 μ L which is enough to fully saturate the cell layer ($\approx 2\mu$ L). The seeding density was $7 \times 10^6 \frac{\text{cells}}{\text{ml}}$

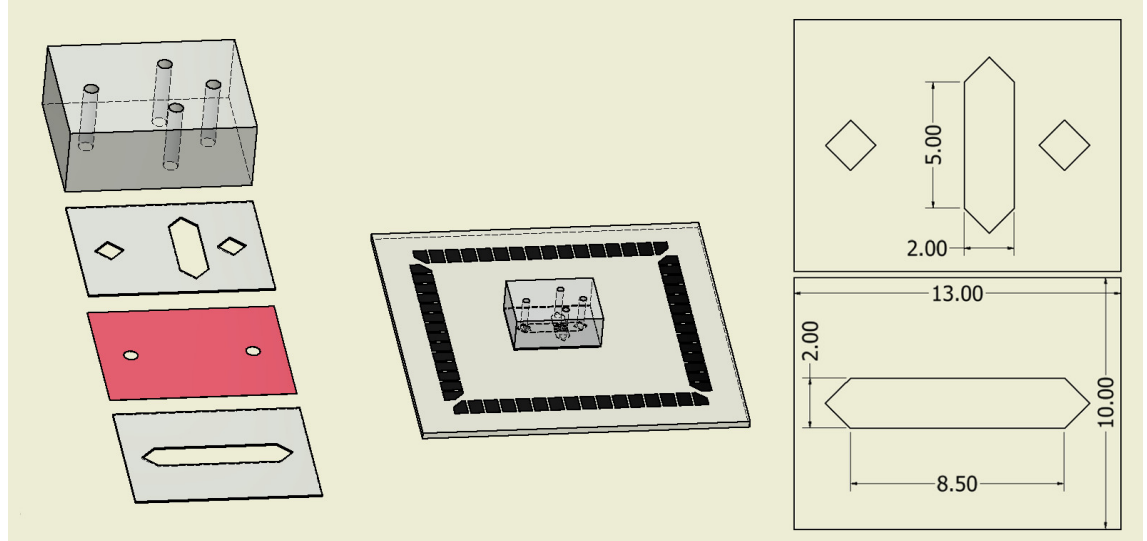


Figure 5.1: **Illustration of the cross flow devices.** Illustrations showing the constituent layers of the device laid out as well as assembled and joined to an MEA. The semi-permeable membrane is optional and shown in red. The dimensions of the flow and cell layers are also shown in millimeter units. Further details about the device fabrication are found in the text.

which was calibrated to achieve an area density of $\approx 1000 \frac{\text{cells}}{\text{mm}^2}$ in the central electrode pads area. Cultures seeded in such devices typically developed well for over a month. This contrasted with the standard 1-layered devices introduced in section 4.2.1 where many of the cultures did not develop past the end of the 3rd week. This could be attributed to the increased volume of the cross flow devices which would be associated with improved nutrient and by product circulation or to the switch to PEI surface treatment which is considered better for neuronal adhesion. Maintenance of the seeded devices was as described in 2.4 and completely follows the protocol achieved in section 4.2.1.

5.3 Activity under flow for young cultures

The first set of experiments were performed on cultures at ages 12-15 days *in vitro* which were termed ‘young’ cultures. This age range is similar to the one used for the viability study in section 4.3 so the results shown here probably best reflect the state of the cultures in that study. The recordings in this chapter were all performed in the presence of electrical stimulation in the form of a single test pulse delivered to a single MEA electrode every 5 seconds. The stimulating electrode and the pulse voltage amplitude were selected before the experiment so that an observable network response would be elicited by the stimulation. The reason for using stimulations is twofold: firstly, spontaneous activity is known to be inherently volatile as it probably depends on stochastic processes of intrinsic excitability and synaptic noise. Since the aim of these experiments is to identify conditions where the activity is stable we were concerned that variability associated with spontaneous activity would be

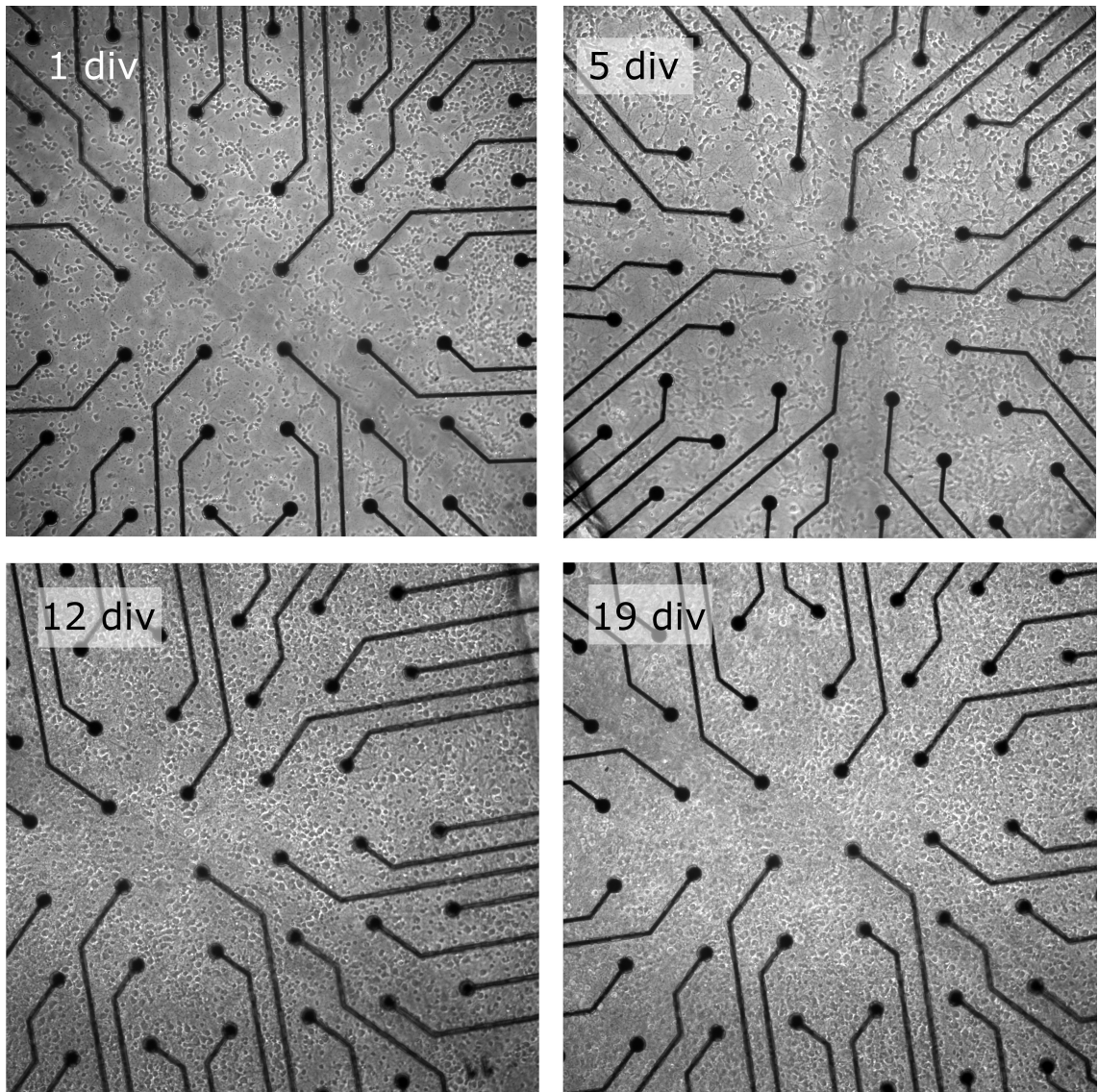


Figure 5.2: Neuronal cultures develop well in cross flow devices for over 3 weeks *in vitro*. Images of neuronal culture growing in the cross flow devices at several developmental time points. The images were taken in the area of intersection between the flow and cell channels. The electrodes are spaced $200\mu\text{m}$ apart for length reference.

confused with the destabilizing effects of flow. Thus, we argued that electrical stimulation which is more deterministic than spontaneous activity might be a more adequate basis for assessing the stability under flow. Secondly, the ability of neuronal ensembles to respond to stimulation underlies their facility for representing and transforming external information. We therefore found it is important to include a criteria where the response to stimulation would be maintained under flow.

The extracellular recordings and data analysis pipeline as well as the stimulation protocol are specified in section 2.5 and have been further described in sections 3.2 and 3.3. All the experiments described in this chapter were initiated with a 30-60 minute period of baseline

recording before the sample was plugged into the flow system. When self media was used, it was withdrawn from the sample and flushed through the system after the baseline recording.

5.3.1 Effect of flow rate

We found a strong flow rate dependent effect on the activity which is exemplified in figure 5.3 which shows baseline as well as slow and fast flow data for a young culture. In the baseline recording, the culture exhibited typical synchronized bursting dynamics which are typical for rat cultures of this age (sections 3.2 and 3.2.2). These synchronized dynamics were manifested in vertical lines in the raster plots and with high values of correlation throughout the correlation matrix. Additionally, the culture responded to test stimulation pulses with a network reverberation, although these sometimes failed to appear. Immediately upon initiation of the fast flow, these synchronized dynamics broke down with the neurons initially switching to a fast tonic firing and then gradually becoming silent. The tonic firing was manifested in a dramatic reduction in the correlation values. Additionally, the stimulation response was all but completely abolished with the activity not occurring preferentially after the stimulation but tonically spread in the observed time window (figure 5.3 B). Remarkably, even the direct responses (low latency, low jitter responses appearing as straight lines in the response rasters) were abolished under flow which suggests that the basic biophysics of the neurons had been compromised. Under slow flow, there was no sign of these dramatic perturbations to the activity. Indeed, it is evident that the slow flow induced some changes to the activity but overall the synchronized bursting dynamics and the stimulation responses were maintained and the structure of the correlation matrix was preserved.

To make sure that the phenomena reported above were indeed consistent we ran several such experiments with slow and fast flow rates and show the statistics in figure 5.4. The results are presented through 3 measures: global firing rate (i.e., total number of spikes recorded over all electrodes), mean correlation (i.e., the mean of the correlation matrix without the diagonal elements) and stimulation response ratio which is explained next. Stimulation response ratio refers to the ratio between the total spike count (over all electrodes) in a $200ms$ window just following the stimulation and a window of the same size 2 seconds later. The reason for this definition is that a measure that counts only the spikes following the stimulation is very sensitive to the background spontaneous activity. Thus we employed a second window at a distance from the stimulation under the assumption that its spike count is attributed solely to spontaneous activity. The ratio measure therefore represents the relative increase in firing rate due to the stimulation relative to the ongoing spontaneous activity. As some of the conditions used here caused large changes in intensity and temporal distribution of the spontaneous activity, using a simple stimulation response measure would have been meaningless. The firing rate and stimulation response ratios are further normalized to the baseline values of these measures (i.e., from the baseline recording period prior to connection of the tubes). Measures for control cultures were normalized to the mean value over the first

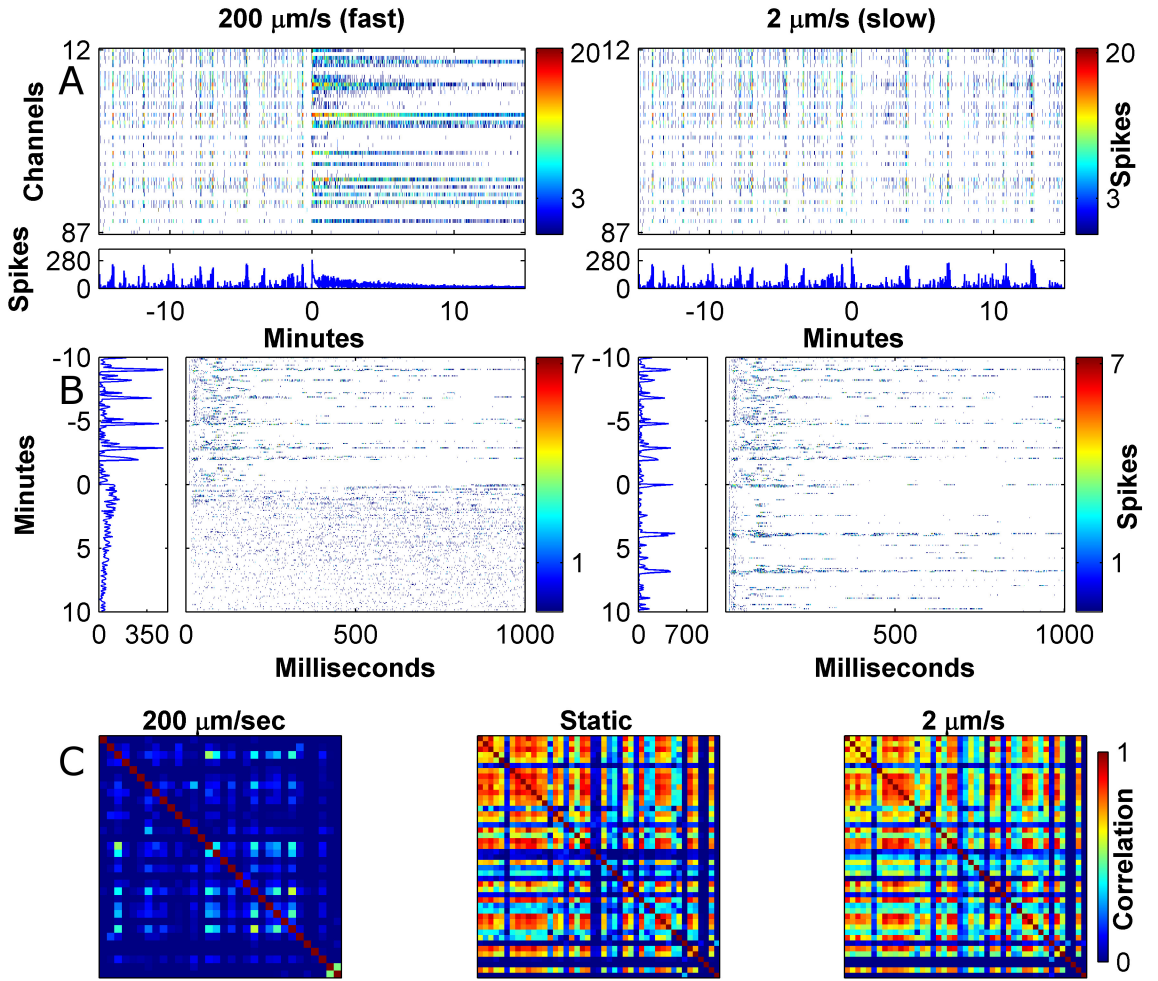


Figure 5.3: Young cultures placed under flow with self media suffer a flow rate dependent disruption to the activity. (A) Network raster plots showing the activity of the culture before (negative times) and just after (positive times) initiation of slow and fast flow (left and right panels, respectively). Note the immediate switch to a tonic and desynchronized regime in the case of the fast flow (B) The culture's network responses to stimulation before and just after initiation of slow and fast flow. Note the immediate loss of the temporally localized stimulation response in the case of fast flow (C) Correlation matrices representing the culture's activity in static conditions and under flow. All matrices are based on 10 minute activity samples. In the case of flow the samples were taken 15 minutes into the flow session. To obtain the shown data, the culture was initially recorded for 30 minutes in baseline conditions following which the flow tubes were connected and 20 minutes of slow flow were recorded. The flow was then increased to the fast rate and remainder of the session was recorded in this setting. This experimental sequence was an exception which was made to observe different flow rates applied to the same culture. In the typical case (figure 5.4) slow and fast flow regimes were conducted in separate experimental sessions.

hours of recording.

The above-mentioned activity measures are shown in a brief 40 minute window following flow initiation (figure 5.4 A-C) to observe the immediate consequences and also for an extended period of over 3 hours (figure 5.4 D-E) to assess the longer term behaviour. The short term window was also used for statistical testing. Cultures placed under fast flow with self media showed a rapid reduction in firing rates and synchronicity and their response to stimulation was immediately abolished (difference from control was verified through 2-way ANOVA with $p = 0.005$, 5×10^{-10} and 3×10^{-9} , respectively. P values shown are the lower between the group and the interaction effect). Cultures under fast flow were not able to recover their activity and all the measures tended to zero in the long run. Cultures placed under slow flow did not show a significant difference in firing rate or in stimulation response and had just a marginal decrease in correlation (2-way ANOVA, $p = 0.61$, 0.20 and 0.04, respectively). It is evident from the long term plots for the firing rate and correlation that there was a high degree of variability associated with the initiation of slow flow (connecting the tubes probably causes a sudden flush of media internally in the device). However, over time the cultures were able to adapt to the conditions and the variability subsided. In the case of the response to stimulation, a dramatic increase was observed from about the 3rd hour of the flow session. This later effect shows that even the slow flow induces changes and instability to the culture over time. However, the mechanism behind this non-trivial effect is probably different from those operating immediately at the onset of flow and was not investigated further in this work.

5.3.2 The semi-permeable membrane approach for shear reduction

The results in the previous section reveal a flow rate threshold which cannot be exceeded if the culture is to maintain a stable network activity. Unfortunately, using direct flow at the permissive rate is incompatible with the rapid drug delivery which is the concern of this work and which requires flow speeds in the order of $1 \frac{mm}{s}$ (see section 4.2.1). Thus we decided to explore an approach of decoupling the flow from the cells by means of a semi-permeable membrane. In this approach high flow rates would be maintained over the membrane to allow rapid drug delivery to the cell area above the membrane. The next step of the delivery would then be carried out via diffusion / slow convection through the membrane. Since the membrane can be positioned in close proximity to the cells the second delivery can potentially be made as quick as necessary. After all it is known that neurons use diffusion over short distances for inter-cell signalling which can be extremely fast (e.g., synapses). For example, if a $10\mu m$ membrane was to be positioned $5\mu m$ above the cells giving a total of $15\mu m$ drug travel distance then, by using the estimated diffusion time relation $t \approx \frac{x^2}{4D}$ with $D = 400 \frac{\mu m^2}{s}$ (typical diffusion coefficient value for a neurotransmitter sized molecule [63]), the drug delivery time would be $\approx 140ms$ which is easily compatible with the total required drug pulse time scales. In the case of the devices used here the height of the cell compartment

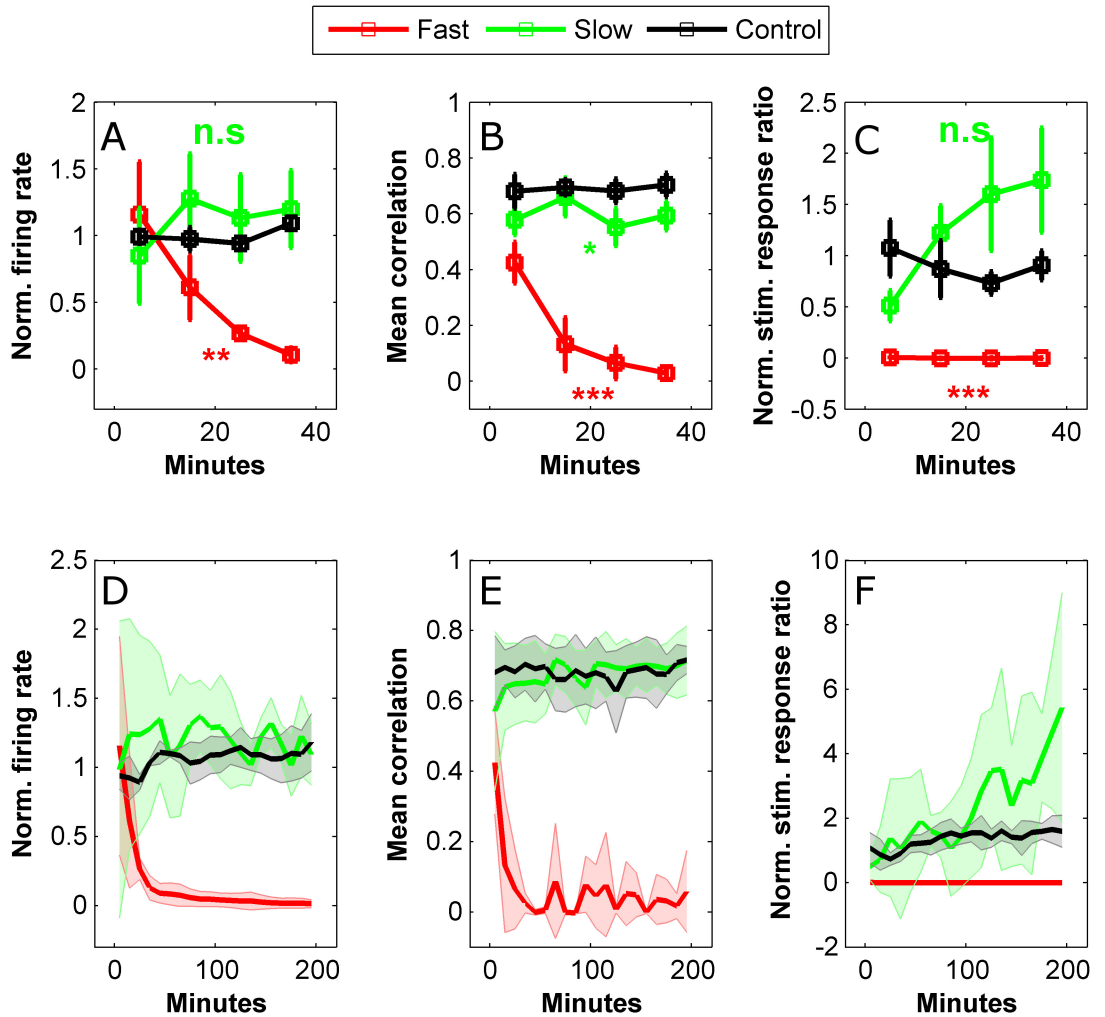


Figure 5.4: **Young cultures placed under flow with self media suffer a flow rate dependent disruption to the activity which does not recover over time.** (A-C) Averaged measures of firing rate, mean correlation and stimulation response ratio in a 40 minute interval immediately after initiation of flow for 2 different flow rates and for recordings in static conditions (color coded). The measures are calculated in 10 minute bins. Error bars indicate SEM. A detailed definition of the measures can be found in the text. Time course of the 3 measures for the 2 flow rates is compared to control by means of a 2-way ANOVA. The statistical significance is determined by the lowest of the p values for group and interaction effects and is indicated by *, **, ***, n.s which refer to confidence levels of 95%, 99%, 99.9% or <95%, respectively. (E-F) Same measures as in A-C in an extended observation period of 200 minutes. All 3 measures crash immediately with fast, but not slow, flow onset. Shaded area represent the standard deviation of the measures. Firing rate and stimulation response ratio measures are normalized to their averaged value in the baseline recording prior to flow (or to the first hour in the case of the control). Data are based on n=4, 5 and 3 experiments for the fast flow, slow flow and control conditions, respectively.

is dictated by the thickness of the tape $\approx 100\mu m$ so the distance is far greater than that required for rapid delivery. However, the aim here is to test the applicability of the approach and the correct distances can be implemented as needed in drug pulsing devices. Indeed this approach has been implemented before for shear free agonist gradient generation to cultured neurons [45, 66]. In that study an analytical estimate was developed for the maximal flow speeds which could be experienced by the cells underneath the membrane as a function of the flow speed over the membrane, of the membrane properties and of the device geometry. Applying this estimate to our devices provides a flow speed of $20 \frac{nm}{s}$ in the cell compartment at most for the highest possible flow speed over the membrane. This estimate is 2 orders of magnitude lower than even the slow flow rate that was shown to be permissive of proper electrophysiological function in section 5.3.1 so this approach holds a potential to sustain the network function.

Young cultures growing in membrane devices were subjected fast flow under the same protocol as in the previous section (figure 5.5 shows images of a culture stained following one such experiment). The results are compared to the fast flow on the non-membrane devices in figure 5.6. Remarkably, the introduction of the membrane did nothing to change the effect of the fast flow on the culture activity with all observed measures crashing with a very similar time course to that of the non membrane devices.

We also include here the data from a single experiment where the MEA central area which contains the recording pads was not located directly underneath the membrane but was shifted to be entirely inside the non exposed area (figure 5.5). Since this was only a single experiment it cannot be included in a rigorous hypothesis testing analysis so it is shown only in the long term plots for impression. This experiment did not include electrical stimulation. The recorded activity and the synchronicity in this case maintained a stable level for the full extent of the flow session. The level of synchronicity was markedly low compared to control but nevertheless stable. These data demonstrate that culture regions which are not placed directly underneath the membrane opening are able to maintain stable electrophysiological function. This experiment provides a positive control for the type of coupling that the culture can have with a flow environment while still sustaining its activity.

5.3.3 Considerations of diffusive flux

The above showed that despite the presence of the membrane the disturbance to the network activity remained as it was before. At first glance, this is surprising because one would expect that the decrease in convective flux due to the presence of the membrane would assist in both in diminishing the shear stress and in maintaining a stable chemical environment under the membrane. Thus it could be expected that regardless of the cause of the disturbance, shear stress or convective flux, the membrane should afford protection. However, this intuition does not take into account the diffusive flux which becomes dominant for short distances. Thus, in what follows, we compare the diffusive flux present in the case of the membrane

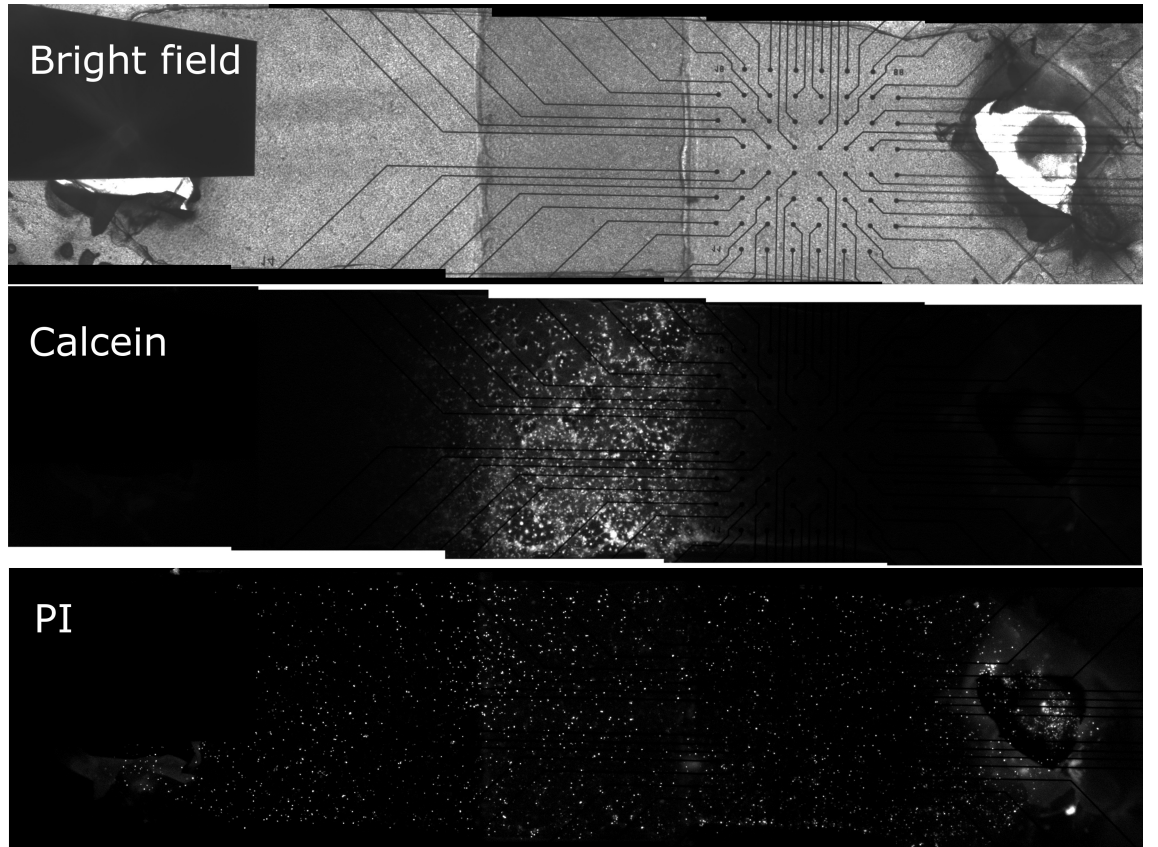


Figure 5.5: Dead live stained Neuronal culture in a semi-permeable membrane device. Polycarbonate membrane is not optically clear so cells are hard to distinguish in bright field image. The culture had been under flow with propidium iodide (dead cell stain, see sections 2.8 and 4.3.2) for 8 hours so the stain had diffused through the membrane opening to the extents of the culture channel. The live cell stain, Calcein-AM, had been introduced into the flow line only for the final 30 minutes of the flow session so that staining is present only immediately underneath the membrane opening. In this case the recording pads were not positioned directly under the membrane opening but rather shifted to one side.

experiments to the convective flux induced by the slow flow.

Considering a certain conditioning factor species which is produced by the culture and normally present at a concentration $C \frac{\text{moles}}{\mu\text{L}}$. Then in the case of direct flow through the channel this species would be carried away by the flow and removed at a flux:

$$J_{conv} = QC = 1 \times 10^{-3} C \frac{\text{moles}}{\text{s}},$$

where $Q = 1 \times 10^{-3} \frac{\mu\text{L}}{\text{s}}$ is the volumetric flow rate for the slow flow.

In the case of the membrane experiments, we assume that the aforementioned conditioning species is not present in the flow media so its concentration over the membrane is null. We further assume a linear concentration gradient for the species between the cells and the

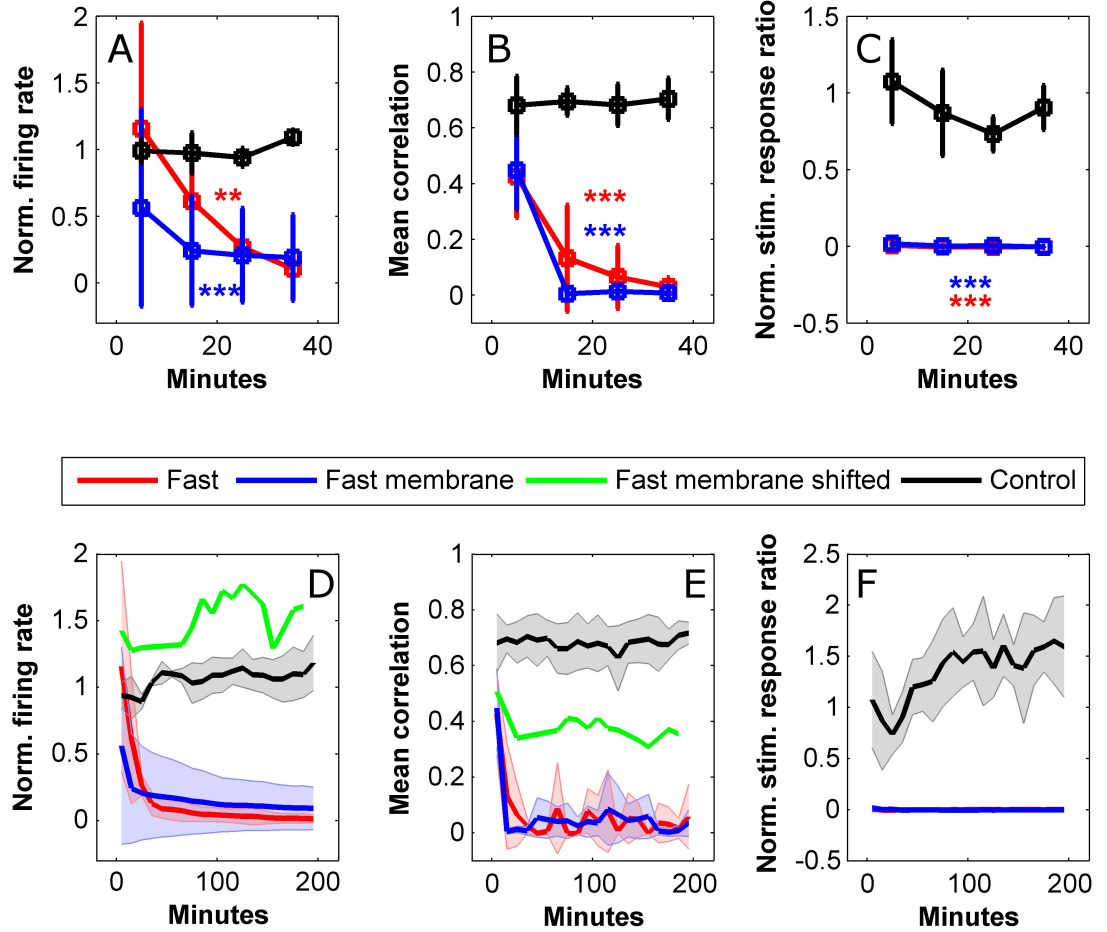


Figure 5.6: **Introduction of a semi permeable to decouple the cells from the flow does improve the activity disruption under fast flow.** Measures are as in figure 5.4 which also contains further information about the data presentation. Note the flow over the membrane (i.e., with $\approx 100\mu m$ distance imposed between the flow interface and the culture) generates exactly the same effect as direct flow. Data are based on n=4, 3, 3, 1 experiments for conditions of fast flow, fast flow with membrane, control and membrane with shifted recording, respectively.

top of the membrane. Then, according to Fick's law the diffusive flux density between the membrane from the cells across the gap and through the membrane is:

$$j_{diff} = D \cdot \frac{C}{h} = 4 \times 10^{-3} C \frac{\text{moles}}{\text{s} \cdot \text{mm}^2},$$

where $D = 4 \times 10^{-4} \frac{\text{mm}^2}{\text{s}}$ is the diffusion coefficient for neurotransmitter sized molecules and $h = 0.1\text{mm}$ is the height of the cell compartments. To get the total flux through the

membrane we multiply the flux density by the area of the membrane opening $A = 4\text{mm}^2$:

$$J_{diff} = j_{diff} \cdot A = 1.6 \times 10^{-2} C \frac{\text{moles}}{\text{s}}.$$

Thus the total diffusive flux of the considered conditioning species through the membrane is actually more than an order of magnitude **higher** than its convective flux during the slow flow experiments. It should be noted that the above calculations include only diffusive flux for the membrane scenario and therefore subliminally assume that the membrane is an ideal diffusive barrier. However, in the case of a real membrane (which is never ideal) the removal flux would be yet more extreme. Another heuristic which emerges from these calculations is that the diffusive flux is inversely proportional to the height of the cell compartment (i.e., the distance between the neurons and chemical sink). In order to equalize the factor removal flux to that of slow flow scenario the membrane needs to be located about $1 - 1.5\text{mm}$ away from the cells. This would explain why standard perfusion systems, which exchange media only from the top surface of the culture bath do not exhibit issues with the network activity as seen here. This heuristic fits well with the results from the experiment where the recorded portion of the culture was shifted relative to the membrane opening. In that experiment the recorded cells were positioned at distances between $400 - 2000\mu\text{m}$ from the membrane which means they were only partially in the ‘safe’ region. Indeed the stable synchronized network activity in that experiment persisted but the effect of the flow was still evident through a decrease in synchronization level compared to the control.

The diffusive flux considerations discussed here give rise to an important heuristic: drug delivery through a diffusive barrier designed to introduce a certain agonist at a given rate would inevitably remove agonists of a similar size at the same rate unless they are also present in the delivery media. The results of the membrane experiments, therefore strongly suggest that the self media used for flow does not fully reflect the chemical environment in the internal volume of the devices, even though it was extracted from the same culture dish. In the next section we provide evidence that, in the case of older cultures, this discrepancy is reduced thus providing means to achieve stable activity under rapid flow.

5.4 Activity under flow for old cultures

In this section we describe a set of experiments measuring the activity of cultures aged 20-23 days *in vitro* placed under fast flow with various media formulations. Section 5.3.1 described how, when young cultures were placed under fast flow with self media, the network activity was immediately abolished. Remarkably, when an identical experiment was performed on old cultures, the synchronized network dynamics persisted under flow with little interruption, namely with the spontaneous activity proceeding in the form of synchronized bursts, with high values in the correlation matrix and with stable responses to stimulation (figure 5.7). Nevertheless, the initiation of flow was still evident in some subtle yet distinctive changes to

the activity structure. Specifically, some of the channels exhibited tonic discharges in discord with the bursts. This can be seen directly in the raster plots (figure 5.7 A, right panel) and also in the correlation matrices which, despite generally maintaining their structure, contained some channels whose correlation values were reduced under flow (figure 5.7 C, compare middle and right panels). Additionally, the stimulation responses intensified and became somewhat longer (figure 5.7 B, right panel).

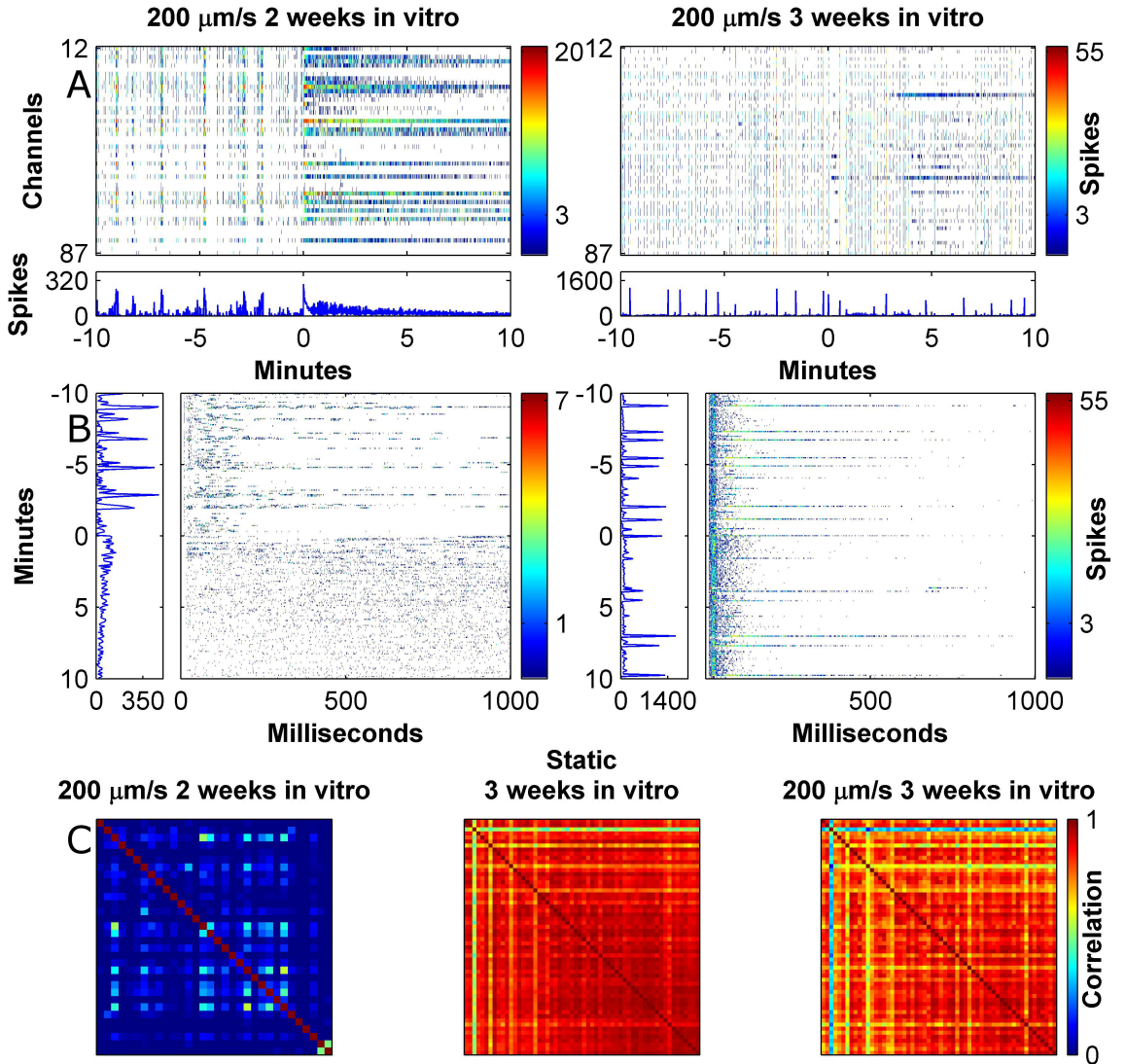


Figure 5.7: Old cultures under fast flow maintain a stable network activity. Data presented as in figure 5.3 only in this case two different cultures (young and old) are compared rather than flow rates on the same culture. In this case the activity and stimulation responses are maintained under fast flow with only small modulations. The correlation matrix for static conditions shows the data from the old culture before it was subjected to flow.

The stability of activity under flow was consistent over several old cultures from several platings as is shown in figure 5.8 which compares the 3 activity measures introduced in

the previous section for young and old cultures under flow as well as for control (static) cultures of the same age groups. The firing rate and synchronicity measures for old cultures are indistinguishable from their controls (2-way ANOVA, $p = 0.084$ and 0.35 , respectively. P-values given are the minimum between the group and interaction effects). The reported lengthening of the stimulation response was manifested as a significant two-fold increase in the stimulation response ratio as compared to controls (2-way ANOVA, $p = 2.7 \times 10^{-5}$) but the response was stable throughout the observation period.

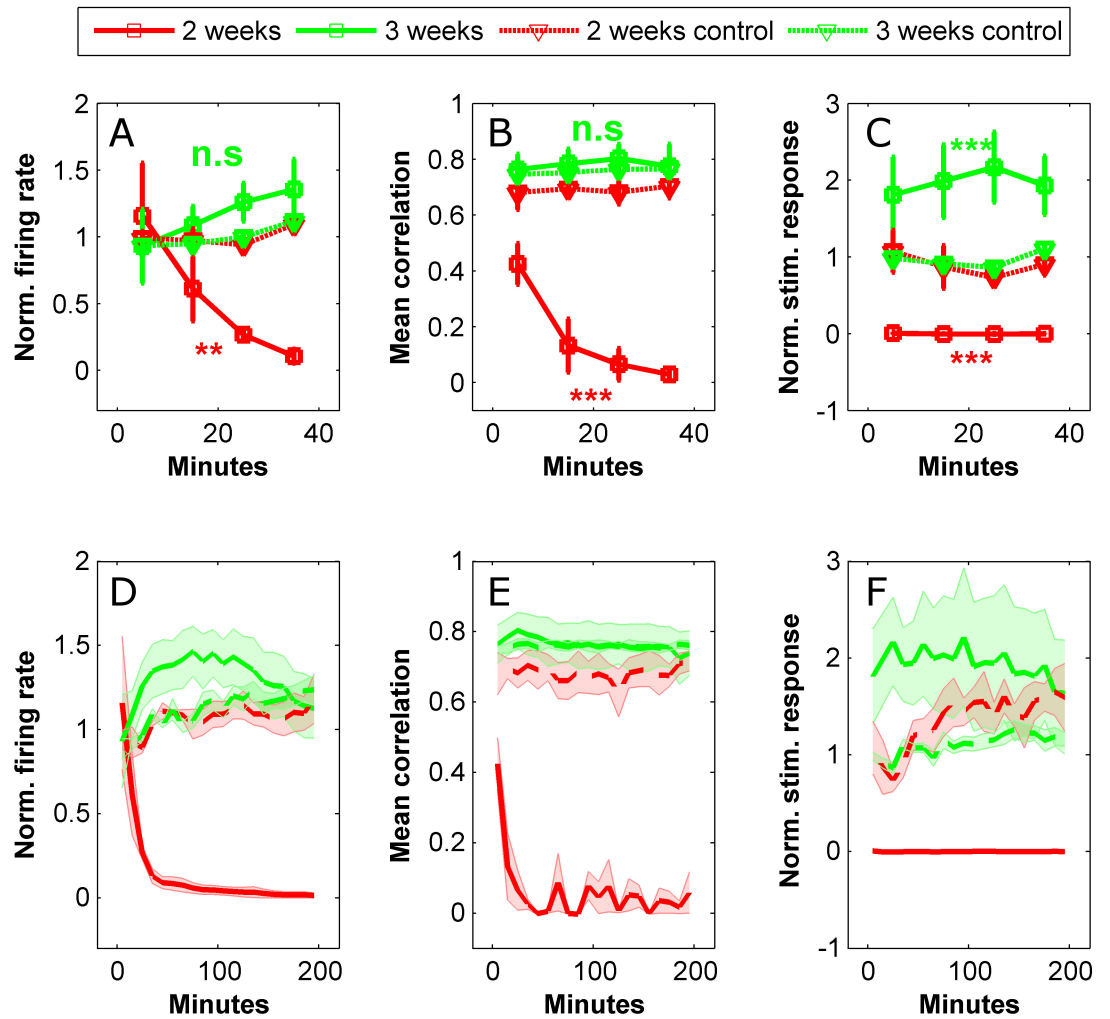


Figure 5.8: Old cultures under fast flow maintain a stable network activity for and extended period of time. Measures are as in figure 5.4 which also contains further information about the data presentation. Data are based on $n=4, 4, 3, 5$ experiments for conditions of fast flow young, fast flow old, young control and old control, respectively.

5.4.1 The effect of the media source

It is quite evident from figure 5.7 that young and old cultures are conspicuously different in their response to stimulation. In both cases the responses are bi-modal in strength, i.e., usually take the form of a short network reverberation of $\approx 200ms$ but occasionally produce a long response of a second or more. However, in the case of old cultures the short reverberations are stronger and more consistent as compared to young ones. As mentioned in section 3.2.1, although synapse density peaks at the end of the 2nd week *in vitro* [67], there is evidence that other synapse related processes such as pruning and changes to the GABA system still significantly affect the network dynamics at later stages (3rd and 4th weeks). The observed increase in the reliability of reverberative response to stimulation might be another manifestation of these later maturation processes although their exact nature is not completely understood. In the present context, it is possible that these age-related changes to the network structure render it more robust to environmental perturbations and therefore could explain why activity is maintained under flow with only minor perturbations. Another age related process which may have to do with the results is ECM formation. It is known that the ECM content in neuronal culture increases over the the 3rd and 4th weeks and that its presence facilitates synaptic function by preventing spill over [12]. It is possible that increased ECM content in the old cultures serves as a protective barrier which allows them to sustain the network activity under flow. The results of the membrane experiments in section 5.3.2 suggested that the self media lacks important conditioning factors which consequently get removed by the flow causing the activity disruption. It therefore possible that the developed ECM help to sustain a localized chemical environment by tethering important conditioning factors even if they are not present in the flow media. It is also possible that the more developed synapse formation renders the activity more stable and makes the culture insensitive to perturbation in the environment chemistry. We wanted to test if indeed old cultures are characterized by a reduced sensitivity to the culture media as this information could inform future flow applications. We therefore conducted two more sets of flow experiments. In the first one we used media from young cultures for flow. In the second one we used self media again but performed the experiments 1-3 days following a media change whereby 25% of the culture's media was replaced with fresh media (the previous self media experiments in section 5.4 were performed 6-9 days following a media change).

Figure 5.9 shows the results of flow with the two media types described above. Interestingly, flow with media taken from a young culture (blue curves) resulted in a dramatic disruption to the activity of a similar nature to the one observed in the young cultures, namely that all 3 measures rapidly crashed. However, there were also some obvious differences: Firstly, the total firing rate initially jumped 4-fold and despite dipping rapidly it stayed elevated compared to the control for the first 40 minutes (2-way ANOVA, $p = 5.0 \times 10^{-5}$). In fact, the firing rate decreased to a level lower than control only after about 100 minutes

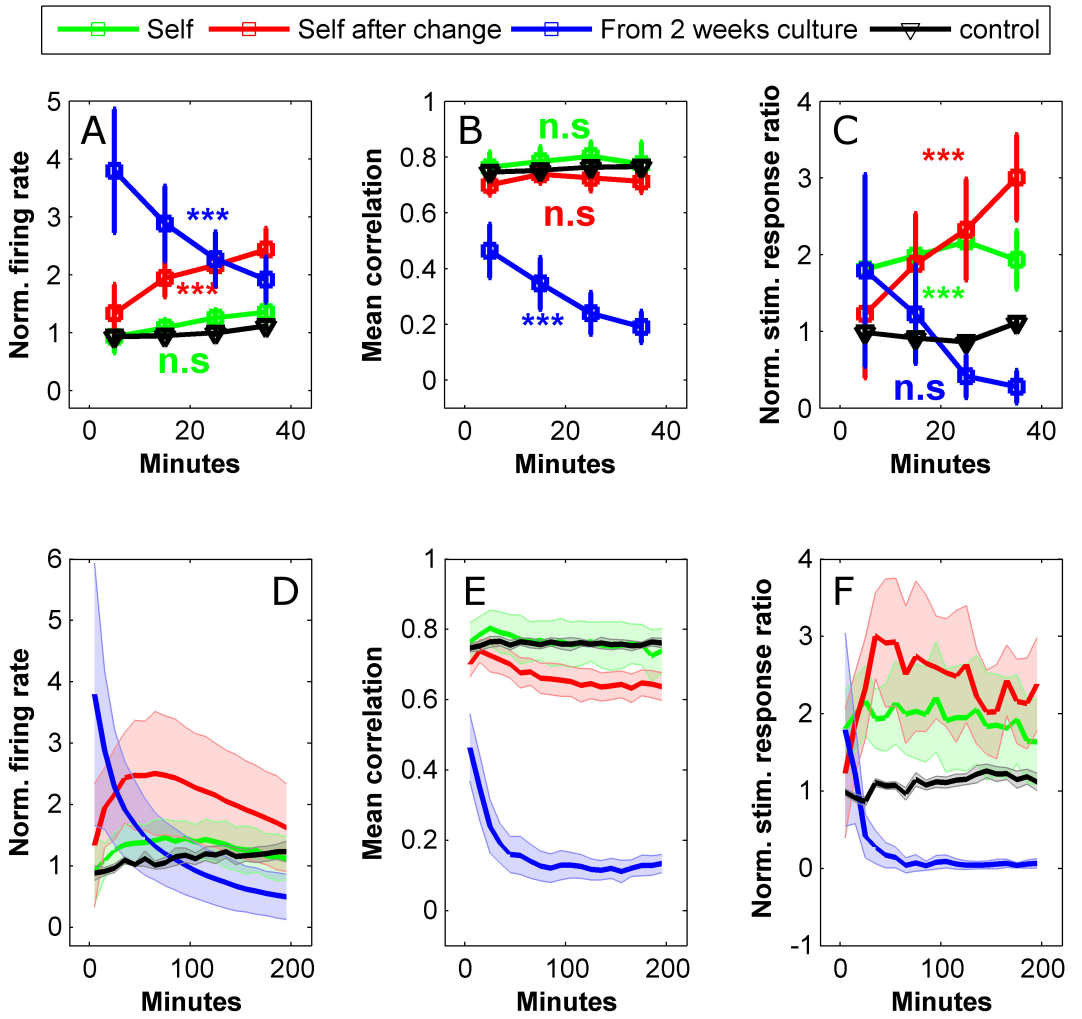


Figure 5.9: **The type of media used for flow strongly modulates the activity of the cultures and can cause the activity can crash.** Measures are as in figure 5.4 which also contains further information about the data presentation. Data are based on $n=4$, 4, 4, 5 experiments for self media, media from young cultures, changed media and control respectively.

and was never abolished completely. Secondly, the correlation levels were significantly reduced as compared to control immediately with flow onset (2-way ANOVA, $p = 1.0 \times 10^{-12}$) but deteriorated more gradually compared to the young cultures (compare to figure 5.6) and were never completely abolished. Finally, the response to stimulation initially persisted (2-way ANOVA on the first 40 minutes did not reveal a significant difference from control, $p = 0.90$ for group effect and 0.28 for interaction effect). However, after 40 minutes the response was already significantly below control (unbalanced t-test on the final sample of panel C, $p = 0.0038$). This time course of loss of the response to stimulation was slower than

in the young cultures where the stimulation response was abolished virtually immediately with the onset of flow.

Figure 5.9 also demonstrates that the mere action of changing the media can significantly affect the culture's response to flow with this media (red curves). In a 40 minute window after flow initiation this was mainly evident in increase in firing rate as compared to control (2-way ANOVA, $p = 6.5 \times 10^{-6}$) whereas the synchronicity was reduced only with a 90% level of confidence (2-way ANOVA $p = 0.054$ for group effect). The stimulation response was significantly stronger than control ($p = 7.3 \times 10^{-4}$) but an increase with the same level of confidence was found for the original flow experiment with self media on old cultures. The long term trends show a less stable behaviour under flow with recently changed media in all 3 measures. Nevertheless, the effects of the media change were quite subtle and these culture generally seemed to maintain basic network function under flow and considered useful for experimentation.

The results provided in this section show that, even in the old cultures, the formulation of the media used for flow is crucial for sustaining a stable network activity. Indeed, as we noted, the old cultures performed better as compared to the young ones but this improvement was marginal given the overall trend. Thus older cultures exhibit a strong sensitivity to the contents of the flow media despite their increased ECM contents and mature synaptic configuration.

5.4.2 How old conditioned media performs on young cultures

The results of the previous section suggest that media drawn from old cultures contains chemical species that enable stable network function under flow and that these species are absent in media from young cultures. This led us to ask whether these enabling features of old media are specifically linked to old cultures or are they more universal and would facilitate stable network function under flow for young cultures as well. To answer this question, we conducted a final set of experiments where media taken from old cultures was used for flow on young cultures. Figure 5.10 shows the results of these studies using the same measures used before. Interestingly, old media did in fact improve the performance of young cultures. These cultures generally did not exhibit the high rate tonic firing that characterized cultures under flow with young media (not shown) and indeed the firing rate in the first 40 minutes was not significantly different from control (2-way ANOVA, $p = 0.5$ for group effect). The mean correlation did dip significantly (2-way ANOVA, $p = 0.0016$) but was initially stable. The stimulation response was also stable but interestingly was significantly **lower** than the control (2-way ANOVA, $p = 0.0027$) rather than higher which was the case when the same media was used with old cultures. Nevertheless the longer term performance was unstable as most of the cultures gradually became silenced in the extended period of observation (figure 5.10 D-F). Additionally, it should be noted that these averaged measures are somewhat misleading as the individual measurements in this case

were highly variable as could be understood from the thickness of the shaded areas in the extended period panels. Out of 5 cultures measured, 2 had their activity abolished and 3 lost their stimulation response almost immediately. On the other hand, the 2 other culture performed very well under flow. These results demonstrate that the beneficial effects which old conditioned media has on old culture are partially carried over to young cultures. Some of the cultures sustain a stable network activity but only for a short while and in highly variable fashion. These results are not surprising as one might expect that the flow media chemistry needs to match the specific identity and developmental stage of the observed culture.

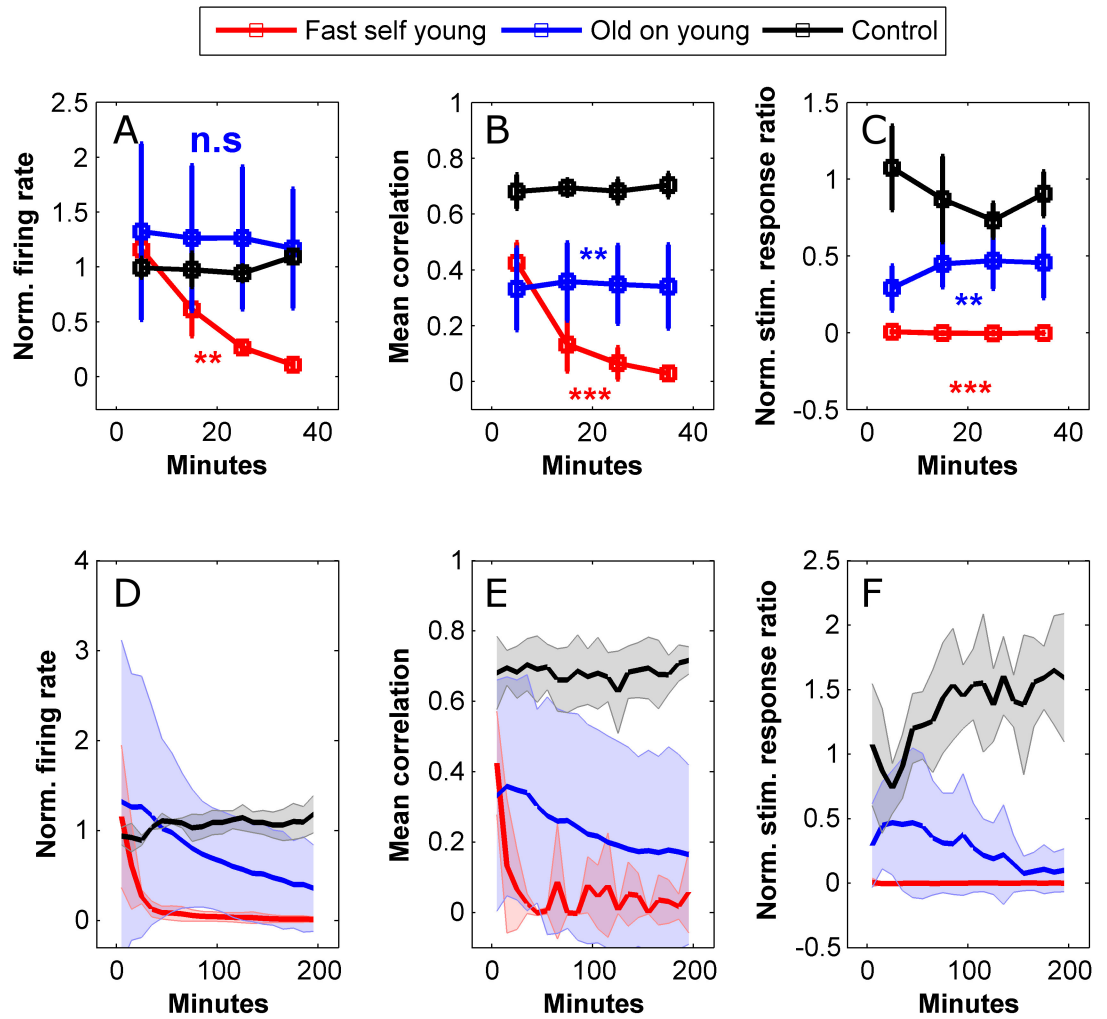


Figure 5.10: **Old media improves the performance of young cultures under flow**
 Measures are as in figure 5.4 which also contains further information about the data presentation. Data are based on $n=4, 5, 3$ experiments for self media, media from old cultures and control respectively.

5.5 Interpretation of the activity under flow results

In the previous chapter we have reported that conditioned media can sustain neuronal viability under flow. However, the nature of interaction between the media and culture and cause of the degeneration remained unclear. In this chapter, we extended the flow experiments to observe the network action potential activity under flow and gained valuable insight as to how flow bears on the culture tissue. Previous flow microfluidic work focused on the need of mitigating shear [45, 46] which neuronal tissue is exposed to and attributed the positive effects of the chemistry of the flow media on the viability to ‘shear protection’ by molecules secreted specifically for that purpose [65]. In this work we observed a strong disruption to the network activity under fast flow. Indeed this could be attributed to shear activating stretch receptors or simply tearing up the cellular membranes and eliciting an inflammatory response. However, using a semi-permeable membrane shown to reduce the shear to negligible levels [66] did not result in any improvement whatsoever. Furthermore, the membrane results were consistent with an assumption that a neuromodulator sized chemical species ($D = 400 \frac{\mu\text{m}^2}{\text{s}}$ [63]) is being diffusively removed through the membrane opening. Calculation based on this scenario predicted that cells located at a distance of $1 - 1.5\text{mm}$ from the diffusive sink would be ‘safe’ from the removal. Indeed the shifted recording experiment showed that a culture area partially located in the safe distance maintained its activity with only minor modulation. Had we performed the calculations with diffusive coefficients of ions ($D = 4000 \frac{\mu\text{m}^2}{\text{s}}$) or small proteins ($D = 40 \frac{\mu\text{m}^2}{\text{s}}$) then we would have expected either a disruption to occur over the entire culture area of the device or no disruption at all, respectively. However, these predictions are in disagreement with the results thus pointing specifically to neurotransmitter sized molecules as the culprits. Given the obvious importance of neurotransmitters to neuronal activity we argue that the immediate activity effects observed here are best explained by action of neurotransmitters on their respective receptor ion channels and that other explanations involving shear should be rejected on the basis of an Occam’s Razor reasoning. The results shown in this chapter do not rule out the possibility that shear contributes to other long term effects but they definitely demonstrate a that a disruption to neuronal signalling is a strong part of the effect of flow which needs to be taken into account.

In section 5.4 we showed that the activity in old cultures was maintained under fast flow with self media although these cultures were very sensitive to changes in the media chemistry (for example, their activity was disrupted in similar fashion to what was observed in young cultures, when media from such young cultures was used for flow). This result suggests that self media in old culture is chemically more matched with the micro-environment around the cells than in young cultures. Nevertheless, as the self media is in direct contact with the culture one would expect chemicals secreted by the cells to quickly diffuse to the bulk, especially in the case of small neurotransmitter molecules, so it may seem surprising that a strong gradient would develop between them. However, as mentioned in section 3.2.1,

the period of development occurring between the young (beginning of 3rd week) and old age (beginning of 4th week) time frames is characterized by fast changes to the neurotransmission systems. HPLC measurements of the glutamate and GABA contents of neuronal culture media show that the levels of both these major neurotransmitters rise over the first month *in vitro* and saturate only at around day 35 [15]. In particular, the GABA levels do not rise monotonically but remain low for the first 3 weeks and then jump sharply to reach the final saturated levels. This sharp rise in the media GABA content might correlate with the induction of the astrocytic GABA [68] or maturation of late interneurons [16]. Additionally, some reports claim that synaptogenesis in culture extends into the forth week which might also explain the increase in neurotransmitter production during the preceding period [69, 70]. Although the exact nature and timing of these maturation processes has not been completely clarified, there is ample evidence that the tonic neurotransmitter levels strongly depend on the culture age. In our devices, a large support culture comprising 250k cells is seeded on the outside (compared to 14k inside) and this external culture is probably the main source for diffusible factors in the bulk media. A possible explanation for the mismatch of the self media in young cultures could therefore be that the external support cultures were at a considerably different developmental stage as compared to the internal cultures and so the self media was not well matched to the latter. Indeed it has been shown that cultures grown in microfluidic devices develop faster than standard ones, possibly due to localized buildup of conditioning factors [71]. In the case of older devices, which are one week more developed, both the internal and external cultures may have entered a saturation in development so they were more similar. Another possible explanation for the self media mismatch is that during periods of accelerated development the rate of changes to the local neurotransmitter environment exceeds the rate of diffusion so that the bulk media is ‘lagging behind’ in accumulating the chemicals from the microenvironment. After all, even though neurotransmitters are small molecules they would take about 17 hours to diffuse through a media reservoir of height 10mm (note that the bulk media volume per sample was bigger in the cross flow devices to allow enough supply for the flow session).

The afore-mentioned delay in development of some GABAergic elements of the neurotransmission system raises the possibility that it is indeed GABA that is lacking in the flow media. Indeed it has been shown that the action of tonic extrasynaptic GABA exerts inhibition that is several times **stronger** than that of the fast synaptic one [72, 73] which could explain how drastic the effects of flow are. Some specific features in the response to flow provide further indication that an inhibitory transmitter is involved. Namely, when young media was used on old cultures the response was an immediate 4 fold increase in the spiking activity followed by a gradual decay, possibly due to depletion of resources. This could be interpreted as a release from strong inhibition. On the other hand, when old media was used on young cultures the stimulation response immediately decreased and the activity became silenced after a while. This could be explained by the young cultures being accus-

tomed to lower levels of tonic inhibitor compared to the old cultures and hence becoming silent when exposed to media from the latter. Indeed GABA is recognized as the major inhibitory neurotransmitter operating in the CNS and its extrasynaptic function has been receiving growing interest [73, 68, 74]. Nevertheless, the activity patterns observed under fast flow with young conditioned media are inconsistent with results from application of GABA antagonists [12, 75]. These studies did not report a decrease in synchronization but rather an increase in burst frequency and burst length so removal of GABA alone is probably not enough to explain the observed disturbance. Intrinsic volume transmission comprises an assortment of other signals including the major excitatory neurotransmitter glutamate [76] as well as ATP, NO and various neuropeptides [77, 78]. Thus the observed disturbance cannot be attributed to any specific species and is more likely a holistic effect associated with perturbations to all the intrinsic volume transmission processes at varying degrees. We believe that our results warrant an in depth investigation into the source of the disruption as it could entail a novel signalling species. Such an investigation could proceed by applying a cocktail of receptor blockers matching the known volume transmission signals to see if the effects of flow may be induced in this manner.

Even when the media is matched the flow could still affect more than just the extrasynaptic tonic concentrations of signalling molecules. This is explained next. The accepted paradigm is that neurotransmission proceeds in two distinct compartments, intra- and extrasynaptic. The most recognized neurotransmission action is the fast synaptic one where vesicle release on the presynaptic side causes an extremely rapid (time constant $< 1\text{ms}$) phasic increase in the neurotransmitter content in the synaptic cleft. The time course of these phasic signals is mainly determined by outwards diffusion to the extrasynaptic space [79]. Although the phasic dynamics are the hallmark of synaptic function it has also been established that there is an appreciable tonic concentration of neurotransmitters in the synaptic cleft which is enough for a continuous activation of postsynaptic receptors [80]. The source of this tonic transmitter level is most probably simply diffusion from the extrasynaptic space. In contrast to the intrasynaptic compartment where only neurotransmitters are known to operate, the extrasynaptic compartment contains a mixture of neurotransmitters and neuromodulators operating through both ionotropic and metabotropic receptors. In recent years, more focus has been given to the extrasynaptic species which were shown to have a strong effect on network dynamics and therefore a computational importance [81, 82, 83, 84, 76]. Such extrasynaptic neurotransmitters and neuromodulators are usually referred to as the 'tonic environment'. However, this terminology could be misleading by giving the impression that this environment is completely static whereas in fact it is temporally varying (i.e., it has phasic aspects) or else it would not be able to modulate the network activity. Since this intrinsic volume transmission is based on discrete secretion events from specific cells it stands to reason that it will have a spatial organization as well (this was shown for the case of adenosine in [81]). Thus, to summarize,

both intra- and extra-synaptic compartments contain signals with tonic and phasic components and they are not completely segregated but rather coupled via diffusion (e.g., synaptic spill over contributes to the phasic extrasynaptic signals and changes to extrasynaptic concentrations of non-synaptic origins can influence the tonic activation of the synapses).

Out of the signalling modes mentioned above, The phasic synaptic one the least likely to be affected by the flow because the neurotransmitter pulses are extremely quick and the concentrations are dependent on release from vesicles which are located intracellularly. Nevertheless there is a concern that if rapid convective flow is channeled through the synaptic cleft then it could wash away the neurotransmitter molecules as they are released and therefore to significantly modify the temporal profile of activation. To check if this could indeed be of concern we compared the diffusive flux out of a synapse with the expected convective flux due to flow assuming that the synapse is indeed open and that the flow is directed perpendicularly to the transmission line as depicted in figure 5.11. The calculations are as follows: assuming a parabolic flow profile (using the laminar flow between parallel plates approximation because channel height \ll channel width [85]) the flow velocity around the synapses is

$$u = u_{avg} \left(1 - \frac{y^2}{h^2}\right) \approx 15 \frac{\mu m}{s}$$

where $u_{avg} = 200 \frac{\mu m}{s}$ is the average flow velocity, $h = 50 \mu m$ is half the channel height and $y = 48 \mu m$ is the location of the synapses relative to the horizontal center of the channel, i.e., $2 \mu m$ from the surface. The diffusive flux out of the synapse is

$$J_{diff} = D \frac{c - b}{d} (4A) \approx 32(c - b) \frac{moles}{s}$$

where $D = 400 \frac{\mu m^2}{s}$ is the diffusion coefficient for a neurotransmitter sized molecule in free media, c and b are the intra- and extra-synaptic neurotransmitter concentrations, respectively in $\frac{moles}{\mu m^3}$, $d = 0.2 \mu m$ is the diffusion distance and $A = 0.2 \times 0.02 = 0.004 \mu m^2$ is the area of one external face of the synaptic cleft (taking the cleft gap to be $0.02 \mu m$ and cleft width to be $0.2 \mu m$) ($4A$ is then the entire face area available for diffusion). The total convective flux is

$$J_{conv} = J_{flowout} - J_{flowin} = Auc - Aub = Au(c - b) = 0.06(c - b) \frac{moles}{s}.$$

Thus, somewhat unintuitively and owing to its nano-scale dimensions, the outwards flux out of the cleft due to diffusion (which is the main determinant of the temporal concentration

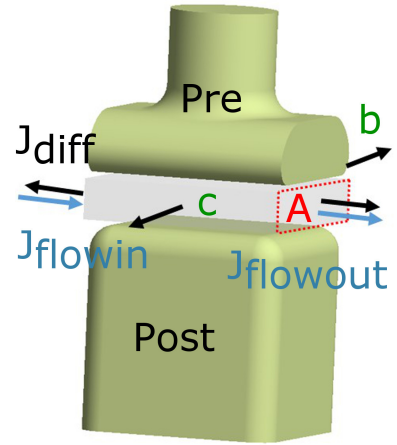


Figure 5.11: Illustration of the synaptic cleft geometry and symbols used to compare the convective and diffusive flux in the case where the flow runs directly through the synapse.

profile during synaptic activation [79]) is 3 orders of magnitude larger than the that due to convection even if the cleft is completely open to the flow. In reality, the synapses are usually enveloped in neuronal and astrocytic membranes which are unlikely to allow any degree of flow through. Thus we would expect phasic synaptic dynamics to be maintained even under much faster flow rates or shallow device geometries (i.e., where the flow velocity at the boundaries would be higher). However, the same cannot be said about the phasic extrasynaptic signalling which is much slower and operates over much larger space scales and about tonic synaptic concentrations. Thus, fast flow, beyond the obvious effect of changing the basal extrasynaptic species concentrations, could have generated the observed disruptions by indirectly changing the tonic receptor activation within the synapses and also by disturbing the phasic (and spatially organized) aspects of the intrinsic volume transmission.

Despite recent research into the diversity of volume transmission mechanisms, the fundamental paradigm is still that the functional identity of the network is stored in its synaptic connections and that extrasynaptic processes play only a supporting role. Given this view it is surprising that the effects of flow, when the media was not matched, were so profound and seemed to drive the network outside its functional regime (inability to maintain any level of activity and abolishment of the stimulation response). Thus these results serve as a reminder of the importance of intrinsic volume transmission processes and promote the view that the fast synaptic currents in fact only modulate the neuronal activity on top of a much stronger signal that is carried by the former. In these cases the functional properties of the circuit were not restored even after a few hours under flow. This demonstrates that the neurons lack other homeostatic mechanisms (e.g., intrinsic or synaptic) that can operate within hours to restore the activity. An accepted paradigm in contemporary neuroscience is that neuronal activity is governed by a balance between excitation and inhibition. These results raise the possibility that this balance is strongly dependent on volume transmission processes rather than on synaptic ones. On the other hand, we have argued that the experiments with old cultures and self media represent a scenario where the extracellular concentrations were roughly maintained because the flow media was matched to the local microenvironment. In this case, it likely that the fast flow, which was in direct contact with the culture, perturbed the fine spatial details of the volume transmission signalling and, to a certain extent, forced it to be truly tonic, i.e. temporally constant without an ability to respond in feedback from the neuronal activity. In this scenario, the fundamental functional identity of the circuit was maintained in the sense that the activity measures that we used as well as the structure of the correlation matrix were roughly maintained (figures 5.8 and 5.7). This supports the original view that intrinsic volume transmission only holds a supporting role with regards to network function. Nevertheless, these latter experiments still exhibited a doubling in the intensity of the network stimulation response and an increase in its length. This could point to an interruption in feedback mechanisms operating through phasic volume transmission to control neuronal excitation. Such mechanisms were observed for GABA [86], adenosine

[81] and ATP [87]. This could suggest that indeed some of the network activity stabilization mechanisms which operate via phasic volume transmission have been compromised by the flow.

5.6 Chapter conclusion

We have argued that the fast microfluidic flow operates as a 'concentration clamp' because it delivers chemical species faster than the culture can uptake or metabolize. This claim has not been fully tested here and doing so might require use of biosensors to directly measure some of the extrasynaptic species. Nevertheless, if this is indeed the case, we propose that, apart from the obvious rapid agonist delivery application, rapid microfluidic flow offers a novel way of holding extrasynaptic concentrations of signalling molecules at set levels. Since neuroactive chemical like neurotransmitters and neuromodulators are directly controlled by the tissue, applying them to the bath is ineffective so the study of their function is classically performed via pharmacology to block the associated receptors. However, this approach ignores potential indirect effects of the presence of these agonists, e.g., elevated extrasynaptic glutamate may operate both through extrasynaptic metabotropic receptors as well as through tonic activation of excitatory synapses. Thus it would be beneficial to be able to control the extracellular concentration of the chemicals to check for remaining effects beyond the obvious receptor blockade. Indeed direct control over extracellular concentration is made possible through enzymatic degradation or chelating agents (e.g., [88]) but that approach is less accurate and depends on availability of specific pharmacology. Thus the so called concentration clamp offers a method of holding an entire tissue at a specific concentration. Additionally, by applying the rapid agonist delivery approach, one could artificially generate volume transmission pulses of specific agonists while keeping others at a constant level. This would require adaptation of the microfluidic geometry and application paradigm to the required time scales but offers a novel way of studying intrinsic volume transmission processes in neural tissue.

Finally, The control experiments presented in this chapter and in section 4.3.2 suggested that the imposed 'concentration clamp' is the main culprit in the observed effects of flow, both in terms of activity as well as viability. Because of the strong action of diffusion at short distances the only way to restore volume transmission processes that are perturbed by the flow is to increase the distance to the flow interface. This may have implications on the level of functionality and viability that may be achieved while preserving the time scales of the drug delivery.

Nevertheless, we have identified conditions where the network activity is adequately maintained under fast flow. The flow protocol described in this chapter will be the basis for the final phasic neuromodulatory signalling system described in the next (and final) chapter.

Chapter 6

Rapid programmatic agonist delivery to a neuronal microculture

6.1 Introduction

In this chapter we combine all the components developed in previous chapters to construct a system with the capability of second-scale agonist pulsing over an entire neuronal microculture. To this end, we started by providing a new design for micowell devices, taking into account the lessons learnt from the pilot design in section 4.2.2, and growing neuronal microcultures in them. Specific further tweaks to the protocol which were needed to achieve satisfactory results are discussed. Secondly, we tested the device’s pulsing performance by visualizing the agonist time course using a fluorescent molecule. We further showed that the pulsing performance can be accurately predicted using a numerical fluid dynamics simulation in Comsol. We used this simulation to gain information about the precise agonist concentrations specifically around the cells (bottom of the micowell) and suggested how it can be used to design devices that meet bespoke pulsing requirements. The ability of the devices to generate a biological response at the required time scales was demonstrated via pulsing of glutamate and recording the neuronal activation on microelectrode arrays. Finally, the devices were used to generate dopamine pulses coupled to electrical stimulations. These preliminary experiments were not able to produce long term plasticity but they demonstrate the usability of the system. Control experiments where the pulses were performed without an agonist showed the the physical pulse action does not perturb the culture activity. By running these final experiments we effectively realized the Izhikevic thought experiment (section 1.2.2) and achieved the declared goal of this Ph.D.

6.2 Fabrication and establishment of long term Neuronal microcultures

The devices were based on a 2-layer design comprising a PDMS microwell layer and a tape-based flow layer. The design is illustrated in figure 6.1 and the fabrication process is described next. The PDMS layers used in this section were manufactured using thin film spinning (section 2.1, either 120 or $80\mu m$ thick). They were based on the design introduced in section 4.2.2 which includes a main experimental microwell together with a large rectangular support well. The distances were selected so that the support well would be placed on top of the internal reference electrode of the MEA to allow it contact with the media. The microwell was created using a $0.8mm$ biopsy punch whereas the support well was cut manually using a scalpel. In this manual procedure, the dimensions were adhered to by placing the cured PDMS sheet on top of a printout of the layer design for reference. The earlier pilot study showed that microcultures exhibit a high rate of degeneration, depending on their size, and that the largest microwell sizes used in that study, $400 \times 400\mu m^2$, were able to match the gold standard viability of macro-cultures. The punched microwells in the new design were of average diameter of $675\mu m$ placing them further in the safe zone. The flow layer was cut out of a $50\mu m$ silicone transfer tape (section 2.1). The assembly process started by joining the flow layer to a pre-cured PDMS bulk and punching of the ports. All elements were then heat sterilized in $120^\circ C$. Next, the microwell layer was placed on top of a commercial MEA pre-coated with PEI (section 2.3) while aligning the microwell and the support well with the central recording and the reference electrode, respectively. A reversible hydrophobic bond is generated when PDMS is put in contact with a glass surface. This was followed by joining of the flow layer (and the PDMS bulk) with the top surface of the microwell layer while making sure that the microwell is positioned as close as possible to the apex of the channel. The device was completed by gluing a glass chamber around the device to hold the growth media (figure 6.1 bottom images). The devices were seeded by pushing $2\mu L$ of seeding suspension at a density of $12 \times 10^6 \frac{cells}{ml}$. The effect of the density will be discussed later. After 1 day of incubation the devices were flushed to remove excess cells from the top of the PDMS sheet. In contrast with how the microcultures were prepared in section 4.2.2, the surface-then-bonding approach used here guaranteed that only the microwell surface was cell adhesive so the cells on top of the PDMS sheet were not strongly attached. This allowed us to use a more delicate flushing routine to avoid any removal of cells from the microwell. This proceeded by using a syringe driver to apply a controlled flow rate of $50 \frac{\mu L}{min}$ for about 20 seconds which was effective at removing the excess cells (figure 6.5 A-B). The MEAs used in the study were either with the standard 8x8 layout with $200\mu m$ inter-electrode spacing or HDMEAs where the electrode pads were closely packed together in 2 blocks of 5x6 configuration at $30\mu m$ spacing. In the first case the microwell was aligned so that 9 electrodes would be contained within its area. In the second case one block of 30 electrodes

could fit into the microwell area. An example for the later case may be seen in figure 6.5. Data sheets of the MEA layouts are provided in appendix A.1.

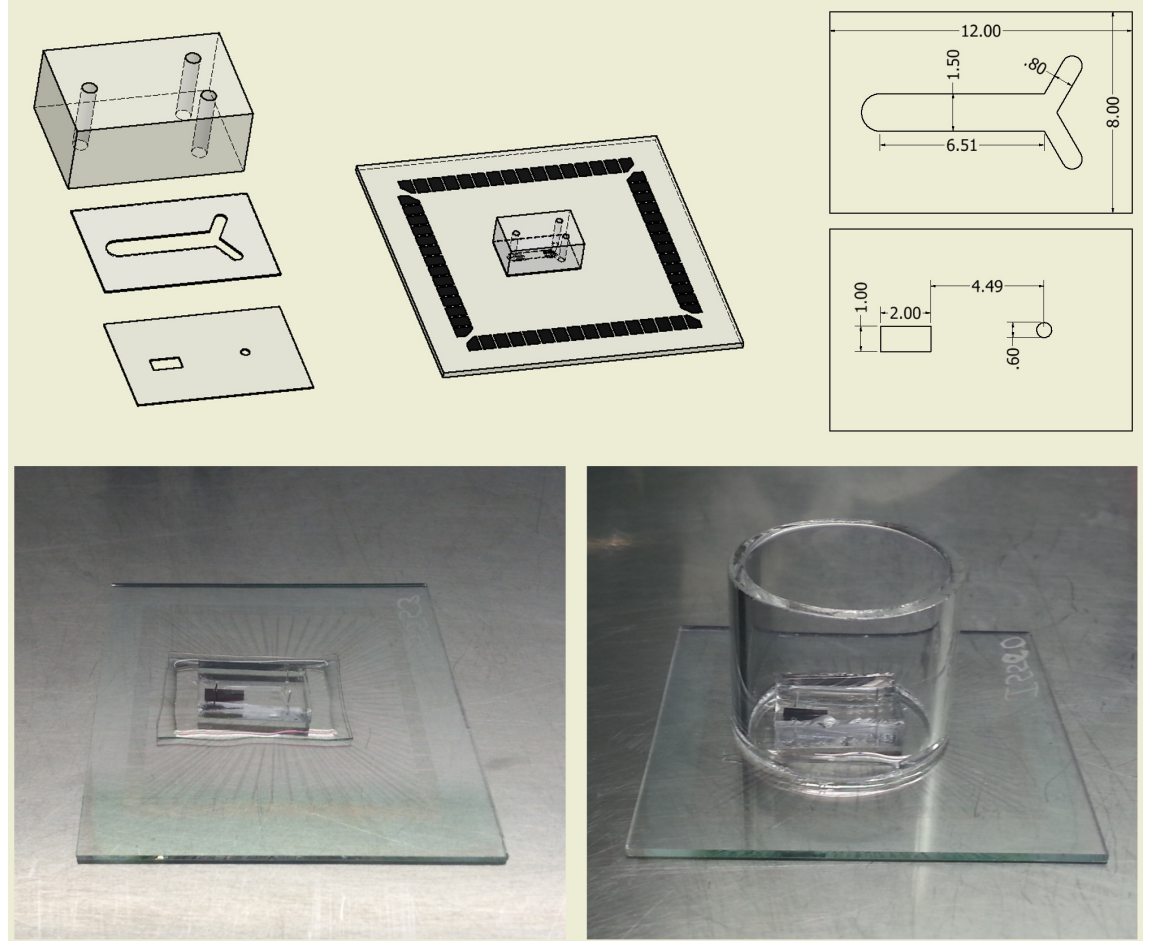


Figure 6.1: **Illustration of the micowell devices.** Illustrations showing the constituent layers of the device laid out as well as assembled and joined to an MEA. The dimensions of the flow and micowell layers are also shown in millimeter units. Also shown are images of the device before and after gluing of glass cylinder to hold the media reservoir. Further details about the device fabrication are found in the text.

6.2.1 PEI-then-all-tape devices

In preliminary versions of the device the micowell layer was composed of silicone transfer tape as this was expected to improve the bonding between the layers and reduce leaks. However, despite the good results obtained with devices made purely out of tape in section 4.2.1.3, the microcultures in this case exhibited poor adhesion and did not develop normally (figure 6.2). In a previous study toxic effects of leaching from PDMS, which is generally considered safe, presented themselves in microfluidic devices of extremely small geometries [49], presumably because of an increased leaching surface to media volume ratio. We reasoned that a similar issue arises in our devices but with tape being the source of the leaching so we

switched to extracted PDMS (section 2.1) for production of the microwell layer. Indeed this modification succeeded in providing the right conditions for microculture growth, as shown next.

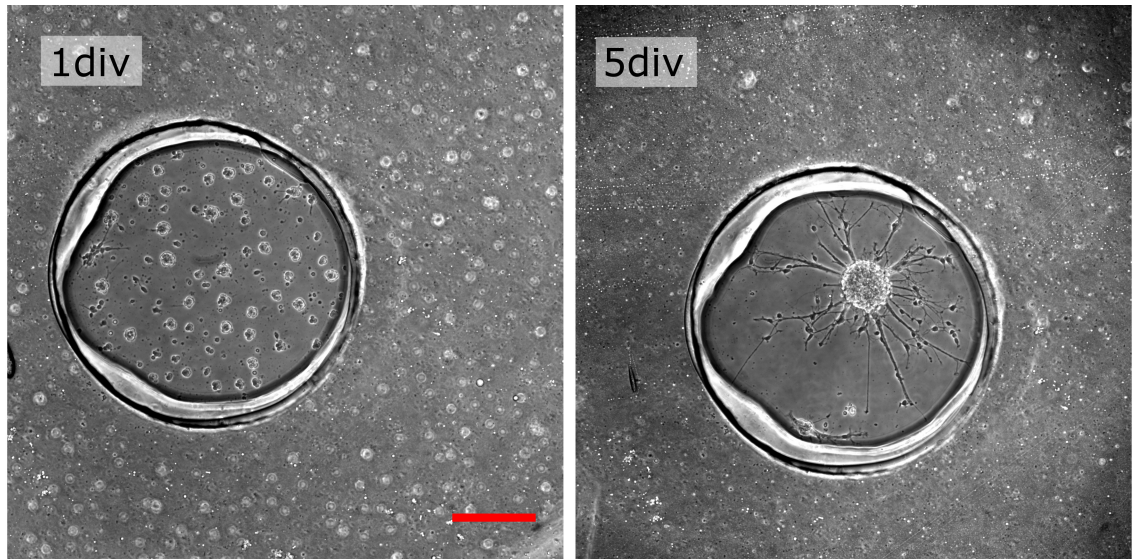


Figure 6.2: Devices made purely out of silicone transfer tape are unsuitable for neuronal adhesion. Images of a culture seeded into devices where both flow and microwell layers were made out of silicone transfer tape (50 and 125 μm thick, respectively). The cells aggregated immediately after plating and formed a single cluster after a few days. Scale bar is 200 μm long and is consistent across both images.

6.2.2 PEI-then-PDMS-tape device

Microcultures generally grew well in the PDMS / tape chimera devices and were usually viable into the 4th week *in vitro* (figure 6.3). However, an interesting side effect of the surface-then-bond approach where the surface outside the microwell is not rendered cell adhesive was revealed: Older microcultures seemed to condense so that the microwell area occupied by the culture tissue became gradually smaller (figure 6.3 19div). This shows that the process of generation of the culture tissue involves buildup of internal tension which is normally balanced by the adhesion forces. In the case of the microcultures the limited adhesion surface did not afford enough adhesion to keep the tissue from condensing. This effect was not observed for the microcultures produced with the bond-then-surface approach in section 4.2.2. It is likely that those microcultures were able to extend outside the microwell area so the balance between tissue mass and adhesion was more favorable for the latter.

We performed immunohistochemical staining on the cultures to make sure they develop normally and to receive further information on their cellular composition. We used antibodies for specific neuronal and glial structural proteins (β -tubulin and GFAP, respectively) as well as nuclear staining (DAPI) to visualize the location of the cell somas (Figure 6.4).



Figure 6.3: Devices with a PDMS microwell layer are conducive to good neuronal adhesion and development. Images of a culture seeded into devices where the flow layer was made out of $50\mu m$ tape and the microwell layer was made out of a $120\mu m$ thick PDMS sheet. The cells adhered well and developed similarly to standard cultures. After about 3 weeks the tissue began collapsing inwards. Scale bar is $200\mu m$ long and is consistent across all images.

Interestingly, the neurites seem to be extremely tightly packed, to the level that they form a seemingly solid tissue. This might be a consequence of their confinement to the small area of the microwell and would explain why internal tissue tensions would exceed those of surface adhesion, driving the tissue to collapse on itself. Additionally, the cultures comprise a dense population of astrocytes. In recent years, it is becoming progressively accepted that astrocytes are an integral part of the synaptic structure and that they participate in the synaptic signalling [89]. Thus, astrocytes are necessary for neural function and their presence holds a promise that the microcultures, despite their unorthodox size, indeed may represent a functional cortical circuit.

In section 4.2.2 we mentioned that the microwell devices that were based on the bond-then-surface paradigm were ineffective at keeping the microcultures confined to microwell area as neurites grew out onto the PDMS surface. In the case of the device of concern here, the microcultures did not grow out of the microwells and remained well restricted for over 3 weeks *in vitro*. This is shown in figure 6.5 which shows the PDMS sheet around a microwell at days 1 and 19 *in vitro*. The PDMS sheet remained clear of neurites throughout the development period. Some seeded cells were not cleared by the flushing but these remained completely latent and no observable connections with the main microculture were observed.

The microculture confinement is further demonstrated in figure 6.6 which shows immunohistochemical staining of the same culture as in figure 6.4 (at 23 days *in vitro*) but focusing on the top surface of the PDMS sheet. The nuclear staining clearly shows that cell somata are present outside the microwell area this stage. However, these somata are strictly co-localized with astrocytic (GFAP) staining whereas neuronal staining (β -tubulin) is completely absent from the top surface. This example serves to demonstrate that by 3

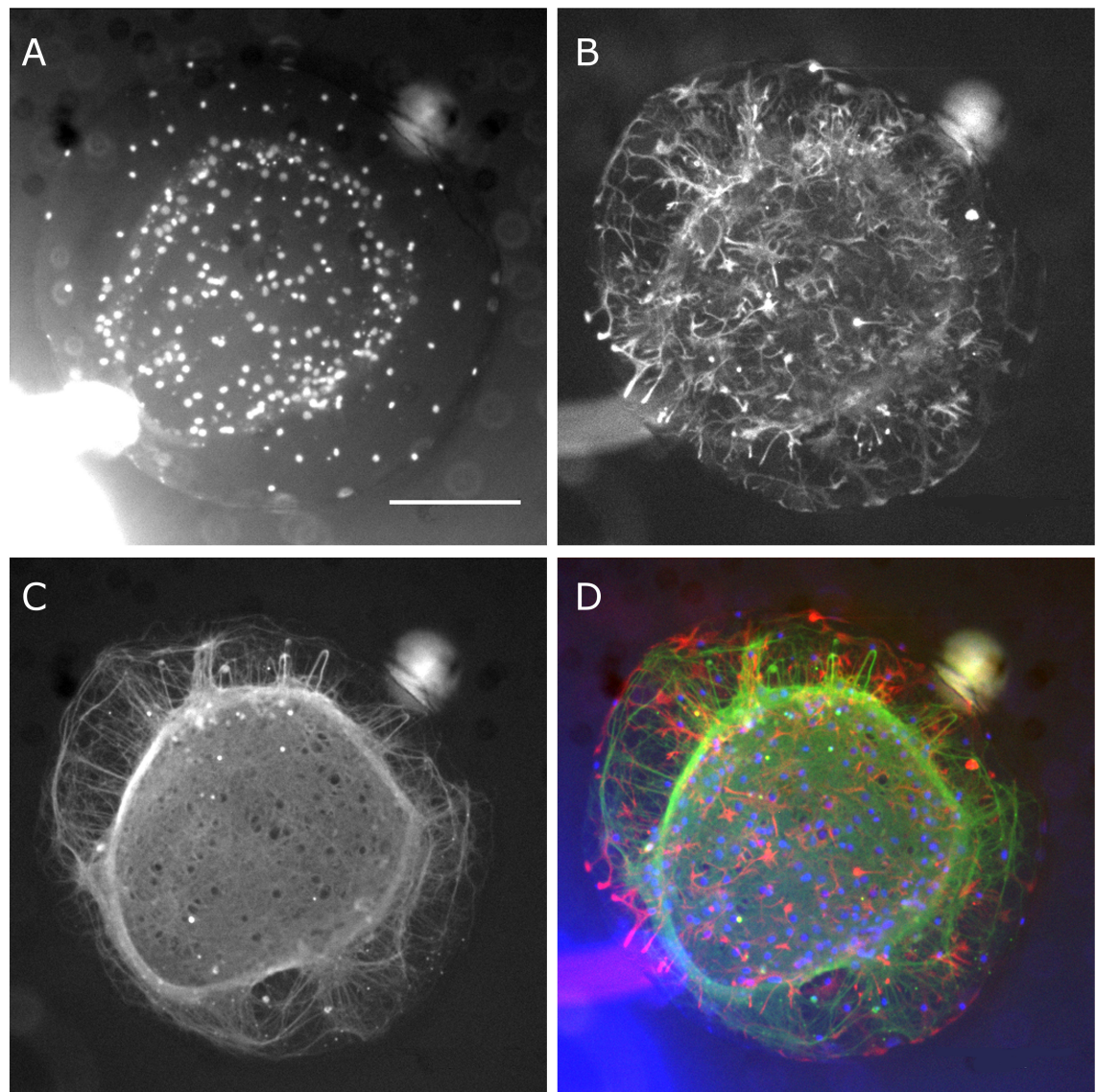


Figure 6.4: Immunostaining of the microcultures indicates the presence of intact neuronal and astrocytic structural elements. Images of immunohistochemical staining of the same culture shown in figure 6.3 at 23 days *in vitro*. Staining agents are (A) DAPI, (B) anti-GFAP and (C) anti- β -tubulin. (D) Overlay of above staining images with pseudo colors. Staining shows a dense astrocytic presence and an intact neuritic network. Scale bar is 200 μ m long and is consistent across all images.

weeks *in vitro* some astrocytes have migrated outside the microwell onto the surrounding PDMS. Nevertheless, even though one may suspect that these renegade astrocytes could serve as a substrate for subsequent neuronal migration, such a process has yet to occur at this point.

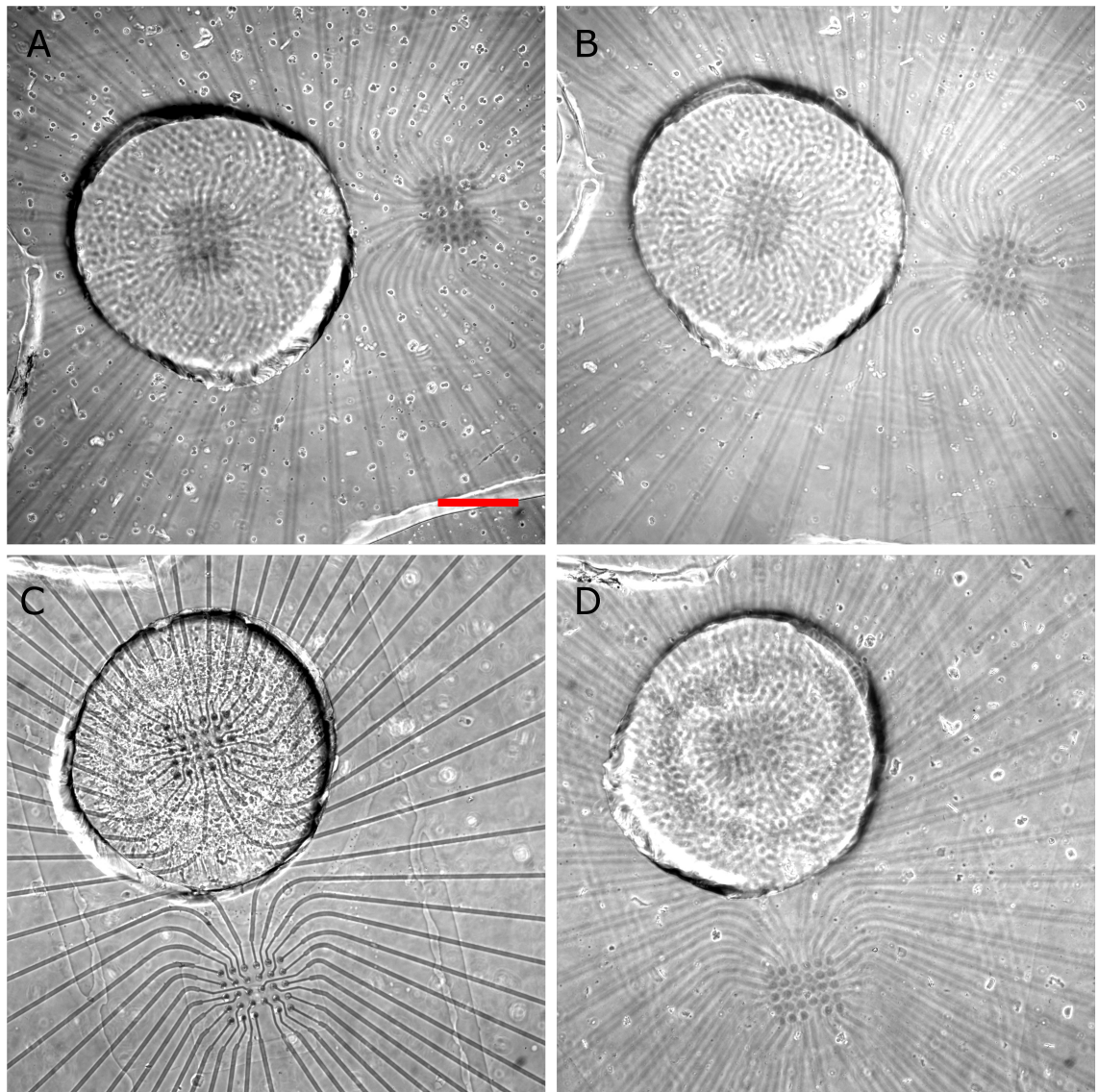


Figure 6.5: No neuritic growth into the top of the PDMS sheet is seen even after 3 weeks *in vitro*. Images of a seeded microculture and the surrounding top surface as follows: (A) Top surface after 1 day *in vitro* before flushing. (B) Same as A following removal of excess cells via flushing. (C) Microculture at 19 days *in vitro* (top surface is out of focus). (D) Top surface of C. Scale bar is $200\mu m$ in is consistent across all images.

6.2.3 Network Activity in microcultures

We performed a pilot study where we monitored the spontaneous as well as evoked activity of the the microcultures at two different plating densities. The selection of the plating density was based on the earlier microculture viability study (section 4.2.2 where it was established that a minimum area density of $1500 \frac{cells}{mm^2}$ is required for the microcultures to develop properly (i.e., not exhibit an increased degeneration rate as compared to standard cultures)). Since the microcultures used here are bigger than the ones in the earlier study we decided to attempt using a lower density in hope that it would reduce the collapse of the

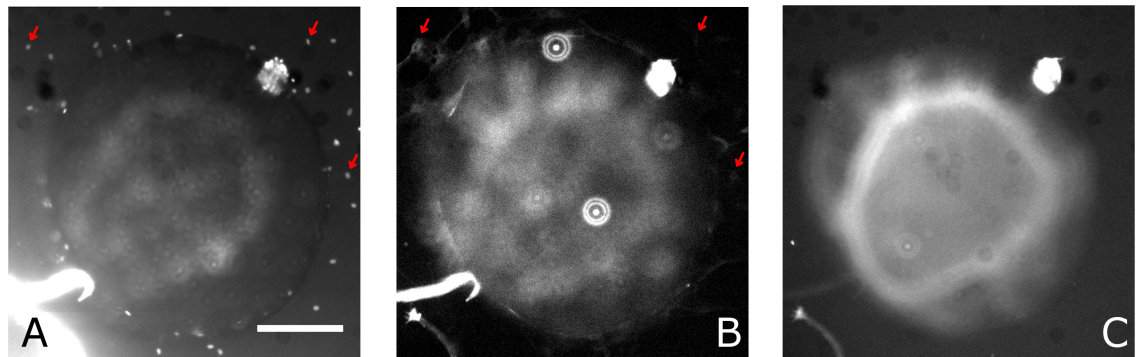


Figure 6.6: No neuritic growth into the top of the PDMS sheet is seen even after 3 weeks *in vitro*. Immunostaining images of the same culture as in figure 6.4 focusing on the top surface. Staining agents are: (A) DAPI, (B) anti-GFAP and (C) anti- β -tubulin. Although some cells are present on the top surface they are co-localized with astrocytic staining (examples are indicated by red arrows) whereas neuronal staining is completely absent. Scale bar is 200 μ m and is consistent across all images.

tissue described above but still sustain the viability. Thus the plating densities we explored were either 6×10^6 or $12 \times 10^6 \frac{\text{cells}}{\text{ml}}$. (corresponds to area densities of ≈ 1000 or $2000 \frac{\text{cells}}{\text{mm}^2}$ and termed ‘single density’ or ‘double density’, respectively). In the case of the single density microcultures, we found it hard to generate consistent evoked responses by means of electrical stimulations (i.e., most of the electrodes either did not generate responses at all or induced weak and inconsistent ones) which might indicate that the synaptic communication was not fully formed. Indeed immunohistochemical staining performed on these microcultures showed that in many of them the neuronal tissue was heavily fragmented and there was no appreciable astrocytic staining.

Strong differences between single density and double density microcultures were also presented when the cultures were placed under flow. The flow sessions were preformed on old microcultures at ages 18-22 days *in vitro* and consisted of fast flow with self media as these conditions were shown to allow stable network activity (section 5.4). The age range used here is slightly lower than in the original study because in some cases the tissue collapse dictated earlier experimentation. Out of 7 single density cultures subjected to flow only 2 maintained any form of stimulation response, in one of them, this response was abolished within 20 minutes. Out of 24 double density microcultures, 14 maintained a consistent stimulation response for an extended period of time (hours). The final protocol therefore used the double density parameter. It should be noted that the inconsistency exhibited by the microcultures is quite different from how the standard cultures in chapter 5 responded to flow. In that case, all old cultures maintained functionality under flow with self media, without exception. In section 5.5 we hypothesized that the performance of a culture under flow is determined by how well the chemistry of the flow media is ‘matched’ with the local chemical microenvironment around the culture which, in turn, depends on its developmental

stage. An explanation for the inconsistency might therefore be that the microcultures, with their unorthodox size, have a different developmental time course and so the self media, which reflects the developmental stage of the external support culture, is more likely to be unmatched. Nevertheless, the 60% success rate was found to be adequate and so we proceeded with the above-mentioned flow protocol.

The microcultures generally exhibited synchronized bursting dynamics similar to the standard (macro) cultures at the same age group. This was manifested in a similar level of synchronization and burst rate (figure 6.7 A, unbalanced t-test, $p = 0.28$ and 0.11 , respectively). However, the level of activity in the microcultures was significantly lower (unbalanced t-test, $p = 0.033$). It is important to note, though, that the distribution of activity levels was not trivial. Out of 5 monitored microcultures, 2 exhibited activity levels within the literature range (0.7 and 1Hz , literature range is $0.4 - 1.5\text{Hz}$, see section 3.5) whereas 3 were almost completely silent (0.1 , 0.02 and 0.03Hz). The silent cultures still had bursts detected in them but these consisted of single or very few spikes on a small portion of the electrodes. Nevertheless, the low activity level did not mean that these microculture were not able to generate strong reverberative activity as, remarkably, when they were continuously stimulated with test pulses at 0.2Hz the recorded activity levels went up to $\approx 1\text{Hz}$ (figure 6.7) and the PSTHs were as intense as in the macro cultures (will be shown later in section 6.5). Thus to summarize, provided that electrical stimulation is applied, the microcultures exhibit reverberative network activity and are therefore appropriate for use in the context of neuromodulator signalling and plasticity.

6.3 Pulsing performance in microculture devices

This section describes a visualization of the dynamics of agonist delivery within the microwell devices through imaging of the pulse action with a fluorescent tracer (fluorescein). It will also present data from an accompanying numerical simulation in Comsol. The reason for developing the numerical simulation is twofold: Firstly, the imaging, which is performed with dark field microscopy, is effective at discerning the agonist distribution in the plane parallel to the device axis. The Z axis distribution (i.e., the distribution along the height of the device), however, is not available and is recorded only as the sum of the fluorescence along that axis. Thus, to obtain an explicit account of the agonist concentration around the cells (i.e., bottom of the microwell), a 3D model is required. We therefore used the visualization to fine tune the model parameters and make sure that it produces a realistic output. The model was then used to extract the concentration at the cells. Secondly, once the model is shown to be realistic it can be used as a design tool for achieving specific pulsing patterns. We demonstrated how this may be used to achieve pulsing time scales that match phasic dopamine signalling in densely innervated brain areas.

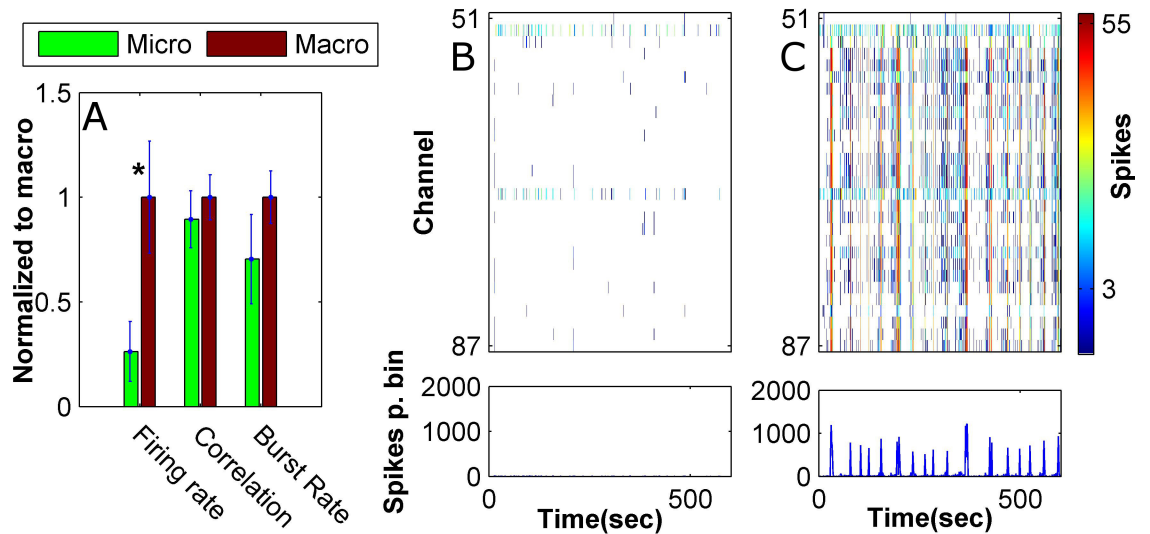


Figure 6.7: Microcultures show synchronized activity dynamics but sometimes require electrical stimulation to produce network wide events. (A) Comparison of activity and bursting measures between macro- and micro-cultures. (B-C) Example raster plots of a microculture which exhibited low levels of spontaneous activity with and without electrical stimulation at 0.2Hz , respectively. The shown time frame is too large to discern individual synchronized events and is shown to convey the dominance of the stimulations. Raster plots use bins of 1.2 seconds. Asterisk indicates a statistically significant difference between macro and microcultures at the given measure at a 95% level of confidence.

6.3.1 Analysis of pulsing visualized by fluorescein

The visualization of the pulse dynamics was performed with the same imaging system as described in section 2.8 but with an X4 objective which allowed the entire channel width to fit within the view field. In these experiments, DDW was used to for the blank (media without agonist) stream and 0.002% (w/v) fluorescein was used for the agonist stream. This concentration of fluorescein was found to provide a linear relationship between the cross section depth and the intensity of the measured fluorescent signal (this was tested in the cross flow devices from chapter 5 where the layers are known to be of the same height). The pulse dynamics are controlled through switching between two flow modes: the ‘baseline’ mode where the flow rates were set to 100 and $5\frac{nL}{s}$ for the blank and agonists channels, respectively, and a ‘pulse’ mode where these rates were flipped. When these modes are continuously set the microwell is completely contained within the respective stream. The pulse action was generated by transiently switching to the pulse mode for 1.5 seconds and then reverting back to baseline. This period was found sufficient for the agonist stream to shift just enough to cover the entire microwell area before shifting back. An example of such a fluorescein-visualized pulse sequence is shown in figure 6.8.

We now describe the full procedure used to obtain quantitative temporal data from the

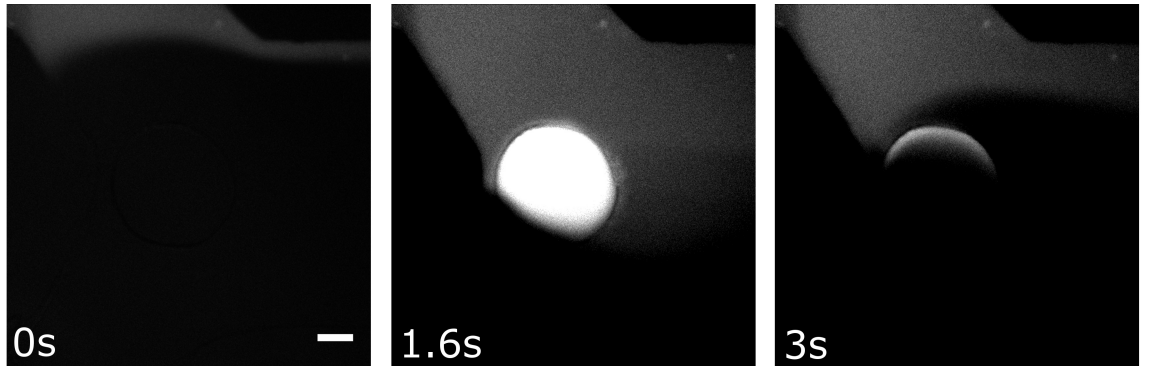


Figure 6.8: The time scales of the concentration transient are interrogated using fluorescein in the agonist stream. Scale bar is $200\mu\text{m}$ long and is consistent across all images.

fluorescein measurements. A pulsing visualization session was initiated by setting the system to pulse mode for 120 seconds. This assured that the microwell would completely fill up with agonist and provided a reference value for microwell saturation. This was followed by 120 seconds of baseline to make sure that the microwell was completely cleared of the fluorescent tracer after which 10 pulses (i.e., switching to pulse mode for 1.5 seconds and then back to baseline) were applied at 20 second intervals. The analysis of the data commenced by defining ROIs where it is desirable to know the concentration time course and extracting fluorescence traces (averaged over the ROIs). For each of the ROIs a square pulse was fitted to the segment of the fluorescent trace where the microwell was entirely inside the agonist stream to obtain a saturation value. The pulse waveforms were then collected, averaged and normalized to this value. The resultant signal represents the time course of saturation during a pulse (i.e., the proportion of the device volume inside the ROI occupied by agonist). This analysis pipeline is illustrated by figure 6.9 for two large ROIs, one encompassing the microwell and the second outside of it. Figure 6.9 D shows the the microwell ROI saturation signal reaches a lower value and persists longer than the outside ROI even though the latter is positioned further along the flow line. This reflects the extra time required for the microwell to become filled up and then depleted of agonist. The normalization method described here allows to directly compare the experimentally derived concentration pulse time course to the one generated by the model and also allowed averaging experiments performed on different devices in different lighting and optical conditions. Such ROI saturation time courses will be compared to numerical simulations in the next section.

6.3.2 Numerical simulation of drug pulsing

We used the finite element solver software Comsol to generate a simulation of the pulse action in a 3D geometry closely mimicking the microwell devices. as reviewed in section 1.3.1, a hallmark of microfluidic technology is that the low flow rates and the miniature

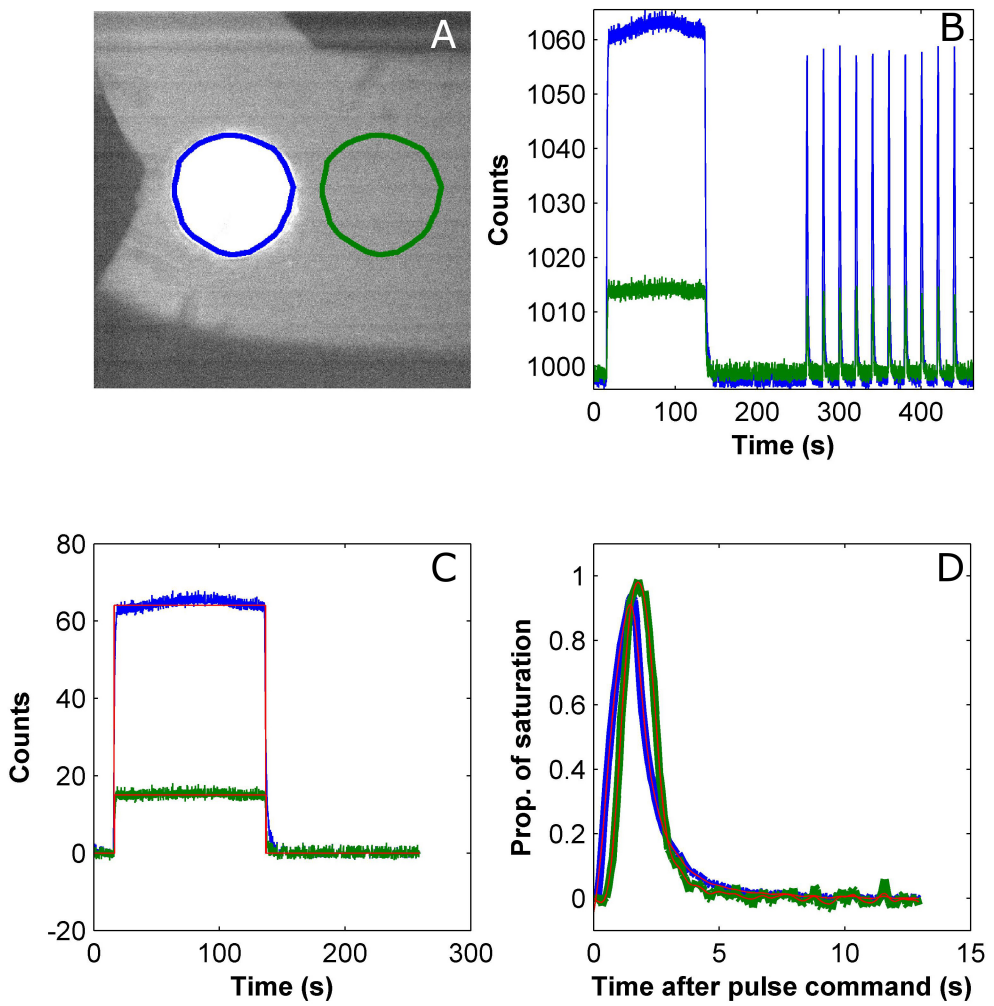


Figure 6.9: **Fluorescence data is analyzed to generate the time course of ROI saturation.** (A) Sample regions of interest of identical shape. (B) Fluorescence traces extracted from the ROIs shown in A. The fluorescence pulsing experiments included an initial 2 minute period where the well was fully saturated with agonist to obtain a reference value. This was followed by 2 minutes of clearance and then 10 agonist pulses at 20 minute intervals. (C) Square pulse fits to the saturation segment of the fluorescence trace after baseline removal. (D) Saturation time courses obtained by normalizing the fluorescence traces to the fitted saturation values in C and averaging over all 10 pulses.

dimensions dictate a laminar flow regime. In cases where the Reynold's number is $<< 1$ the inertial elements in the Navier-Stokes equation may be completely neglected resulting in a simplified model named creeping flow which includes only the hydrostatic and viscous terms [85]. We calculated the Reynold's number for the the microwell devices of concern to be $Re \approx 0.05$ and therefore used the 'creeping flow' physics module to model the velocities in

the device. We further employed the ‘transport of diluted species’ module and coupled it to the velocity field from the former module to model the convective and diffusive transport of the agonist. We used a diffusion coefficient of a neurotransmitter sized molecule ($400 \frac{\mu m^2}{s}$). Geometry parameters were measured in microscope images and averaged over all the devices that participated in the visualization. The well height was measured prior to bonding using a clean room profiler. The channel height was calculated from the ratio between the fluorescent signal inside the well to that outside in locations fully saturated with agonist. This calculation resulted in a mean channel height of $40 \pm 3.7 \mu m$ which shows that the silicone tape becomes compressed by 20% during the assembly process (as $50 \mu m$ tape was used for the channel layer). A complete listing of the model parameter values is provided in appendix A.2. The flow rates were applied as boundary conditions in the device ports. To properly model the switching of the flow rates we collected and averaged flow sensor data just after pulse commands. Figure 6.10 shows the averaged data from all 3 inline flow sensors (2 inlet and 1 outlet). The data show that following a flow switch the flow rates overshoot the set point and oscillate a few times. This is because the flow PID settings were purposefully adjusted to minimize the switch time at the cost of these minor oscillations. To model the flow switching, we disregarded the oscillations and assumed linear transition in flow rates between the set points over a switch time as in the original data (300ms, dashed line in figure 6.10). We verified that this approximation did not impact the results in the model by also running simulations with the original flow data as input.

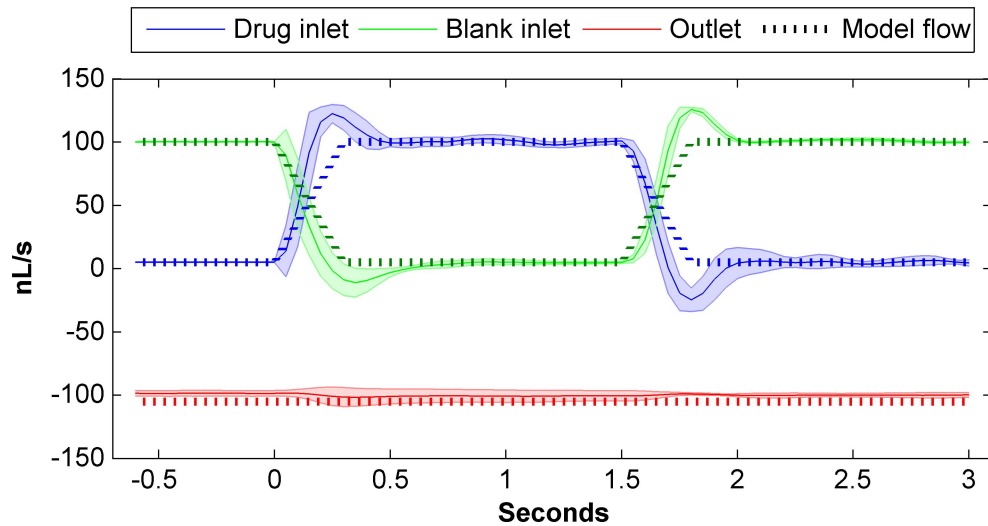


Figure 6.10: Flow switching is modeled as a linear transition between the set flow rates. The input flow rates are set to 100 and $5 \frac{nL}{s}$ at baseline. To generate the agonist pulse the flow rates are flipped for 1.5 seconds. The measurements show that the flow rates oscillate briefly and are not completely symmetric in their switch kinetics. Nevertheless, modelling the switch as a linear transition between the set points over 300ms provided a good match between model and experiment.

To validate the model through comparison to the experiments, we chose 3 equally spaced locations of measurement within the microwell along a line at a 45° angle from the longitudinal channel axis (figure 6.11). We extracted saturation time course as described in the previous section from 10×10 ROIs centered at these locations. These were compared to the predicted mean concentration along vertical lines at the same locations in the model. The data show a striking resemblance between the model generated and the experimental time courses, particularly in the temporal features (e.g., the asymmetry between the rising and decay phases). A certain discrepancy between model and experimentation is observed at the spatial location farthest from the agonist port where the concentration peak was lower in the latter case.

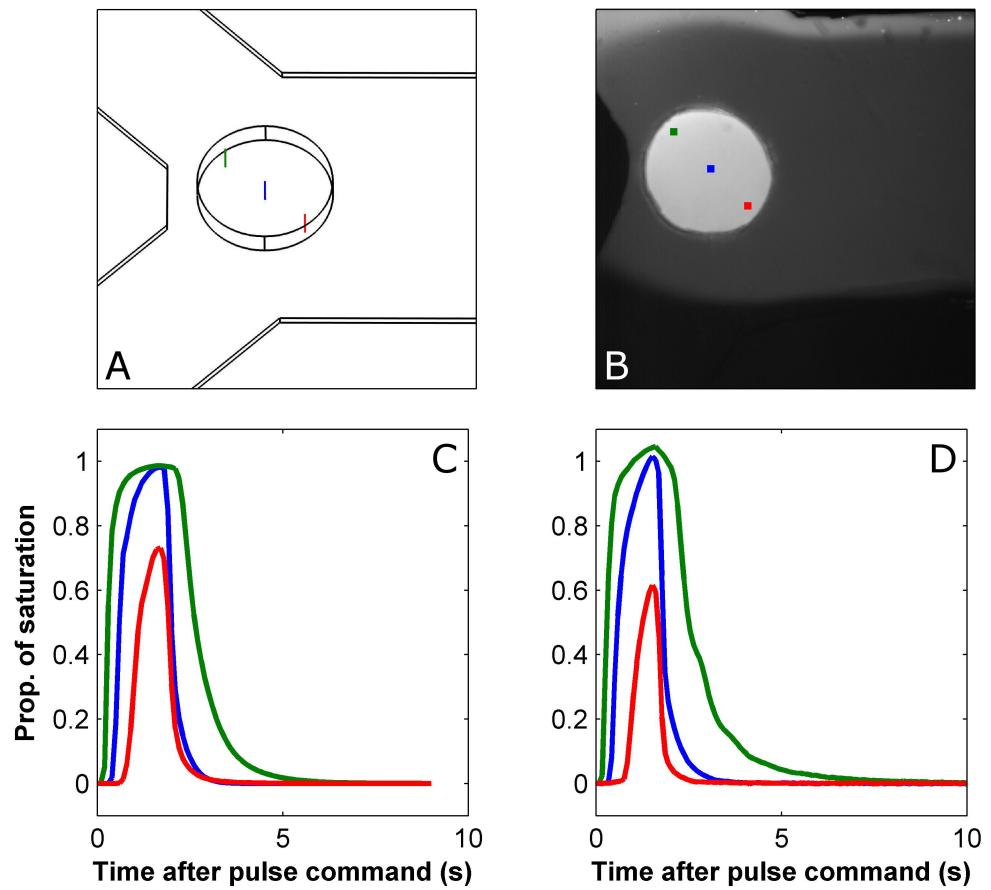


Figure 6.11: The model captures the fine kinetic details of agonist transients in different locations across the microwell. (A) Model geometry generated in Comsol and showing the three lines of examination. (B) Image of device during a fluorescence visualization showing 3 points of examination matching the lines in A. The agonist concentration averaged across the model lines is considered proportional to the fluorescence at the corresponding point because of the low Z axis resolution of the wide field microscopy. (C) Concentration traces averaged over the lines shown in A (agonist concentration in the model is arbitrarily set to 1). (D) Normalized saturation traces at the points shown in B extracted as described in section 6.3.1.

To further compare the model prediction to the measurements we present an overlay of the model data on averaged measurements in figure 6.12. This figure also shows the standard deviation of the experimental measurements which probably reflects the variability in device fabrication. This comparison shows a striking match between model and measurements in the onset of the rising phases of concentration pulses. This shows that the model predicts the travel time across the micowell well. On the other hand, the experimental time courses in all 3 spatial locations seemed sluggish as compared to the model with both rise and decay times somewhat longer in the former. We suspect that the sluggishness is related to the presence of the bubble traps in the flow lines (see section 2.8). These bubble traps are essentially PDMS devices with large cavities that are meant to collect bubbles which may interfere with the flow. Because of their elasticity, the traps function as capacitive elements with respect to pressure changes and therefore dampen sharp transitions in the flow rates (e.g., during an agonist pulse). Thus further improvements to the accuracy of the model may be achieved by measuring the flow rates down the line from the bubble traps or by changing them to a stiff material. Nevertheless, even as is, the model's predictions are within one standard deviation from the measurements. We therefore argued that further improvements would only provide marginal benefit and decided to continue with the model as is.

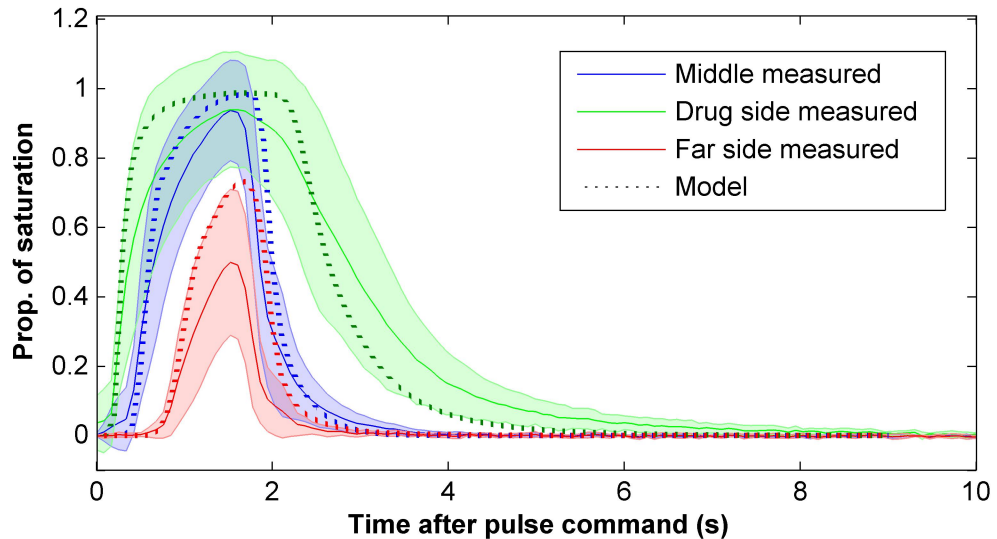


Figure 6.12: Measured transients are in good agreement (albeit slightly more sluggish) with the model. Overlay of the model and measured transient data at 3 locations in the micowell as indicated in figure 6.11. Experimental transients are averaged over $n=5$ devices. Shaded area represents standard deviation.

The establishment of the finite element model provides us with estimates of detailed agonist concentrations in the 3D volume of the device. This allows us to generate detailed agonist distributions around the cells (the micowell bottom) during an agonist pulse (figure 6.13). This data shows that the cells are already exposed to significant concentrations of

agonist within a second from the pulse command. This type of information can be consulted with for applications with requirements on the concentration density across the tissue. At present there is no clear cut information regarding how evenly neuromodulators are distributed in the tissue during a transient so we will restrict discussion to the concentration time course averaged over the entire well area from now on. Figure 6.15 shows the averaged concentration time course during an agonist transient in devices with $120\mu m$ deep microwells. The transient lasts for about 5-6 seconds before decaying back to baseline levels. Data from amperometric dopamine sensing studies show that reward associated dopamine transients can last between 1 and 7 seconds, depending on the the brain region under examination [90, 91, 53]. This places the transients shown here on the slow end of the spectrum and they can be taken to represent release in a brain region with a low density of dopaminergic innervation where the molecules linger in the extra cellular space for several seconds before being fully uptaken. Other neuromodulatory systems generate transients in the same range of time scales [92, 93, 94]. Another distinctive difference between the transient generated by our system and amperometric data is the rise time. In *in vivo* conditions the concentration transient is generated by a synchronized quantal release event occurring in many synaptic sites across the tissue. This process generates sharp concentration increases which normally peak within less than a second. In the case of our interface shifting approach the rise time depends on the rate at which the interface is swept across the microwell, which may be controlled by adjusting the flow rate. The purpose of this work was not to account for specific kinetic details of the neuromodulator transient but show that the physiological range of time scales may be achieved. Also, it not clear which of the features is specifically critical to the functional aspects of the phasic neuromodulatory signalling. However, this does not mean that the interface shifting methods is not conducive to generating transients with specific features. To demonstrate this, the next section will show that by manipulating device and flow parameters faster time scales may be achieved. These will be compared to amperometric data from our collaborators.

6.3.3 Shortening of the transient time scales by changing microfluidic parameters

We argued that transient time may be shortened by increasing the flow rate and by making the microwell shallower. Both of these changes are expected to reduce the time taken to fill up the microwell and subsequently empty it from the agonist. However, reduction of in the fill time also needs to be accommodated by a reduction in the pulse width (the duration of time that the flow rates are held in pulse mode during the pulsing sequence, see section 6.3.1). A correct selection of the pulse width is critical as holding it for too long will lengthen the transient and cutting it short may prevent the agonist from reaching all of the cells. To reconcile these contradictory requirements we defined the optimal pulse width for a given

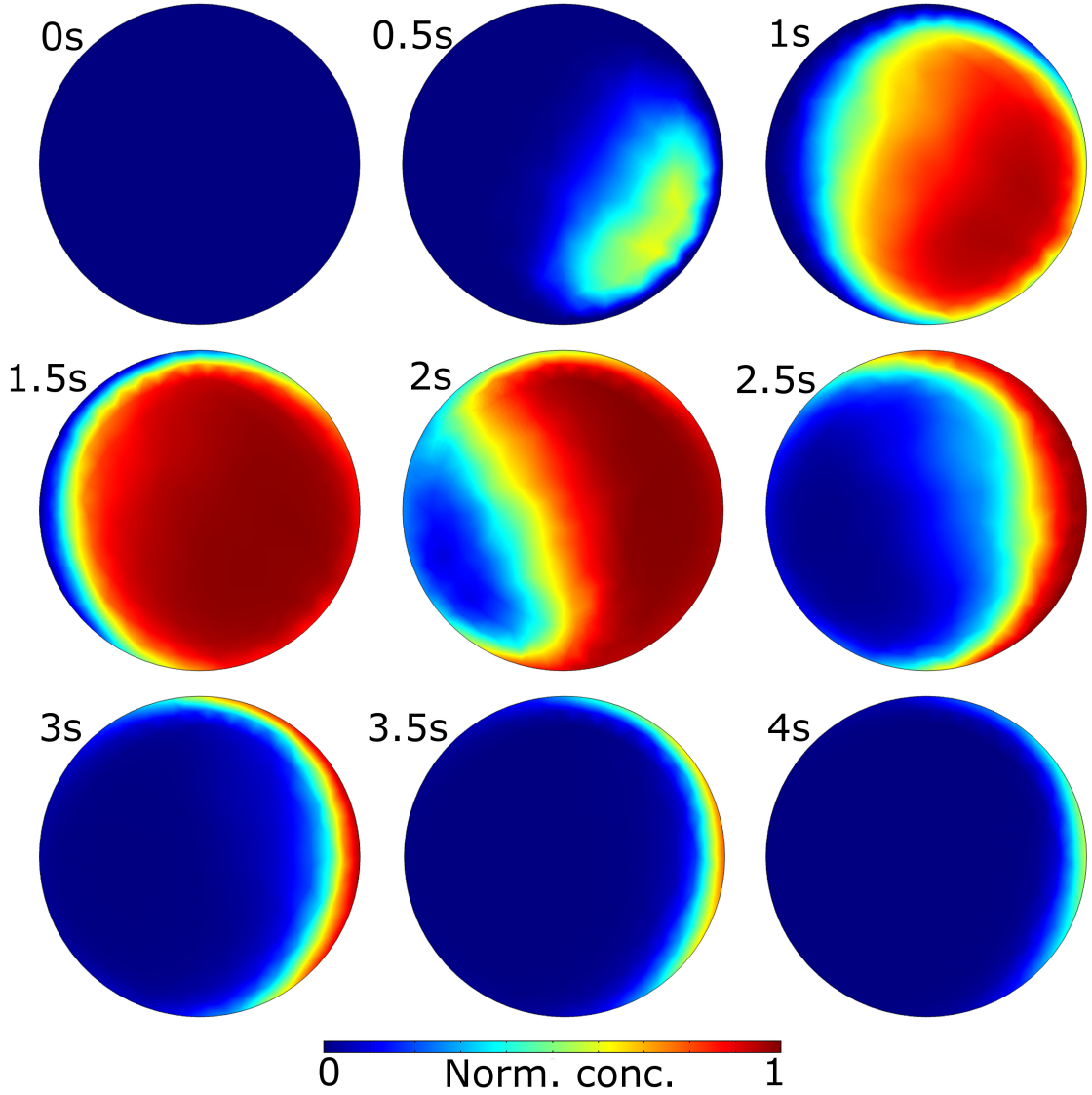


Figure 6.13: **The microwell is widely inhabited with agonist within a second from the pulse command.** Model derived agonist distributions across the microwell (in a parallel plane $6\mu m$ from the bottom surface) at fixed time points following a pulse command.

flow rate / geometry to be the shortest pulse where the agonist concentration in at least 95% of the microwell bottom area had reached at least 95% of the its concentration in the input stream. The reason for not requiring 100% saturation is that we found that the very final stages of filling process take a disproportionately long time compared to the earlier ones and so demanding a complete fill is counterproductive in the given scenario. In order to find the optimal pulse width which complies with this criteria we ran numerical simulations of agonist pulses with a range of pulse widths (while fixing all other parameters). For each of these runs we computed the time course of the microwell fill. This was taken as the proportion of the well surface (i.e., a parallel plane, $6\mu m$ from the well bottom) where the concentration had reached at least 95% of the input. The maximal fill values were used to generate a plot

of maximal fill as a function of pulse width which was normally monotonically increasing. The optimal pulse width was finally taken as the intersection of the plot with 95% fill. This process is demonstrated in figure 6.14 A-B.

Using the above procedure, we simulated the optimal agonist transients for flow rates between $100 - 600 \frac{nL}{s}$ and a well depth of $10\mu m$. These transients are shown in figure 6.14 D. These data show even for the flow rate used in the other sections, $100 \frac{nL}{s}$, the transient is appreciatively narrower (compare with figure 6.15 B) owing to the use of the shallow well. The same panel also shows a dopamine transient obtained through amperometric measurements in the rat striatum. These data were provided courtesy of Dr. James McCutcheon from The University of Leicester. As the striatum is the one the brain regions with the highest density of innervating dopamine terminals the amperometry-measured transient probably represents the fastest in the time scale range. Nevertheless, as shown by the comparison the microfluidics can readily match these time scales and even exceed them. This demonstrates that the interface shifting paradigm can generate phasic neuromodulator signalling at any physiologically-relevant time scale and highlights the usefulness of using fluid dynamics numerical simulation in calibrating the microfluidic parameters.

6.4 Glutamate pulsing

To further demonstrate the ability of the system to generate a biological response in the predicted time scales we made several recordings where pulsing was performed with $100\mu M$ glutamate. Figure 6.15 shows an example PSTH from one culture as well one averaged over 3 such experiments. The predicted glutamate concentration transients averaged over the well bottom is overlayed for reference. The data show that the cultures reacted to the glutamate transients with a burst of action potentials starting $\approx 500ms$ after the pulse command. The spiking activity returned to the baseline levels after ≈ 6 seconds, in good agreement with the predicted time scales of the agonist transients. At first glance, the activity transient seems not to comply well with the predicted glutamate concentration time course because the spiking activity surge mostly terminated before the glutamate was washed away. However, in interpreting these results one should take receptor desensitization into account, as explained next. The time course of the activity transient was evidently composed of two parts: an initial intense phase consisting of a sharp increase in the firing rates which is significantly shorter lived than the agonist transient and an ensuing phase of sustained firing at much lower levels (but still evidently above baseline). Ionic glutamate receptors are known to undergo rapid desensitization under prolonged exposure to the agonist. In particular, the AMPA receptor desensitizes completely after just a few milliseconds [95]. The NMDA receptor desensitizes more slowly [96] and not completely, as it was shown to produce tonic currents in the sustained presence of glutamate [80]. Thus it is plausible that the initial intense activity phase is associated with a temporary opening of both AMPA

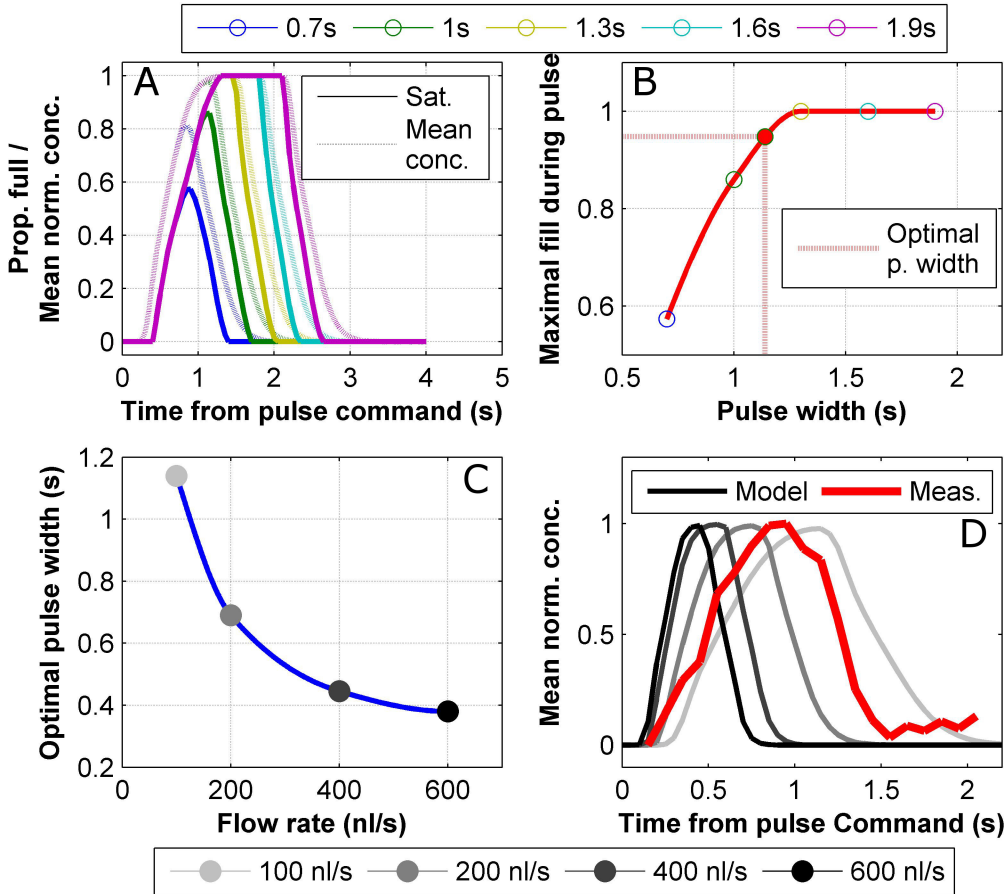


Figure 6.14: By increasing the flow rates and using a shallow microwell, transients may be generated that are narrower than those observed in the striatum. (A) Time course of well filling during agonist pulses simulated at several pulse widths and a flow rate of $100 \frac{nl}{s}$ in a $10\mu m$ deep microwell. Time course of agonist concentration averaged over the well surface is also shown for information. Precise definition of proportion fill measure is given in the text. Pulse widths longer than the time needed to completely fill the well (transients with a prolonged plateau) or ones too short to achieve complete filling are suboptimal. (B) Maximal well fill as a function of pulse width. Open circles are the maxima of the curves shown in A. Optimal pulse width is the one generating 95% fill. Red curve is a piecewise cubic hermite interpolation of the open circles. (C) Optimal pulse width as a function of flow rate computed as shown in A-B. $10\mu m$ deep microwells were used in all cases. Blue curve is an interpolation of the data points as in B. (D) Optimal agonist concentration transients averaged over well surface for several flow rates. Also shown is a dopamine transient measured via amperometry in rat striatum and presented after baseline correction and normalization to its own peak. These data were provided courtesy of Dr. James McCutcheon of The University of Leicester.

and NMDA channels which deactivate quickly, leaving just a partial NMDA associated depolarizing current responsible for the second phase. The shorter time scales of the first

phase as compared to those of the predicted agonist concentration should therefore not be taken as undermining the model validity.

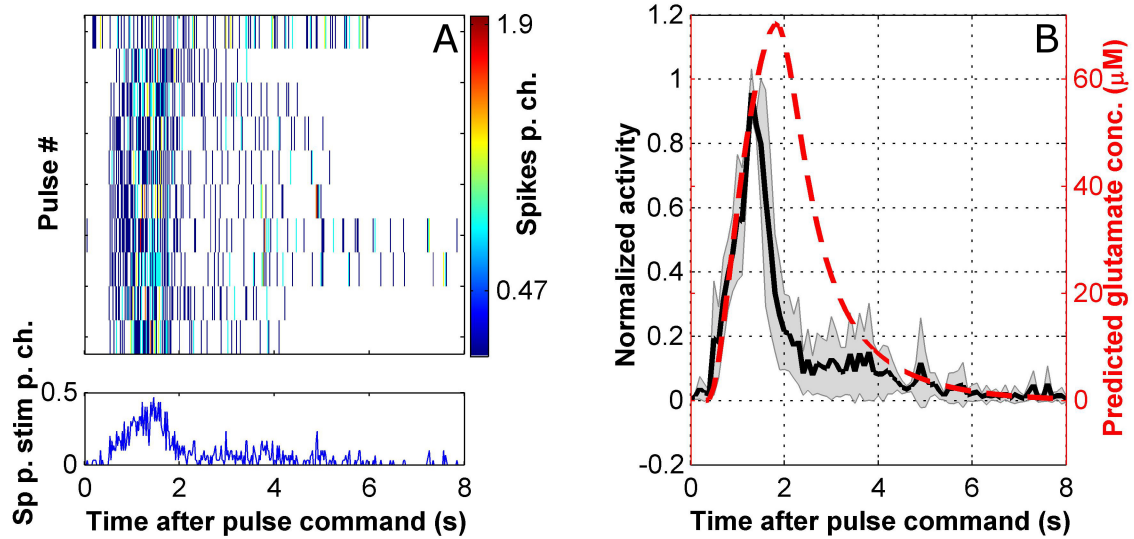


Figure 6.15: The culture responds to glutamate pulses with intense firing events of length matching the predicted agonist time course. (A) Example post pulse rasters and time histogram showing the responses to 10 glutamate pulses applied at 20 second intervals. (B) Averaged post pulse time histogram (PPTH) overlayed with the predicted glutamate time course (spatial average of the concentration across a parallel plane $6\mu\text{m}$ from the well bottom). PPTH is average of data from $n=3$ microcultures. Shaded area represents standard deviation. These experiments were conducted in devices with $120\mu\text{m}$ deep microwells.

6.5 Dopamine pulses

In previous sections, we have demonstrated that our realization of the interface shifting paradigm can generate agonist transients at time scales of phasic neuromodulatory signalling. What remains to be demonstrated is that the microcultures sustain a stable network activity under flow (i.e., that the macroculture results of chapter 5 are transferrable to the microcultures), that the pulsing action does not perturb the activity, and that the cells are responsive to neuromodulators, even under flow. To address these gaps and finalize the validation of the system, we designed an experimental inspired by the Izhikevich thought experiment (section 1.2.2). We placed microcultures under flow while being subjected to electrical stimulations that induce a network reverberatory response. During a defined epoch, the electrical stimulations were coupled to pulses of dopamine (or blank media). The stimulation responses before, during and after the pulsing were monitored for short and long term effects of the pulse action and the dopamine coupling. The pulsing commands were given 200ms prior to

the coupled electrical stimulations to offset the delay in arrival of the agonist. The reasoning behind the precise time delay value is addressed later in the text. The experimental paradigm is further outlined in figure 6.16. Beyond the validation of the system, the results of this section bear relevance to the results of the plasticity induction experiment carried out in section 3.4, which will be discussed as well.

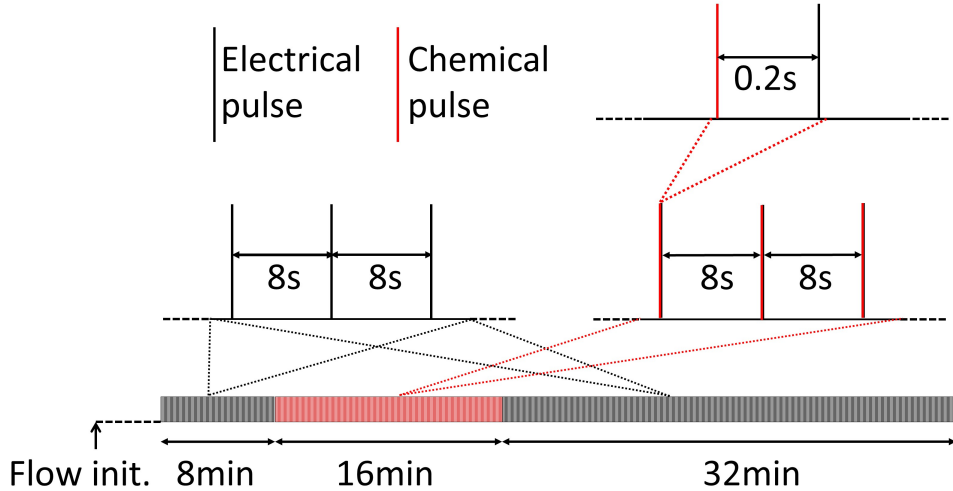


Figure 6.16: **Illustration of the dopamine pulsing experimental protocol.**

Figure 6.17 shows full response rasters (averaged over all channels) of two example experiments, one with dopamine one control. The stimulation responses that were coupled to dopamine pulses (marked by the red bar) were depressed (i.e., smaller in length and intensity) as compared to those induced before and after the coupling. The control data show that this depression is not a result of the pulse action itself (i.e., the sweeping of the interface across the microculture) as the responses persisted seamlessly through the pulsing epoch.

Many of the experiments exhibited a marked increase or decrease in the intensity of the responses as the experiments progressed. However, these changes were observed both for the dopamine and control conditions. Figures 6.18 and 6.19 show such response changes broken down into the constituent channels (i.e., channel-resolved response rasters and stimulation maps). These data show that changes in the total stimulation response intensity were expressed as a general inhibition or excitation across all channels while maintaining their individual roles within the network, i.e., individual channels maintained their response latencies and their proportional firing rate. Thus, as far as this analysis can tell, the noted changes to the response intensity reflect a general drift in the excitability of the microculture rather than a change in the functional organization. In chapter 5 we argued that the fast flow interferes with intrinsic volume transmission processes within the tissue because it effectively imposes a particular concentration for the extracellular species (their concentration in the flow media). Part of the role of the extracellular environment is to dynamically

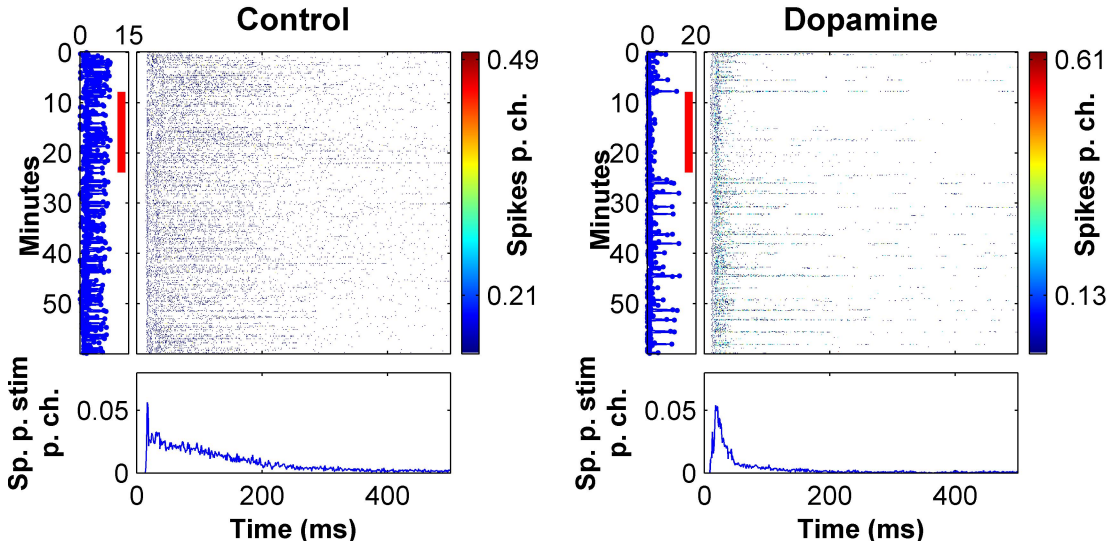


Figure 6.17: Coupling electrical stimulations to dopamine pulses suppresses the responses whereas blank pulses have no effect. Complete response rasters and PSTHs are shown from example control and dopamine pulsing experiments. The experimental epoch where the stimulations were coupled to dopamine are marked by red bars in the response sum panels (on the left of response rasters). Raster plots use 1ms bins.

respond to changes in the global activity to maintain homeostatic control and the loss of this control is likely to be responsible for the observed drift. Nevertheless, the sustainment of the functional identity of the circuit shows that the conclusions of chapter 5 are valid for the microcultures as well, i.e., that useful experimentation can be performed under these flow conditions. In practical terms, the excitability drift is reflected in the variability of experimental data and this can be seen in figure 6.21 where the variability of the overall firing rate increases over experiment time.

As noted above, the dopamine (or control) pulse commands were given 200ms prior to the associated electrical stimulation. Nevertheless, taking into account the predicted delay in the arrival of the agonist, the cells experienced an appreciable increase in dopamine levels only after most of the stimulation-associated activity had subsided (figure 6.20 A). This precise temporal arrangement has been purposefully selected to make this experimental protocol relevant to the notion of distal reward, as explained next. Distal reward, as reviewed in section 1.2.1 refers to the fact the dopamine transients associated with discrete rewarding events arrive in delay compared to the neuronal activity that was responsible for the attainment of the reward. To link the dopamine transient to the preceding neuronal activity, it was suggested that active synapses become tagged with an ‘eligibility trace’ which decays at a time scale of several seconds [97]. A synapse will be reinforced only if the dopamine transient arrives before its eligibility trace has completely decayed. Recently, such an ‘eligibility’ time window has been demonstrated for plasticity of synaptic spines in

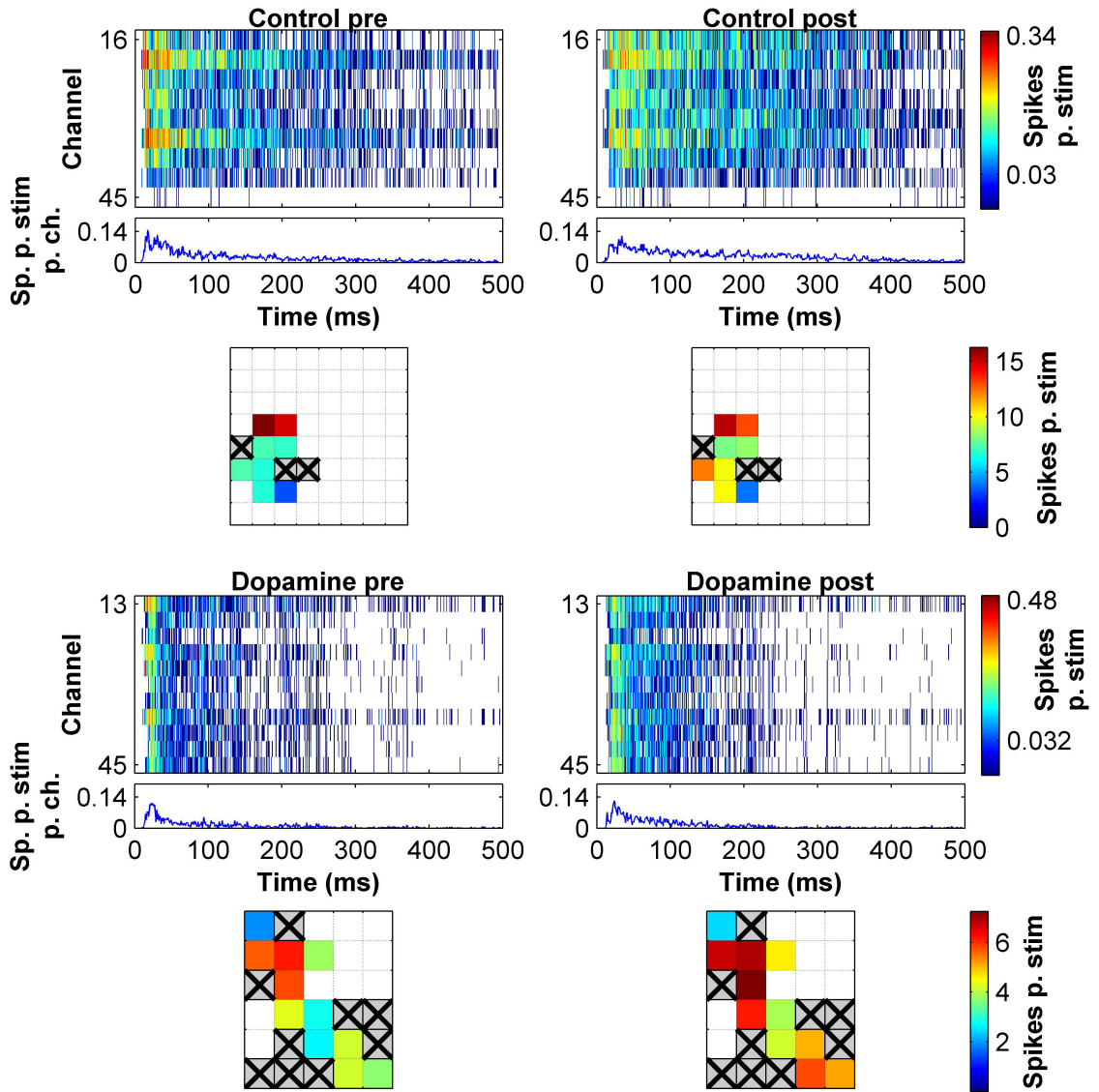


Figure 6.18: Some of the dopamine and control experiments exhibited an increase in response intensity following the pulsing but without reorganization of relative channel firing rates. Comparison of channel PSTHs and stimulation response maps before and after the pulsing epoch in example control and dopamine experiments. Each of the data sets is based on an 8 minute recording bins. The pre bin refers to the experimental segment prior to the pulsing. The post block refers to the second bin after the termination of the pulsing. These specific data are examples of increases in the global response intensity. The response rasters and particularly the summated PSTHs (panels directly below the channel rasters) show that the difference is mainly associated with a lengthening of the reverberative stimulation response. Stimulating electrodes are marked with X. The control data were collected from a device assembled on a 8×8 MEA. Thus the graphic stimulation response maps show the relative location of the microculture on the electrode grid. The dopamine data were collected on a HDMEA in which case a single 5×6 block is shown.

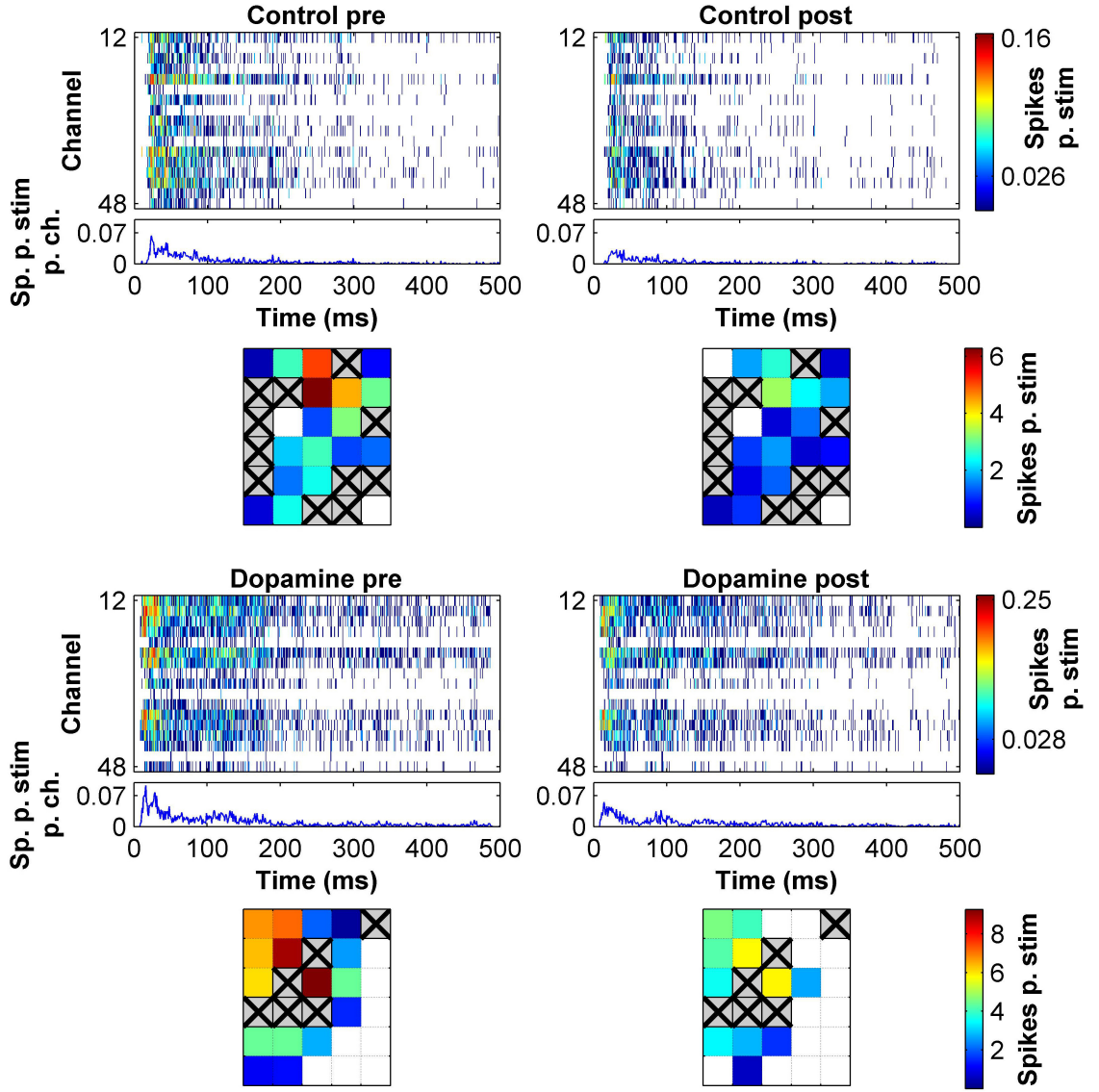


Figure 6.19: Some of the dopamine and control experiments exhibited a decrease in response intensity following the pulsing but without reorganization of relative channel firing rates. Comparison of channel PSTHs and stimulation response maps before and after the pulsing epoch in example control and dopamine experiments as in figure 6.18. These specific data are examples of decreases in the global response intensity. The response rasters and the summed PSTHs (panels directly below the channel rasters) suggest that the difference is associated with a decrease in initial firing rates of the reverberative stimulation response as well as with a shortening in its length.

the striatum [98]. Thus, the experimental paradigm employed here is designed to directly test these ideas in the culture context. Beyond its established interaction with neuronal plasticity, dopamine is also known to directly and immediately modulate neuronal circuits upon exposure [99, 100, 101, 43, 102]. This effect has been linked to the generation of reward-driven behaviour [103, 102]. Thus the delayed administration of the agonist also

aims to test whether these two separate roles of dopamine, delayed reward plasticity and direct activity modulation, can be decoupled from each other. This experimental design highlights the utility of the system in studying rapid volume transmission processes with a high level of temporal control and in a concentration-resolved manner.

To provide an improved grounds for interpreting the results of the experiments we estimated the degree of receptor activation during the dopamine transients using the Michaelis-Menten equation. This approach requires a value for the affinity (dissociation constant) of the dopamine receptors. However, the literature provides contradictory affinity values. In part, this has to do with these receptors having been shown to exist in two states with several orders of magnitude difference in affinities when expressed *in vitro* making it unclear which state they take on *in vivo* [104, 105]. At the same time, direct *in vivo* measurement of the affinity using radioligands is problematic due to nonspecific interactions in the native tissue [106]. Nevertheless, Radioligand studies in intact tissue slices showed that both D1 and D2 receptor appear in rat brain in a mix of high affinity and low affinity states [105]. This suggests that they occur in different brain regions in different affinity states and have the ability to switch between them. The factors which determine such switching remain unknown, though. Given these complications, it is unsurprising that reported affinity values have varied between $K_d = 1 - 3000\text{nM}$. Most of the reports in rats, though, seem to have been clustered at values of $K_d = 1 - 20\text{nM}$ for both main receptor subtypes [106]. Such low values, however, seem inconsistent with the amperometric accounts of dopamine concentration *in vivo*. Such reports have indicated that, in the striatum, dopamine levels fluctuate between 30nM at baseline and $100 - 200\text{nM}$ at the peak of phasic transients [53, 107, 91]. If dopamine levels already exceed the dissociation constant at baseline it would leave little dynamic range for phasic transients to have an impact. Given these arguments, we finally estimated the receptor activation using a dissociation constant of $K_d = 100\text{nM}$ which seems plausible given both the radioligand and the amperometric reports. However, this very rough estimation is used solely to give an impression rather than to draw quantitative conclusions. In this study we used a dopamine concentration of $100\mu\text{M}$ in the agonist stream which is the gold standard for inducing maximal activation of dopamine receptors [106] and is the typical concentration used for bath application experiments (e.g., [4, 98]). However, because this concentration is 3 orders of magnitude higher than the speculated dissociation constant, the effective activation of the dopamine receptors is much wider than is apparent from the concentration transients (figure 6.20 B). Alas, this information depends on a speculative value for K_d but even the lowest reported value is still 2 orders of magnitude lower than the source concentration. Consequently, it should be taken into account that the effective separation between consecutive activations of the dopamine machinery is probably much less than a second.

Despite the programmed delay in the arrival of the dopamine transient relative to the electrical stimulation, the spiking responses became depressed for the period of time

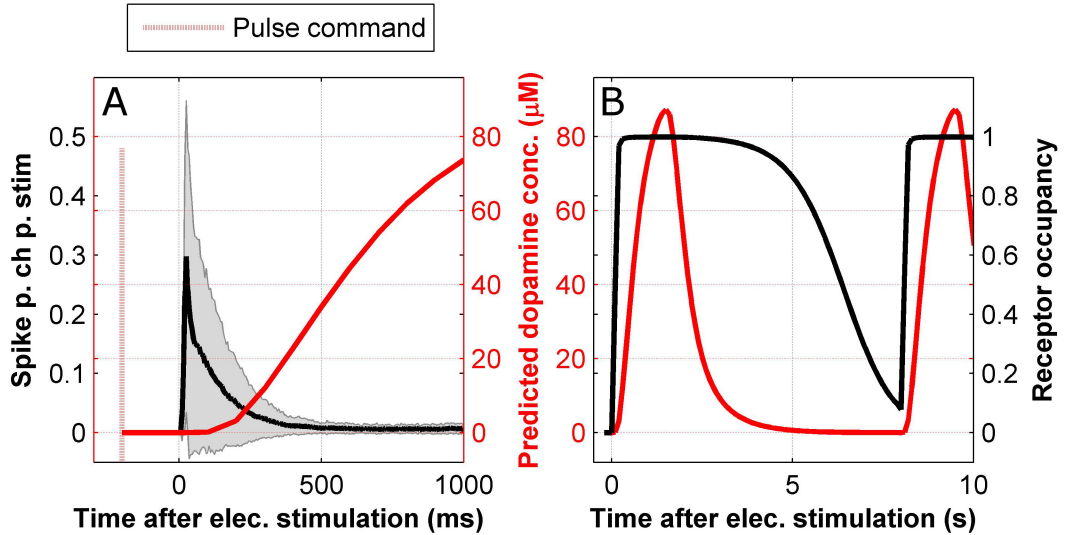


Figure 6.20: The dopamine levels were programmed to increase only after the reverberative stimulation response had mostly subsided. (A) Overlay of the predicted dopamine transient and the averaged PSTH across all pulsing experiments ($n=13$). Shaded area shows the PSTH standard deviation. Pulse command was given 200ms prior to the associated electrical stimulation. The timing of the dopamine transient was purposefully selected to model a ‘distal reward’ scenario. (B) Estimated dopamine receptors activation (black curve) over an entire dopamine transient (red curve) cycle. Receptor activation was estimated using standard Michaelis-Menten equilibrium and an approximate dissociation constant of $100nM$. See text for further information about this estimation. Due to the large discrepancy between the dopamine concentration in the agonist stream ($100\mu M$) and the dissociation constant, consecutive receptor activations were probably less temporally separate than apparent from the dopamine time course. Dopamine pulsing experiments were performed in devices with $80\mu m$ deep microwells.

that they were coupled to dopamine pulses (figure 6.21 A, unbalanced t-test, $p = 0.025$ and 0.028 for the two bins spanning the pulsing epoch) and reverted back to baseline soon after the pulsing was concluded. Such a temporary effect is indicative of a direct influence of the dopamine on the network dynamics rather than of synaptic plasticity. This suggests that the effect of dopamine persisted beyond the physical presence of the agonist and that the pulse configuration used here did not give enough time between transients to allow recovery. These results demonstrate that dopamine neuromodulation is functional in these microcultures. The direct modulation of circuit dynamics by dopamine has been suggested to be linked with transition into mental modes of alertness and motivation [103, 102, 108]. Thus this system might also be suited to study the neural correlates of these such mental processes.

Since synaptic plasticity was not observed in the above-described measure of global

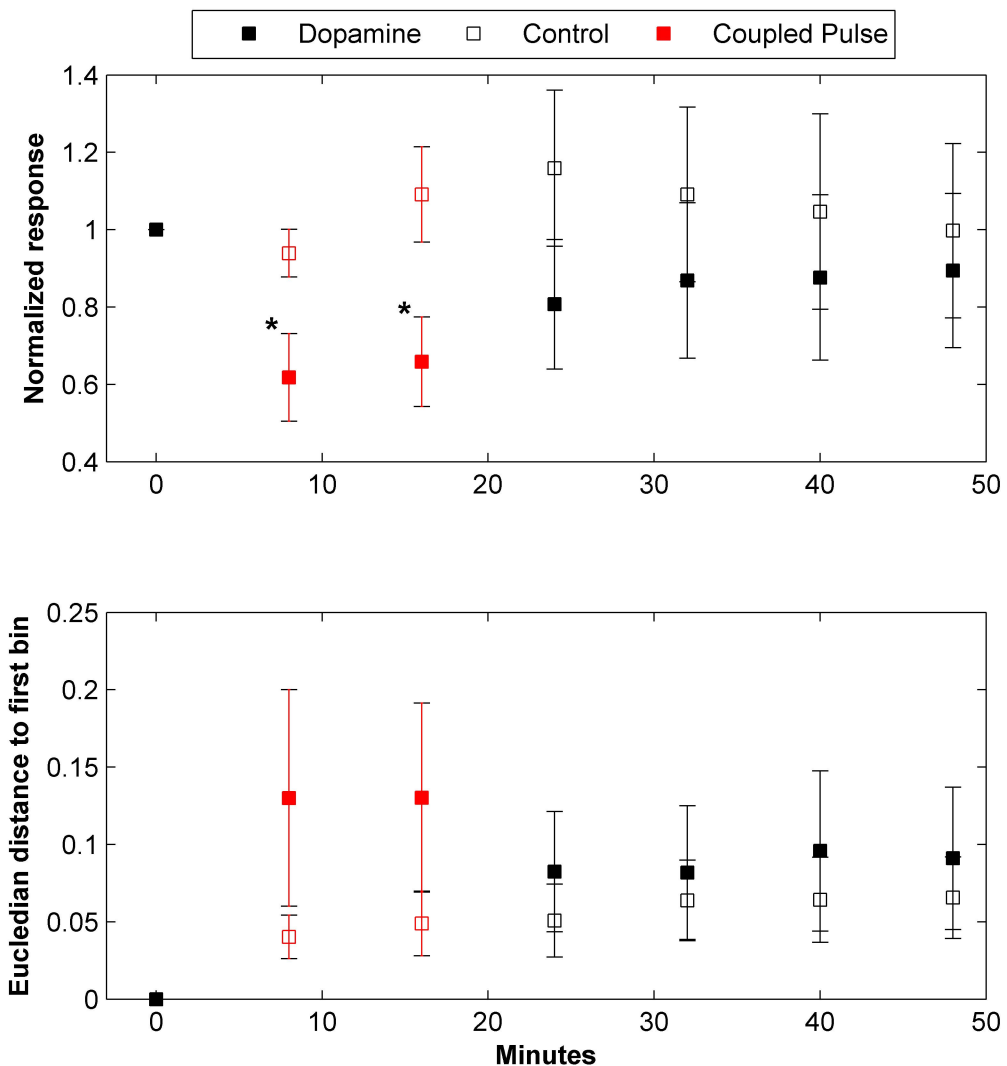


Figure 6.21: Association of the electrical stimulation with dopamine pulses causes a temporary inhibition of evoked responses. (A) Comparison of the time course of global stimulation responses between experimental conditions of dopamine ($n=6$) and blank ($n=7$) pulsing. Stimulation responses are averaged over all channels and all experiments in 8 minute bins. Red squares indicate bins where the electrical stimulations were coupled to dopamine pulsing. Responses are normalized to the baseline epoch (i.e., the block preceding the pulsing) in each experiment. Error bars show SEM. (B) Functional connectivity analysis where the measure is computed over 8 minute bins of activity and presented as in A. Asterisk indicates a statistically significant difference between control and dopamine at the given block at a 95% level of confidence.

response we repeated the analyses performed in section 3.4 and which were designed to detect changes in the detailed response distributions of the channels (figure 6.22) or in the functional connectivity between them (figure 6.21 B). These analyses did not reveal

any significant changes induced by the dopamine pulsing as compared to blank pulsing. Nevertheless, it should be noted that despite the lack of statistical significance there is a visible hysteresis in the global response and functional connectivity, i.e., the time course for these measures in the dopamine case is noticeably different from the control case. This might indicate that there is a certain degree of plasticity which requires a longer induction protocol to emerge as significant or that some components of the direct dopamine effect take longer to decay. We plan to use this system for further exploration of experimental paradigms to uncover the conditions for induction of dopamine-dependent plasticity. We believe that this system will be useful in understanding the principles behind dopamine’s dual role in shaping the network dynamics and in reinforcement learning.

In contrast to the results of section 3.4, where persistent changes were observed after the plasticity induction in the presence of dopamine, no significant long lasting effects were observed with the dopamine induction performed here. The results of these two studies are not directly comparable because the induction method was different (tetanus vs. low frequency stimulation). Nevertheless, the approach followed in this chapter is superior because of its explicit control over the agonist concentration levels and because it inherently avoids artifacts associated with the solution exchange (as the culture is continuously under a steady rate of media replenishment). Thus, the contradiction in results calls for a reevaluation of the compounding factors in the previous study.

6.6 Chapter conclusion

In this chapter we put together the knowledge gathered in the previous ones to construct a system for rapid solution exchange to an entire neuronal microculture at time scales compatible with phasic neuromodulation. Despite of the work performed in the previous chapters some uncertainties had remained uncleared, namely, whether the microcultures would be electrophysiologically functional, whether they would sustain that functionality under flow, whether the pulsing action would perturb the activity and whether the system can indeed match physiological time scales. These gaps have all been addressed here as we demonstrated that the microcultures exhibit spontaneous and evoked reverberative activity, that they are able to sustain that activity under flow with good efficacy, that they are oblivious to the interface shifting in itself and that the agonist transients can be applied with our current system configuration at time scales within the known range of phasic neuromodulatory signals.

We also demonstrated through simulation that faster time scales can be achieved to cover the full reported range *in vivo*. Such options, however come with a caveat that they require increased flow rates. In chapters 4 and 5 we provided data to show that, beyond a certain flow threshold, the viability and functionality of the culture are completely determined by media conditioning and are not modulated by the shear in any way. It therefore stands to

reason that the results shown here apply for higher flow rates as well. Nevertheless, there will be a shear threshold which, when exceeded, will result in physical damage to the tissue and so higher flow rates would need to be tested.

We finalized the work by designing and running a plasticity experiment involving an interaction between phasic dopamine transients and stimulation induced reverberatory activity. This experimental design highlights the usefulness of the presented system in studying how fine temporal features of phasic volume transmission interact with the activity. To our knowledge, this is the first demonstration of programmatic control over the concentration and kinetics of an extracellular chemical species in an entire neuronal circuit. As microfluidics technology continues to advance we expect to see increasingly sophisticated systems involving simultaneous control of multiple extracellular species with a spatial resolution. This work is a first step in that direction.

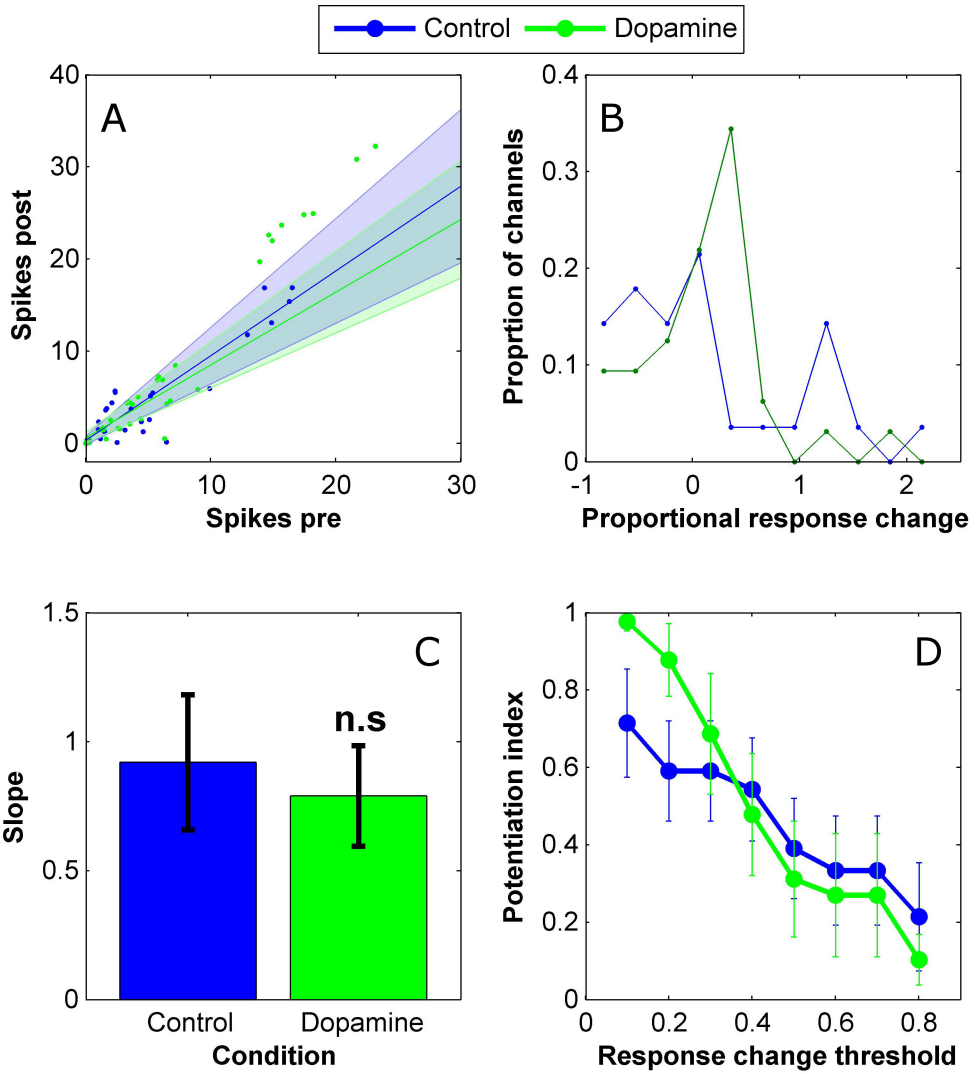


Figure 6.22: In this experimental configuration, coupling electrical stimulation to dopamine pulses did not elicit long term changes to global responses or a significant change in response distributions across the channels as compared to control. The analysis in this figure completely repeats the one performed for the tetanus induction protocol in figure 3.10 for comparative purposes. (A) Scatter plot of pre vs. post channel responses for the dopamine and control conditions. Pre refers to the 8 minute data bin prior to the pulsing and post refers to the second bin of such size after the pulsing has terminated. A line is fitted to the scattered points of each experimental condition. Plotted lines and shaded areas visualize the mean and SEM of these line slopes. (B) Comparison of fitted slopes from A. ‘n.s’ - non significant difference. (C) Distributions of proportional changes induced in channel responses when compared between the pre and post epochs as in A. Potentiation index (PI) is computed based on these distributions as in figure 3.10. (D) Mean + SEM of potentiation index as a function of tested levels of change thresholds (see section 3.4 and figure 3.10).